LBL-31695
UC-410

Lawrence Berkeley Laboratory
UNIVERSITY OF CALIFORNIA

Accelerator & Fusion Research Division

Diffraction Phenomena in Spontaneous and Stimulated Radiation by Relativistic Particles in Crystals

V.G. Baryshevsky and I. Ya Dubovskaya

December 1991

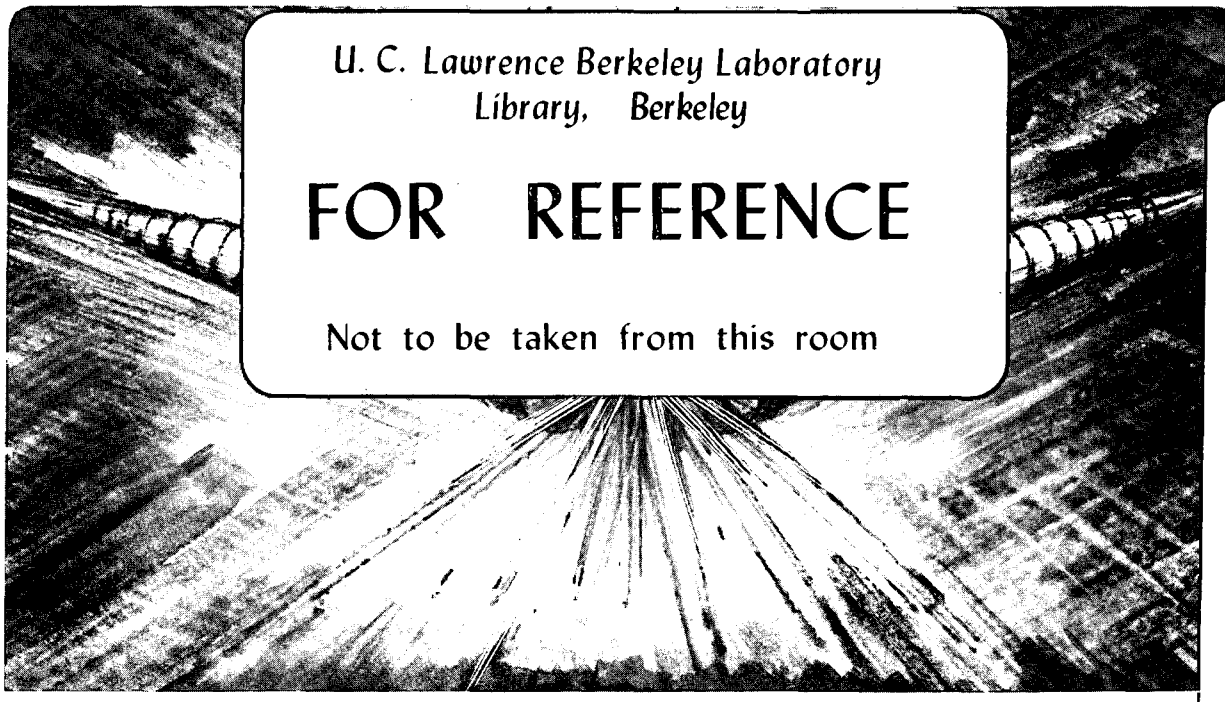

Prepared for the U.S. Department of Energy under Contract Number DE-AC03-76SF00098

DISCLAIMER

LBL-31695
ESG Note-162

DIFFRACTION PHENOMENA IN SPONTANEOUS AND STIMULATED RADIATION BY RELATIVISTIC PARTICLES IN CRYSTALS

(REVIEW)*

V.G. Baryshevsky

Institute of Nuclear Problems
Minsk 220050, USSR

I. Ya Dubovskaya**

Lawrence Berkeley Laboratory
University of California
Berkeley, California 94720

* This review was published in Russia and translated by author. The translation work was supported in part by the Director, Office of Energy Research, Office of Basic Energy Sciences, Materials Sciences Division, of the U.S. Department of Energy under contract No. DE-AC03-76F00098

** Permanent address: Institute of Nuclear Problems, Minsk 220050, USSR

DIFFRACTION PHENOMENA IN SPONTANEOUS AND STIMULATED RADIATION BY RELATIVISTIC PARTICLES IN CRYSTALS (REVIEW)

V.G. Baryshevsky and I. Ya. Dubovskaya

I. Introduction

The emission of photons by relativistic particles in media has been calling attention for a long time. This connects, first of all, with a wide variety of tasks being solved by using different radiation mechanisms, such as: bremsstralung, transition and Cerenkov radiations and so on. In later decades investigation of radiation by relativistic particles in crystals is most interesting. A number of new radiation mechanisms connected with a periodic structure of crystals have been considered theoretically and confirmed experimentally in the Institute of Nuclear Problems (Minsk).

All characteristic properties of radiation, in this case, are resulted in by a crystal periodic structure. The medium can influence radiation processes under the passage of relativistic charged particles through crystals in two ways. First of all, it is well-known that, when a charged particle is incident on a crystal at a small angle relative to crystallographic planes or axes, its trajectory is formed by a series of grazing collisions with atoms of a crystal. As a result, the particle moves in some averaged potential of crystallographic planes or axes. In this case, we tell about channeling phenomenon and can consider the motion of channeled particles as motion inside a potential well - one-dimensional (for the plane channeling) or two-dimensional (for axial channeling). But the particle, moving inside a potential well, according to quantum mechanics, has a discrete spectrum of its energy. In this case, this is the energy spectrum of its transverse motion. Consequently, such particles can be considered as one-dimensional or two-dimensional atoms (oscillators) being characterized by a spectrum of bound states (zones) of transverse energy ε_n, ε_f. The number of bound states and their characteristics depend on the longitudinal particle energy. One can conclude that many phenomena observed for ordinary atoms will manifest themselves under passage of channeled particles through crystals. It is obvious that such excited atoms should emit photons with the energy equal to the difference of energies of atom states ε_n and ε_f. The frequency of

transition is $\Omega nf = \varepsilon_n - \varepsilon_f$ and depends, in a laboratory frame, on the total particle energy. By analogy of an ordinary moving oscillator, the frequency of observed emitted photons is evaluated by Doppler effect and, as a result, is determined by the following expression:

$$\omega = \frac{\Omega nf}{1 - \beta n(\omega) \cos\theta}, \qquad (1)$$

where θ is the radiation angle, $\beta = u/c$, u is the longitudinal particle velocity, $n(\omega)$ is the refractive index of photon with a frequency ω in the medium. It is interesting that the relativistic oscillator can be formed not only by unperturbed crystal channel but also by an external ultrasonic or laser wave which subjects to the crystal and originates a bent crystal channel.

On the other hand, when the wave length of emitted photons is of the order of the interplanar spacing of atoms in a crystal, radiation diffraction can essentially modify photon state. In this case, the radiation process is characterized by several refractive indices $n_i(\omega)$ dependent on the photon momentum direction. In its turn, this leads to the modification of all mechanisms of radiation formation by relativistic particles in X-ray region of spectrum. For example, the radiation at a large angle relative to particle motion direction becomes possible. As a result, the diffraction pattern characterizing a given crystal is formed. The analysis of dielectric properties of a crystal under diffraction condition shows that at least one from several refractive indices $n_i(\omega)$, characterizing the crystal under this condition, becomes more than unity within a frequency interval. As a consequence, the Vavilov-Cerenkon condition can be fulfilled. In this case, the X-ray radiation, being analogous to optical Cerenkov radiation, appears. This radiation mechanism, taking place under the penetration of uniformly moving particles through the periodic medium under diffraction condition of radiated photons, was theoretically predicted by Baryshevsky and Feranchuk and was called Parametric (quasi-cerenkov) X-ray radiation (PXR). It was experimentally observed and investigated in Tomsk synchrotron by collaboration of Institute of Nuclear Problems (Mnisk) and Institute of Nuclear Physics (Tomsk).

Under diffraction conditions, the radiation of relativistic oscillator essentially modifies as well. Now the periodic structure of a crystal affects both to particle motion and photon state. This leads to the formation of diffraction radiation of oscillator (DRO), which can not be reduced to the sequence of two independent processes: radiation by oscillator and diffraction of radiated photons. In this case the process of photon emission and its diffraction are developing simultaneously and coherently and result in the radiation with new properties.

The parametric X-ray radiation generated by a particle uniformly moving through a crystal has threshold behavior the same as the ordinary Cerenkov radiation and its intensity is proportional to the crystal length or photon absorption length. The spectral-angular distribution consists of a series of peaks (reflections), concentrated near characteristic frequencies of PXR $\omega_B = \tau^2 c/2|\vec{\tau}\,\vec{\beta}|$ ($\vec{\tau}$ is a reciprocal lattice vector), and is determined, first of all, by a crystal dielectric constant under diffraction. It is important to stress, that PXR does not should be mixed with so-called "resonance" [1] or dynamical [20] radiations. In the contrary of PXR, which frequencies are determined only by a crystal constant, the frequency of resonance radiation depends on a particle energy [1]. The dynamical radiation takes place only in thin crystals [20]. Its intensity decreases with increasing the crystal length. This is caused by the neglection of the photon refraction inside a crystal [20]. The refraction of photons was taken into account by the authors in [4,21]. Just due to the fact that the refractive index of a photon can become more than unity under diffraction condition, the particle speed inside the crystal becomes more than the phase speed of the photon in the medium. This, in turn, leads to the appearance of radiation with the intensity proportional to the crystal length (in the absence of absorption).

Now many features of PXR, predicted theoretically, have been confirmed in experiments.

The second type of X-radiation (DRO), also connected with a change of dielectric properties under diffraction conditions, was considered in [13] and then in [17-19]. If, in the absence of diffraction, the X-ray spectrum of the oscillator is determined by the complex Doppler effect ($n(\omega) < 1$), then, under diffraction, the refractive index can become more than unity and, consequently, the anomalous Doppler effect possible. In this case the photon emitted by oscillator

is accompanied by the excitation of oscillator itself. This is one of the important features of diffraction radiation of oscillator (DRO). This effect is waiting for own experimental investigation.

So, the modification of dielectric properties in periodic media under diffraction leads to the appearance of two types of radiation with angular distribution forming a diffraction pattern determined by parameters of medium periodic structure. For crystals with parameters of lattice of the order of A°, the spectrum of PXR and DRO is in the region of X-ray and even higher frequencies depending on excited reflex.

It is well-known that in amorphous medium the ordinary Cerenkov radiation can be considered as a specific case of radiation of oscillator with the zero eigenfrequency [10]. In a periodic medium, in the total analogy, the frequency of PXR can be expressed by the formula (1) in the specific case of $\Omega nf = 0$, i.e., $1 - \beta n_i(\omega) \cos\theta = 0$, where $n_i(\omega)$ is the refraction index of a crystal under diffraction conditions.

II. Dispersion Characteristics of PXR and DRO.

Due to the dependence of the refractive index under diffraction on a frequency and a particle motion direction, the relation (1) and (2) determining the radiated photon spectrum are the equations with several solutions [13,17, 19, 27].

For example, let us consider the case of two-wave generation when the diffraction condition is fulfilled only for a reciprocal lattice vector $\vec{\tau}$. It means that two strong waves with wave vectors $\vec{k}$ and $\vec{k}_{\vec{\tau}} = \vec{k} + \vec{\tau}$ are excited under diffraction. For the simplicity of analysis of photon frequencies, let us represent the equation (1) in the form:

$$n(\omega) = \frac{\omega - \Omega nf}{\omega\beta \cos\theta} \qquad (1.1)$$

In this case the refractive index in a crystal under diffraction conditions is characterized by two dispersion branches $n_{1,2}$. By using the well-known expression for $n_{1,2}$ one can rewrite (1.1) as follows:

$$\frac{1}{\beta\cos\theta} - \frac{\Omega_{nf}(1-\delta)}{\omega_B\,\beta\cos\theta} =$$
$$= 1 - \frac{\omega_L^2}{4/\omega^2}\left\{(1+\beta_1) - A\beta_1\frac{\delta}{|g_0|} \mp \sqrt{\left[(\beta_1-1) - A\beta_1\frac{\delta}{|g_0|}\right]^2 + 4\beta_1\frac{|g_\tau^2|}{g_0^2}}\right\} \quad (1.2)$$

for the diffraction radiation of oscillator (DRO) and

$$\frac{1}{\beta\cos 0} = 1 - \frac{\omega_L^2}{4\omega^2}\left\{(1+\beta_1) - A\beta_1\frac{\delta}{|g_0|} \mp \sqrt{\left[(\beta_1-1)^2 - A\beta_1\frac{\delta}{|g_0|}\right]^2 + 4\beta_1\frac{|g_\tau|^2}{|g_0|^2}}\right\} \quad (1.3)$$

for parametric quasi-Cerenkov radiation (PXR), generated by a particle passing through the crystal with a constant velocity.

We have introduced the following notations: $\alpha = \frac{2(\vec{k}\vec{\tau}) + \tau^2}{\omega^2/c^2}$, is the deviation from exact Bragg condition,

$$\alpha \cong \alpha_{\omega_B} + \left(\frac{\partial\alpha}{\partial\omega}\right)_{\omega_B}(\omega - \omega_B) = -\frac{\tau^2c^2}{\omega_B^3}(\omega - \omega_B) = -A\delta\ ,$$

where $A = \frac{\tau^2c^2}{\omega_B^2} > 0$, $\delta = \omega - \omega_B/\omega_B$, $\omega_B = \tau^2c^2/2|\vec{\tau}\,\vec{\beta}|$ is the Bragg frequency, corresponding to $\alpha = 0$, $\beta_1 = k_z/k_z+\tau_z$ is the geometry factor of diffraction asymmetry, the axis Z is chosen as a normal to the target surface directed inside the crystal. Let us assume the particle with a mean velocity $\vec{u}$ to move along the axis Z, $\beta = u/c$, g_0, g_τ are the coefficients in a series expansion in terms of the reciprocal lattice vectors of the crystal dielectric susceptibility. For simplicity, we will assume a crystal to be center-symmetric and the absorption to be neglected, $\omega_L^2 = 4\pi e n_0/m_e$ is the Langmuir frequency of the medium.

Let us consider in detail the condition of the existence of parametric X-ray radiation. Indeed, for the existence of this radiation it is enough the relation (1.3) to be fulfilled although for one from the two refractive indices characterizing the crystal at a given frequency. On the left-hand side of (1.3) there is a term more than unity ($\beta < 1$ and $|\cos\theta| < 1$). Consequently, for the existence of the solution of Eq.(1.3), the expression, on the right-hand side of (1.3), between the figure brackets, should be less than zero. Far from Bragg condition, $\delta \to \infty$ and we transit to the well-known case of amorphous medium, i.e. to the refractive index $n(\omega) = 1 - \omega_L^2/2\,\omega^2 < 1$ for any frequencies from X-ray region. As a result, Cerenkov radiation is impossible in this region. The analysis of (1.3) near Bragg condition $|\alpha| \lesssim |g_0|$ shows that the expression between the figure brackets is always positive for one dispersion branch, corresponding to the sight (–); consequently, the fulfillment of Eq.(1.3) is impossible. For the second branch, corresponding to the sight (+), this expression can be negative at $|\alpha| \gtrsim |g_0|$. For example, in the case of

$$\left|(\beta_1 - 1) - A_{\beta_1}\frac{\delta}{|g_0|}\right| >> 4\beta_1\left|\frac{g_\tau}{g_0}\right|^2 ,$$

we can approximately write

$$\frac{1}{\beta\cos\theta} \cong 1 - \frac{\omega_L^2}{2\omega^2}\beta_1\left[1 - A\frac{\delta}{|g_0|}\right]$$

and, obviously, that the fulfillment of Cerenkov condition is possible for Laue diffraction case ($\beta_1 > 0$) at frequencies for which $\left|A\frac{\delta}{|g_0|}\right| > 1$. In Bragg diffraction case ($\beta_1 < 0$) the Cerenkov condition can be fulfilled not only for one dispersion branch but even for two branches at the degeneration point.

The comparison of expression (1.3) and (1.2) shows that the relation (1.2) can be satisfied for both dispersion branches at $\Omega_{nf} > 0$, i.e. for the radiation accompanied by the transition of a particle to the lower energy level ($\varepsilon_n > \varepsilon_f$). It means that two different frequencies are radiated at a

given angle. In this situation, we observe normal complex Doppler effect. In this case, the equation (1.2) is satisfied for radiation angles more than the angle of parametric (quasi-Cerenkov) radiation. At the same time, the fulfillment of (1.2) leads to the strong limitation of particle energy, the radiation angle and the value of deviation from the exact Bragg condition α for the radiation accompanied by the oscillator excitation $\Omega_{nf} < 0$ ($\varepsilon_n < \varepsilon_f$). In this case, according to (1.2), for one from dispersion branches it is possible the radiation of a photon (anomalous Doppler effect) with the wave vector directed relative to the particle motion at an angle less than that for the parametric (quasi-Cerenkov) radiation.

The analytical analysis of Eq.(1.2) can be derived in a specific case, when

$$2\frac{\omega_L^2}{\Omega^2}\phi(\omega,\theta)(1-\beta\cos\theta) << 1 \qquad (1.4)$$

where

$$\phi(\omega,\theta) = \frac{1}{2}\left\{1+\beta_1 - A\beta_1\frac{\delta}{|g_0|} \mp \sqrt{\left(\beta_1 - 1 - A\beta_1\frac{\delta}{|g_0|}\right)^2 + 4\beta_1\frac{|g_\tau|^2}{|g_0|}}\right. \qquad (1.5)$$

Let us represent (1.2) in the form

$$\omega = \frac{\Omega_{nf}}{2(1-\beta\cos\theta)}\left(1 \pm \sqrt{1 - 2\frac{\omega_L^2}{\Omega^2}\phi(\omega,\theta)(1-\beta\cos\theta)}\right) \qquad (1.6)$$

In view of Eq.(1.4), Eq.(1.6) divides into two independent equations corresponding to upper and lower radiation branches in the absence of diffraction.

$$\omega_I = \frac{\Omega_{nf}}{1-\beta\cos\theta} - \frac{\omega_L^2}{2\,\Omega_{nf}}\phi(\omega,\theta), \qquad (1.7)$$

$$\omega_{II} = \frac{\omega_L^2}{2\Omega_{nf}} \phi(\omega,\theta) . \qquad (1.8)$$

Neglecting the dependence of β_1 on ω, one can obtain the frequency solutions of Eqs.(1.7) and (1.8) as a function of a radiation angle:

$$\omega_{I\pm} = \omega_m - \omega_0 \left[\frac{1+\beta_1}{2} - \frac{x}{2} \left\{ 1 + \frac{\omega_m - \omega_B}{\omega_0} \pm \right. \right.$$

$$\left. \left. \pm \sqrt{\left(\frac{1-\beta_1}{x} + 1 - \frac{\omega_m - \omega_B}{\omega_0} \right)^2 - 4 \left| \frac{g_\tau}{g_0} \right|^2 \frac{1}{x}} \right] (1-x)^{-1} , \right. \qquad (1.9)$$

$$\omega_{II\pm} = \omega_0 \left[\frac{1+\beta_1}{2} + \frac{x}{2} \left(1 + \frac{\omega_B}{\omega_0} \pm \right. \right.$$

$$\left. \left. \pm \sqrt{\left(\frac{1-\beta_1}{x} + 1 - \frac{\omega_B}{\omega_0} \right)^2 + 4 \left| \frac{g_\tau}{g_0} \right|^2 \frac{1}{x}} \right] (1+x)^{-1} , \right. \qquad (1.10)$$

where

$$\omega_0 = \frac{\omega_L^2}{2\Omega} , \quad \omega_m = \frac{\Omega}{1 - \beta\cos\theta} ; \quad \omega_B = \frac{\tau^2}{2} \left\{ \left| \vec{\tau}_{||} \right| \cos\theta - \left| \vec{\tau}_{\perp} \right| \sin\theta \cos\varphi \right\}^{-1}$$

$$x = \frac{\beta_1}{\Omega} \left(\left| \vec{\tau}_{||} \right| \cos\theta - \left| \vec{\tau}_{\perp} \right| \sin\theta \cos\varphi \right) ,$$

$\bar{\tau}_{||}$ and $\bar{\tau}_{\perp}$ are the projections of the reciprocal lattice vector to the particle mean velocity direction and to the plane perpendicular to its velocity, correspondingly; φ is the angle between $\bar{\tau}_{\perp}$ and $\vec{k}_{\perp}$. In Fig.1 the dependence $\omega = \omega(\theta)$ for the case of symmetric diffraction $\beta_1 = 1$ is shown.

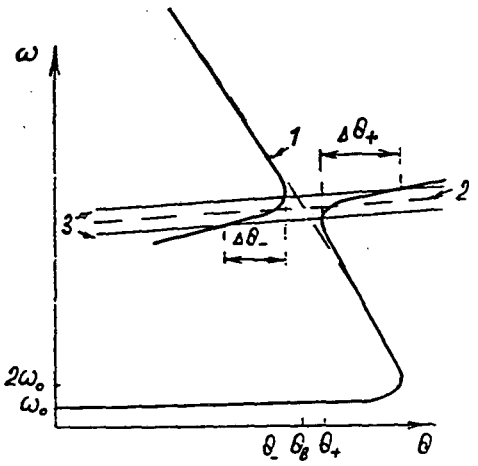

Fig. 1

According to Fig.1 and Exs.(1.9) and (1.10), the spectrum of radiated photons essentially modify under diffraction. Each radiation branch, in the absence of diffraction, splits, in its turn, into two subbranches. Thus, diffraction results in the excitation of an additional branch in the complex Doppler effect with the frequency close to the Bragg one ω_B and in the formation of a radiation non-transparency region in the angular distribution $\Delta\theta = \theta_+ - \theta_- = 10^{-5} \div 10^{-6}$ rad. Under the change of the angle θ the solution is realized first for one dispersion branch than for the another one. In Fig.1 the angular region in which $|\alpha| \le |g_0|$ is pointed out. It should be noted that the radiation frequency of additional diffraction branch changes a little with the radiation angle. As a result, the angular range, in which $|\alpha| \le |g_0|$, may considerably exceed the ordinary angular interval, characterizing diffraction of an X-ray external monochromatic wave when $\Delta\theta$ is of the order of several angular minutes (in Fig.1 this is the angular interval $\Delta\theta = \Delta\theta_+ + \Delta\theta_-$). To obtain the analytical solution is rather complicated, that is why, the numerical calculation of the dependence of $\alpha/|g_0|$ on the radiation angle θ near the Bragg angle θ_B was made for the oscillator moving along the crystal direction $\langle 110 \rangle$ and photon diffraction by crystallographic planes (400) in Si. According to these calculations, the magnitude of $\Delta\theta$ weakly depends on the energy and eigenfrequency of oscillator and maintains within the interval of $10^{-4} - 10^{-3}$. In Fig.2 the magnitude of $\alpha/|g_0|$ shows as a function of the angle θ at the following parameters of the oscillator: Ω = 1eV, $\gamma = 2.10^3$. As you can see $\Delta\theta_- \approx 4.10^{-3}$ rad, $\Delta\theta_+ = 5.2 \cdot 10^{-3}$ rad and the total interval $|\alpha| \le |g_0|$, $\Delta\theta$=9.2 10^{-3} rad.

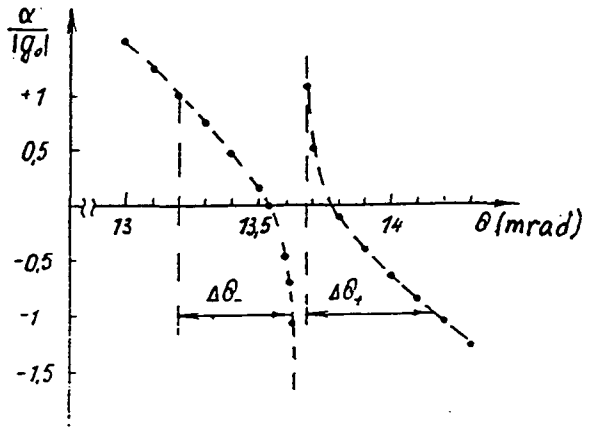

Fig. 2

The values of the angles $\theta_{\pm}$,when $\alpha = 0$, is determined from the equation

$$\omega_B = \omega_m - \omega_0\left(1 \pm \frac{g_\tau}{g_0}\right) . \qquad (1.11)$$

The picture, like the considered one, takes place also for the second branch (see (1.10)). So, if $\omega_0 \neq \omega_B$ and it is possible to neglect the second term under the root in (1.10), then, for example, $\omega_{II+} \approx \omega_B$ and $\omega_{II-} \approx \omega_0$ at $\omega_0 < \omega_B$. It means that, as in the previous case, we have the excitation of the wave with the frequency close to the Bragg frequency in addition to the solution far from diffraction at a given radiation angle θ. As the calculation shows, the magnitude of α keeps practically constant and is determined by the oscillator eigenfrequency in the whole interval of radiation angles, corresponding to the fulfillment of the condition (1.4), in spite of the change of diffracted wave frequency. Although, the parameter α depends on the eigenfrequency of oscillator Ω and is equal to zero at

$$\Omega_{\pm} = \frac{\omega_L^2}{2\omega_B}\left(1 \pm \frac{g_\tau}{g_0}\right), \qquad (1.12)$$

but it remains small ($|\alpha| \leq |g_0|$) within the rather wide interval of the eigenfrequencies. For example, in the case, considered above, $\Omega_{\pm} = 0.092$eV and $|\alpha| \leq |g_0|$ for the interval $\Omega_{+min} = 0.08$eV and $\Omega_{+max} = 0.15$ eV.

It should be noted that the equality (1.10) has the solution also for the negative eigenfrequency of oscillator (at the frequency close to ω_B), that corresponds to the anomalous Doppler effect, i.e. the radiation of the oscillator is accompanied by its excitation. Such process is possible because the refractive index can be more than unity under diffraction condition.

The analysis of dispersion expression for the radiation, propagating at a large angle and for arbitrary geometry of diffraction was made in [29]. Here we discuss the spectrums of DRO and PXR only in the two-wave diffraction case. However, due to crystal symmetry, the diffraction condition can be satisfied for many waves, that is the case of multi-wave diffraction can be realized. In this case the several refraction indices $n_i(\omega)$, corresponding to the different dispersion branches, can be more than unity. It appears that the possibility of new effects in the radiation, such as the effect of the excitation of radiation in a roundabout way takes place. It means, that the PXR intensity in a diffraction peak may differ from zero even in the case when a given reflection is forbidden because of the lattice symmetry. The particular properties in the angular distribution of radiation are observed in the vicinity of the point of the dispersion branches degeneration.

II. Parametric X-Ray (Quasi-Cerenkov) Radiation (PXR).

§1. General Expression for Spectral-Angular Distribution of Radiation Generated by a Particle in a Target.

Both the spectral-angular density of radiation energy per unit solid angle $W_{\vec{n},\omega}$ and the differential number of emitted photons $dN_{\vec{n},\omega}\ \omega = 1/\hbar\omega \cdot W_{\vec{n},\omega}$ can be easily obtained if the field $\vec{E}(\vec{r},\omega)$, produced by a particle at large distance $\vec{r}$ from a crystal, is known [30]

$$W_{\vec{n},\omega} = \frac{er^2}{4\pi^2}\left|\vec{E}(\vec{r},\omega)\right|^2 , \tag{2.1}$$

Here the line means the averaging over-all possible states of the radiating system. In order to obtain $\vec{E}(\vec{r},\omega)$, Maxwell's equation describing the interaction of particles with the medium should be solved. The transverse solution can be found by the help of Green's function of this equation, that satisfies the expression:

$$G = G_0 + G_0 \frac{\omega^2}{4\pi c^2}\left(\hat{\varepsilon} - 1\right) G , \tag{2.2}$$

G_0 is the transverse Green's function of Maxwell's equation at $\hat{\varepsilon} = 1$. It is given, for example, in [31].

By using G,we can find the field being interested in:

$$E_n(\vec{r},\omega) = \int G_{ne}\left(\vec{r},\vec{r}',\omega\right)\frac{i\omega}{c^2} j_{0e}\left(\vec{r}',\omega\right) d^3r' , \tag{2.3}$$

where n, e = x, y, z, $j_{0e}(\vec{r},\omega)$ is the Founier-transform of e-th component of the current, produced by the moving charged particle beam (in the approximation linear in the field, the current is determined by the velocity and the trajectory of a particle, which are obtained from the equation of particle motion in the external field, by neglecting the influence of the radiation field on the particle

motion). Under the quantum-mechanical consideration the current j_0 should by considered as the current of transition of particle-medium system from one state to the another one.

According to [32], the Green's function is expressed at $r \to \infty$, through the solution of homogeneous Maxwell's equation $E_n^{(-)}(\vec{r},\omega)$, containing incoming spherical waves:

$$\lim_{r \to \infty} G_{ne}(\vec{r},\vec{r}',\omega) = \frac{e^{ikr}}{r} \sum_s e_n^s E_{ke}^{(-)s*}(\vec{r}',\omega), \tag{2.4}$$

where $\vec{e}^{\,s}$ is the unit polarization vector, $s = 1,2$, $\vec{e}^{\,1} \perp \vec{e}^{\,2} \perp \vec{k}$.

If the electromagnetic wave is incident on a crystal of finite size, then at $r \to \infty$

$$\vec{E}_{\vec{k}}^{s(-)}(\vec{r},\omega) = \vec{e}^{\,s} e^{i\vec{k}\vec{r}} + \text{const}\frac{e^{ikr}}{r},$$

one can show that the relation between the solution $\vec{E}_{\vec{k}}^{s(-)}$ and the solution of Maxwell's equation $\vec{E}^{(+)}(\vec{k},\omega)$, describing the scattering of a plane wave by the target (crystal), is given by:

$$\vec{E}_{\vec{k}}^{s(-)*} = \vec{E}_{-\vec{k}}^{s(+)} . \tag{2.5}$$

By using (2.3) we obtain

$$E_n(\vec{r},\omega) = \frac{e^{ikr}}{r} \frac{i\omega}{c^2} \sum_s e_n^s \int \vec{E}_{\vec{k}}^{s(-)*}(\vec{r},\omega)\, \vec{j}_0(\vec{r}',\omega)\, d^3r' . \tag{2.6}$$

As a result, the spectral energy density of photons with the polarization s can be written in the form:

$$W^{s}_{\vec{n},\omega} = \frac{\omega^2}{4\pi^2 c^2}\left|\int \vec{E}^{s(-)*}_{\vec{k}}(\vec{r},\omega)\,\vec{j}_0(\vec{r},\omega)d^3r\right|^2 , \tag{2.7}$$

$$\vec{j}_0(\vec{r},\omega) = \int e^{i\omega t}\,\vec{j}_0(\vec{r},t)\,dt = Q\int e^{i\omega t}\,\vec{v}(t)\delta(\vec{r}-\vec{r}(t))\,dt , \tag{2.8}$$

where Q is the charge of a particle, $\vec{v}(t)$ and $\vec{r}(t)$ are the velocity and the trajectory of the particle at the moment t. By introducing Eq.(2.8) into (2.7) we derive

$$dN^{s}_{\vec{n},\omega} = \frac{\omega Q^2}{4\pi^2 c^3}\left|\int \vec{E}^{s(-)*}_{\vec{k}}(\vec{r}(t),\omega)\,\vec{v}(t)e^{i\omega t}dt\right|^2 . \tag{2.9}$$

The integration in (2.9) is carried out over the whole interval of the particle motion.

It should be noted that the application of the solution of homogeneous Maxwell's equation, instead of inhomogeneous one, essentially simplifies the analysis of the radiation problem.

§2. Parametric X-Ray (Quasi-Cerenkov) Radiation (PXR).

The Theoretical Description.

The problem of radiation by a charged particle uniformly moving through a space-periodic medium has a long history [1,5]. While analyzing the optical radiation inside the complex medium consisting of a set of plates with different dielectric constants, Fainberg and Hizhnayk [39] showed that, besides the well-known Vavilov-Cerenkov radiation caused by the difference of medium dielectric constant from the unity, it is possible the other mechanism of radiation. It appears when the radiation wave length is comparable with the dimensional period of the medium and is a result of the change of a photon state in the medium. The considered mechanism of radiation was called the parametric Vavilov-Cerenkov radiation.

The problem of the radiation by a particle uniformly moving through the three-dimensional periodic medium was considered by Ter-Mikaelian in the frame of the perturbation theory [1]. It

was showed that, under the definite interference (resonance) conditions, the "resonance" radiation appeared. One of the main features of this radiation [1] is that the energy of emitted photons depends on the particle energy and increases with increasing the later one.

In 1971 Baryshevsky [15] showed that the refraction and diffraction of emitted photons in the thick crystals led to new, in comparison with an amorphous medium, effects, manifesting themselves in induced Cerenkov, transition and bremsstralung radiations by relativistic particles. The effects of anomalous transition and dynamical diffraction essentially modify the cross-section of electromagnetic processes in crystals.

In [6] Baryshevsky and Feranchuk solved the problem of X-ray radiation by charged particles uniformly moving through a crystal not using the perturbation theory relative to the interaction of emitted photon with the medium. The expressions for the radiation field amplitudes were obtained and the physical reason of the new mechanism of radiation was analyzed. It was shown that, in a such process, photons can be emitted even at large angle θ relative to the particle velocity (for example, $\theta \geq \pi/2 >> 1/\gamma$). This circumstance was suggested to be applied for experimental observation of this radiation. It should be noted that in [16] the integral radiation intensity was overestimated. The correct estimation was given in [16'] and in [34-36]. The comprehensive analysis of X-ray radiation, formed by a particle uniformly moving through a crystal [34-37], allowed to conclude that this radiation had the same physical reason as Vavilov-Cerenkov radiation. By the analogy of optical radiation, considered in [33], this new mechanism of X-ray radiation was called parametric X-ray radiation (PXR). The differential and integral intensity of PXR were derived in [34-37] in the frame both the classical and quantum theories, in the case of two-beam dynamical diffraction. It was shown that there were effects manifesting themselves only in thick crystals and, consequently, cannot be considered by the help of the perturbation theory.

It should be noted that the analysis of the formulae, obtained in [1], shows the presence of interference maxima in the angular distribution of radiation. The angles between the wave vectors of photons, emitted in the direction of diffraction maxima and the particle motion direction can be much more than the angle $\theta \sim 1/\gamma$ being characteristic for the radiation in the amorphous medium.

The presence of such diffraction maxima is the main difference of the radiation by the charged particle in crystals from the radiation in the amorphous medium. However, the results, obtained in [1], do not describe just parametric X-ray (quasi-Cerenkov) radiation, as they are correct only for rather thin crystals, when the photon refraction can be ignored. As a consequence, the formulae from [1] do not give the maximum in the X-ray radiation spectrum in the direction of the particle motion.

The X-ray radiation produced by the particle, moving with constant velocity through a crystal, was also considered by Garibian and Yang C. In their first papers they called this radiation "dynamical" radiation and then, in the book [4], as quasi-Cerenkov radiation. It is necessary to point out that in paper [20], published simultaneously with [16], the results were obtained in the frame of the perturbation theory for the thin crystal and practically coincided with the results by Ter-Mikaelian and did not describe parametric radiation. In [21] the formulae for the differential PXR intensity were derived and the qualitative analysis was made. The analysis of radiation in detail and numerical calculation of the integral intensity into the diffraction peak was performed in [38-41]. The theory of PXR taking into account the multiple scattering of particles by a crystal was derived in [42-46]. The results, obtained by different authors in [47-51], coincide, in general, with the results given in [34-37] and [4,38-41]. In [51] the analytical expressions for the integral PXR intensity in the perfect and imperfect crystals were obtained. The possibility of the effective application of PXR for the solution of different tasks was considered in [52-54]. In [55] the comparative analysis of contributions from the different mechanisms of radiation to the total intensity of X-ray radiation generated by a particle moving through a crystal target was made.

Let us follow below the theoretical consideration of PXR derived in [34-37, 42-46, 56].

According to (2.9), for the calculation of the differential number of emitted photons we need know the solution $\vec{E}^{s(-)}_{\vec{k}}(\vec{r},\omega)$ which was given, for example, in [2,17] for an arbitrary geometry of two-beam diffraction (Bragg and Laue, see Fig. 3). For example, in the Laue case, the photon wave function can be written in the following form [2] (here the system $\hbar = c = 1$ is used):

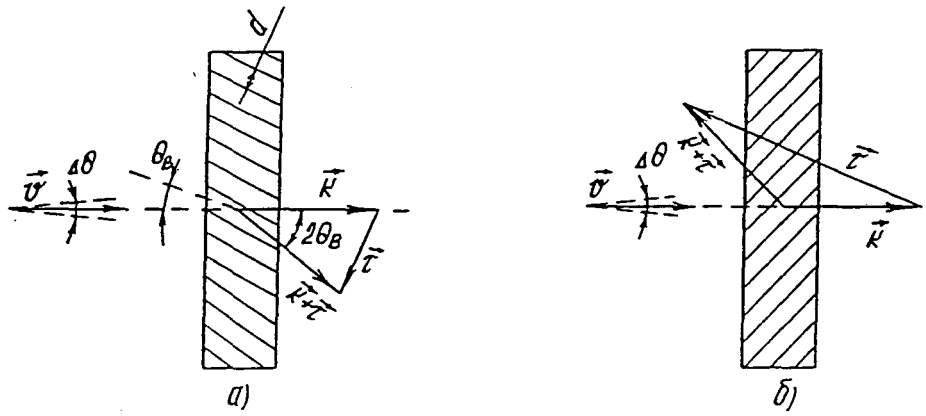

Fig. 3

$$\vec{E}^{(-)}_{\vec{k}_s}(\vec{r},\omega) = \left\{\vec{e}_s e^{i\vec{k}\vec{r}}\left[-\zeta^{\circ *}_{1s} e^{-\frac{\omega}{\gamma_0}\delta^*_{1s}L} - \zeta^{\circ *}_{2s} e^{-\frac{\omega}{\gamma_0}\delta^*_{2s}L}\right] + \right.$$

$$+ \vec{e}_{1s} e^{i\vec{k}_\tau\vec{r}}\beta_1\left[\zeta^{\tau *}_{1s} e^{-i\frac{\omega}{\gamma_0}\delta^*_{1s}L} + \zeta^{\tau *}_{2s} e^{-i\frac{\omega}{\gamma_0}\delta^*_{2s}L}\right]\Big\}\theta(-z) +$$

$$+ \left\{\vec{e}_s e^{i\vec{k}\vec{r}}\left[-\zeta^{\circ}_{1s} e^{-i\frac{\omega}{\gamma_0}\delta^*_{1s}(L-z)} - \zeta^{\circ}_{2s} e^{-i\frac{\omega}{\gamma_0}\delta^*_{2s}(L-z)}\right] + \right. \qquad (2.10)$$

$$\left. + \vec{e}_{1s}\beta_1 e^{i\vec{k}_\tau\vec{r}}\left[\zeta^{\tau *}_{1s} e^{-i\frac{\omega}{\gamma_0}\delta^*_{1s}(L-z)} + \zeta^{\tau *}_{2s} e^{-i\frac{\omega}{\gamma_0}\delta^*_{2s}(L-z)}\right]\right\}\theta(z)\theta(L-z) + \vec{e}_s e^{i\vec{k}\vec{z} - ik_z L}\,\theta(z-L)\ .$$

The crystal target is assumed to be the plate parallel target with the surface perpendicular to the Z axis and with the length $0 \le Z \le L$.

$$\zeta^{\circ}_{1,2s} = \mp\frac{2\delta_{2,1s} - g_{00}}{2(\delta_{2s} - \delta_{1s})},\ \zeta^{\tau}_{1,2s} = \mp\frac{g^s_{01}}{2(\delta_{2s} - \delta_{1s})},$$

$$\delta_{1,2s} = \frac{1}{4}\left\{(g_{00} + \beta_1 g_{11} - \alpha\beta_1) \pm \left[(g_{00} + \beta g_{11} - \alpha\beta_1)^2 + \right.\right. \qquad (2.11)$$

$$\left.\left. + 4\beta_1(\alpha g_{00} - g_{00}g_{11} + g^s_{10}g^s_{01})\right]^{1/2}\right\}\ .$$

$\beta_1 = k_z/k_z + \tau_z$ is the diffraction asymmetry factor, α is the deviation from the exact Bragg condition, g^s_{ik} are the coefficients in a series expansion of the crystal dielectric susceptibility in terms of the reciprocal lattice vector. The crystal dielectric susceptibility is a periodic function relative to the location of the nuclei and atoms and directly connects with the amplitudes of the coherent elastic scattering of photons by electrons and nuclei of the crystal. For the central-symmetric crystal $g_{00} = g_{11} = g_0$, $g^s_{10} = g^s_\tau$, $g^s_{01} = g^{s*}_\tau$, $g^\sigma_\tau = g_\tau$, $g^\pi_\tau = g_\tau \cos\left(\vec{k},\vec{k}_\tau\right)$.

By substituting (2.10) into (2.7) and integrating over the whole particle way, we can obtain the following expression for the differential number of photons emitted within the spectral interval $d\omega$ and into the solid angle $d\Omega$ along the particle velocity direction:

$$\frac{d^2N_s^{(0)}}{d_\omega d\Omega} = \frac{Q^2(\vec{e}_s\vec{u})^2\omega}{\pi^2}\left|\sum_\mu \frac{(2\delta_{\mu s}-g_{01})}{(2\delta_{2s}-\delta_{1s})}\left(L_0^{(0)}-L_{\mu s}^{(0)}\right)e^{i\frac{L}{L_{\mu s}^0}}-1)\right|^2 , \tag{2.12}$$

Besides, the radiation is formed in the direction of diffraction, determined by the vector $\omega_B^\tau \vec{u} + \vec{\tau}$, where ω_B is the Bragg frequency, corresponding to the requirement $\alpha = 0$, $\beta = u/c$. The expression for the number of photons emitted in this diffraction direction has the form:

$$\frac{d^2N_s^\tau}{d\omega d\Omega} = \frac{Q^2\beta_1^2(\vec{e}_{1s}\vec{u})^2\omega}{\pi^2}\left|\sum_\mu \frac{(-1)^\mu g_\tau^s}{2(\delta_{2s}-\delta_{1s})}\left(L_0^{(\tau)}-L_{\mu s}^{(\tau)}\right)\left(e^{i\frac{L}{L_{\mu s}^{(\tau)}}}-1\right)\right|^2 , \tag{2.13}$$

where $L_{\mu s}^{0(\nu)}$ and $L_0^{(\nu)}$ are the coherent lengths of PXR in the medium and in the vacuum, correspondingly.

$$L_{\mu s}^{(\nu)} = \frac{1}{q_{\mu s}^{(\nu)}} = \frac{2}{\omega}\left(\frac{m^2}{E^2} + \theta_\nu^2 - 2\delta_{\mu s}\right)^{-1} ,$$

$$L_0^{(\nu)} = \frac{2}{\omega}\left(\frac{m^2}{E^2} + \theta_\nu^2\right)^{-1} , \nu = 0,\tau . \tag{2.14}$$

Here $q_{\mu s}^{(\nu)} = p_z - p_{1z} - k_z^{\nu}\left(1 + \delta_{\mu s}\right)$ is the longitudinal momentum transmitted to the medium, $\vec{p}$ and $\vec{p}_1$ are the initial and final momentums of the particle, θ_ν is the radiation angle of the photon $\theta_0 = \vec{k}\hat{}\vec{u}$ and $\theta_\tau = \vec{k}\hat{}\omega_B\vec{u} + \vec{\tau}$.

According to (2.14), contrary to the amorphous medium where there is only one coherent radiation length, we now have, in general, four coherent lengths for each direction of the emission. s = 1,2 correspond to two different polarization states of emitted photons, and μ = 1,2 label two different stationary superpositions of electromagnetic waves appearing inside the crystal under the interference of the incident and the diffracted waves.

By analyzing (2.12) and (2.13), we can see that the output of radiation is maximum if the real part of the longitudinal momentum transmitted to the medium $R_e\, q_{\mu s}^{\nu}$ becomes zero. In this case the coherent length of radiation becomes equal to the photon absorption length. The dispersion equation $R_e q_{\mu s} = 0$ determining the condition of PXR formation, is the analogy of the Vavilov-Cerenkov condition in the crystal.

$$\cos\theta_\nu = \frac{1}{\beta} - 2\mathrm{Re}\delta_{\mu s}^{(\nu)} \tag{2.15}$$

In the case of rather thick crystals when it is possible the application of δ-function in the expressions (2.12), (2.13) (see [2]), the analytical expressions for the angular and spectral distributions of PXR in the diffraction peak can be easily obtained.

It is very convenient to choose a new coordinate system for each diffraction reflex. In this case, the Z axis is directed along the vector $\vec{n}_B = \frac{\omega_B\vec{u}+\vec{\tau}}{k_B}$ ($k_B = \omega_B/c$), the X-axis is placed on the plane of the vectors $\vec{u}$ and $\vec{\tau}$, and the Y-axis is perpendicular to this plane (see Fig.4).

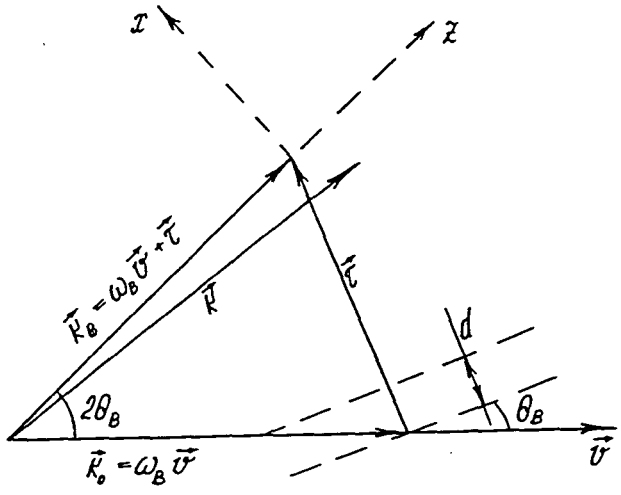

Fig. 4.

In this coordinate system the photon wave vector $\vec{k}$ is always directed at a small angle relative to the vector $\vec{n}$B. Taking into account the smallness of this angle θ_v and integrating the Eq.(2.13) over the frequencies we obtain the angular distribution of PXR into a diffraction peak as follows:

$$\frac{d^2N}{d\theta_x d\theta_y} = \sum_{n=1}^{\infty} \frac{Q^2}{4\pi} \omega_B^{(n)} L_a\left(\omega_B^n\right)\left(1 - e^{-\frac{L}{L_a^n}}\right)\frac{\left|g_\tau\left(\omega_B^n\right)\right|^2}{\sin^2\theta_B} \cdot \frac{\left(\theta_x^2 \cos^2 2\theta_B + \theta_y^2\right)}{\left(\theta_x^2 + \theta_y^2 + \theta_{ef}^2\right)^2}, \tag{2.16}$$

where the angles $\theta_{x,y}$ are determined in the following way

$$\theta_{x,y} = \frac{\left(\vec{k} - \vec{k}_B\right)_{x,y} c}{\omega_B},$$

$L_a(\omega_B) = \left(\omega_B^n g_0''\right)^{-1}$ is the absorption length of photon with the frequency of ω_B. The summation is made over all harmonics of PXR radiated in this direction and

$$\theta_{ef}^2 = \gamma^{-2} + |g_0'(\omega_B)| + \overline{\theta_s^2}\,, \qquad (2.17)$$

determines the characteristic angular divergence of photons in a given diffraction direction, $g_0' \equiv \mathrm{Re}\,g_0'$, $\overline{\theta_s^2}$ is the mean square angle of multiple scattering of the photon by a crystal, $\gamma = m/E$, m is the mass of the radiating particle. It should be noted that the spectral-angular and polarization characteristics of PXR, taking into account the multiple scattering of particles by atoms of the crystal, was derived in detail in [45]. The comparison of the formulae from [45] with the expression (2.16), where the multiple scattering is taken into account by introducing the quality $\overline{\theta_s^2}$, shows that such a phenomenological way of the multiple scattering account gives a good result and allows to describe the experimental results with high accuracy. Besides, as the magnitude of $g_\tau \sim 1/\omega^2$, then the contributions of different harmonics to the total radiation intensity is proportional to $\sim 1/n^3$ (n is the number of reflections) and, as a consequence, the intensity of PXR is determined, in general, by the first harmonic contribution.

Taking into account only the first radiation harmonic let us represent the spectral-angular distribution of radiation in a nondimensional form with the help of the normalized angular coordinates and the normalized radiation amplitude, which are

$$J(x,y) = \frac{1}{N_0}\frac{d^2N}{d_x d_y}\,, \qquad x,y = \frac{\theta_{x,y}}{\theta_{ef}}\,, \qquad (2.18)$$

where N_0 is the total number of emitted photons. As a result, the angular distribution of photons within a diffraction peak is represented by a universal function depending only on the Bragg angle value but not on the parameters of the elementary cell of a given crystal.

$$J(x,y) = \frac{x^2\cos^2 2\theta_B + y^2}{(x^2 + y^2 + 1)}\,. \qquad (2.19)$$

In Fig.5 the two-dimensional angular distribution J(x,y) and the lines of equal intensity are shown for $\theta_B = 25°$. As you can see in Fig.5, the main peculiarity of the angular PXR distribution is the

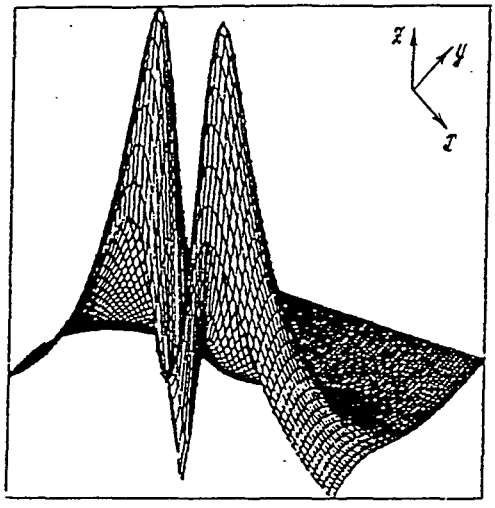

Fig. 5

zero intensity of the radiation in the direction of the vector $\vec{k}_B$. This fact totally corresponds to the angular distribution of the ordinary Vavilov-Cerenkov radiation in the amorphous medium. According to Fig.5, the PXR angular distribution has two separate peaks and is polarized along the Y-axis.

The multiple scattering leads to the appearance of bremsstralung, which can be diffracted by the same set of crystallographic planes and, consequently, gives the contribution of diffraction bremsstralung (DB) to the angular distribution of radiation being observed in the experiment. As a result, the fine structure of PXR spectrum is smoothed, especially in the case of light charged particles and the intensity of radiation at $\theta_{x,y} \to 0$ is nonzero. As in the experimental situation the total intensity of radiation (PXR+DB) is measured, let us give the analytical expression for the one-dimensional angular distribution of the total radiation emitted into a diffraction peak:

$$J(\theta_x) = \frac{1}{N_0}\frac{\partial N}{\partial \theta_y} = \frac{(1+\cos^2 2\theta_B)\left(\theta_y^2 + \frac{1}{2}\overline{\theta_s^2}\right) + \theta_{ef}^2 \cos^2 2\theta_B}{\left(\theta_y^2 + \theta_{ef}^2\right)^{3/2}} \,. \qquad (2.20)$$

There are two maxima in this case and the angular distance between them is determined by

$$\Delta\theta_y = 2\sqrt{2}\left(1+\cos^2 2\theta_B\right)^{-1/2}\left[\left(1-\frac{1}{2}\cos^2 2\theta_B\right)\theta_{ef}^2-\frac{3}{4}\left(1+\cos^2 2\theta_B\right)\overline{\theta_s^2}\right]^{1/2} \quad (2.21)$$

The depth of the gap in the angular distribution depends on the relationship between the radiation angle θ and the mean square angle of multiple scattering $\sqrt{\theta_s^2}$ and for J(y) is given by the relation:

$$\left(\frac{J_{min}}{J_{max}}\right)_y = \frac{1}{\theta_{ef}^2}\left[\theta_{ef}^2\cos^2 2\theta_B+\frac{1}{2}\left(1+\cos^2 2\theta_B\right)\overline{\theta_s^2}\right]\cdot$$

$$\cdot\frac{\left[3\theta_{ef}^2-\frac{3}{2}\left(1+\cos^2 2\theta_B\right)\overline{\theta_s^2}\right]^{3/2}}{\left[2\theta_{ef}^2-\left(1+\cos^2 2\theta_B\right)\overline{\theta_s^2}\right]\left(1+\cos^2 2\theta_B\right)^{3/2}}\cdot \quad (2.22)$$

The angular distribution relative to the variable X is

$$J(\theta_x)=\frac{1}{N_0}\frac{\partial N}{\partial\theta_x}=\frac{\left(1+\cos^2 2\theta_B\right)\left(\theta_x^2+\frac{1}{2}\overline{\theta_s^2}\right)+\theta_{ef}^2}{\left(\theta_x^2+\theta_{ef}^2\right)^{3/2}} \quad (2.23)$$

and the split of the angular peak, pointed above, takes place only if

$$\cos 2\theta_B > \frac{\theta_{ef}^2+\frac{3}{2}\overline{\theta_s^2}}{2\left(\theta_{ef}^2-\frac{3}{4}\overline{\theta_s^2}\right)},$$

and the magnitude of this split is determined by

$$\Delta\theta_x = 2\sqrt{2}\left(1+\cos^2 2\theta_B\right)^{-1/2}\left[\left(\cos^2 2\theta_B-\frac{1}{2}\right)\theta_{ef}^2-\frac{3}{4}\left(1+\cos^2 2\theta_{ef}\right)\overline{\theta_s^2}\right]^{1/2} \quad (2.24)$$

In Fig.6 the angular distributions $J(\theta_y)$ (a) and $J(\theta_x)$ (b) are represented at $\theta_B = 45°$ and $\overline{\theta_s^2}/\theta_{ef}^2 = 0.5$. The relative contributions of two mechanisms of radiation (PXR and DB) are shown.

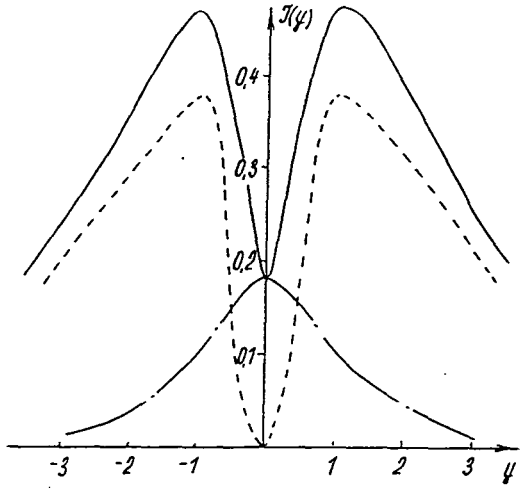

Fig. 6(a)

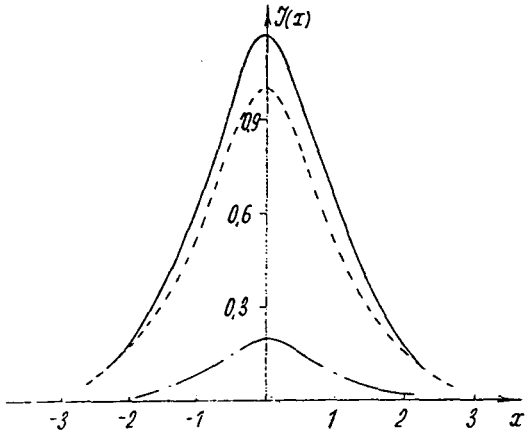

Fig. 6(b)

The angular distribution relative to the azimuthal angle ($\theta_x = \theta \cos\varphi$, $\theta_y = \theta\sin\varphi$) is represented as:

$$J(\varphi) = \frac{1}{N_0}\frac{\partial N}{\partial \varphi} = \frac{1}{\pi}\left[\left(\cos^2\varphi\,\cos^2 2\theta_B + \sin^2\varphi\right)\zeta_1(E,\theta_D) + \right.$$

$$\left. + \left(1 + \cos^2 2\theta_B\right)\zeta_2(E,\theta_D)\right], \tag{2.25}$$

where the functions $\zeta_1(E, \theta_D)$ and $\zeta_2(E, \theta_D)$ are determined by the particle beam characteristics and the conditions of photon detection

$$\zeta_1(E,\theta_D) = \ln\left(\frac{\theta_{ef}^2 + \theta_D^2}{\theta_{ef}^2}\right) - \frac{\theta_D^2}{\theta_D^2 + \theta_{ef}^2}\ln\left[\frac{\rho_D^2 + 1 + \frac{1}{x^2}\left(1 + \overline{\theta_s^2}\right)}{1 + \frac{1}{x^2}\left(1 + \overline{\theta_s^2}\right)}\right] -$$

$$- \rho_D^2\left(\rho_D^2 + 1 + \frac{1}{x^2}\left(1 + \overline{\theta_s^2}\right)\right)^{-1}, \tag{2.26}$$

$$\zeta_2(E,\theta_D) = \frac{\overline{\theta_s^2}\,\theta_D^2}{\theta_{ef}^2\left(\theta_D^2 + \theta_{ef}^2\right)} = \frac{\rho_D^2}{x^2}\overline{\theta_s^2}\left[1 + \frac{1}{x^2}\left(1 + \overline{\theta_s^2}\right)\right]\left[\rho_D^2 + 1 + \frac{1}{x^2}\left(1 + \overline{\theta_s^2}\right)\right]^{-1}, \tag{2.26'}$$

where $\rho_D = \frac{\theta_D}{\sqrt{|g_0'|}}$, $x = \frac{E}{m}\sqrt{|g_0'|}$, $\overline{\theta_s^2} = \frac{E_s^2}{E^2}\frac{L}{L_R}$, L_R is the radiation length, θ_D is the angular size of the detector. The special features of the angular distribution in the vicinity of the degeneration of the dispersion equation roots, being possible in the Bragg case of diffraction, were considered in [58,59]. In [58] it was first shown that the sharp maximum in the spectral-angular radiation density is possible in this case. This effect is the most prominent in the case of multi- wave dynamical diffraction. In [60] the spectral-angular and spectral distributions of PXR were analyzed in the specific case of diffraction - the back scattering geometry of diffraction. The numerical estimations, performed in this paper, showed that the integral intensity in the back reflection direction could exceed the integral PXR intensity in the other diffraction peaks.

By using the δ-function for the integration of (2.13) over the angles, it is possible to write the spectral distribution of the total radiation in the following nondimensional form:

$$J(u) = \frac{1}{N_1}\frac{\partial N}{\partial u} = \left[1 + \left(u^2 + \frac{\overline{\theta_s^2}}{2\theta_{ef}^2}\right)\left(1 + \cos^2 2\theta_B\right)\right](1 + u^2)^{3/2}, \qquad (2.27)$$

where $N_1 = \frac{\pi}{2} N_0$, $u = \frac{\omega - \omega_B}{\omega_B \theta_{ef}} \tan\theta_B$ is the normalized frequency.

The universal spectral distribution $J(u,\theta_B)$ for the different magnitudes of θ_B are represented in Fig.7.

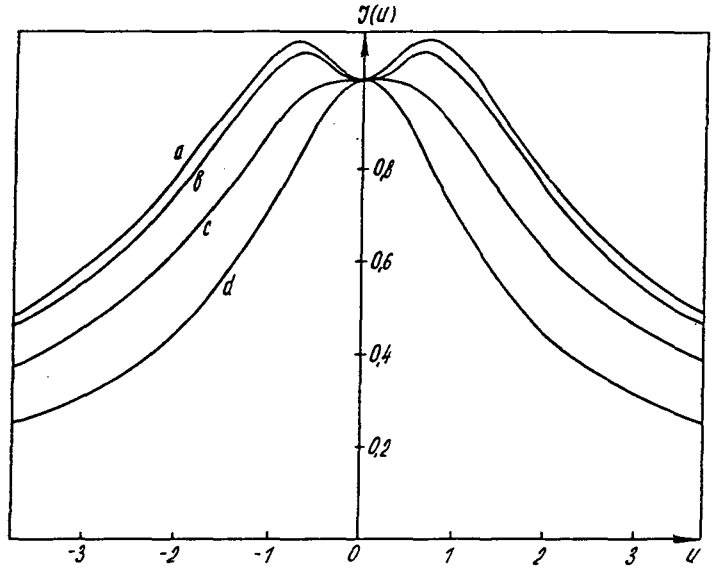

Fig. 7. Here: a) $\theta_B = 5°$; b) $\theta_B = 15°$; c) $\theta_B = 30°$; d) $\theta_B = 95°$.

According to (2.27), there is only a split in the spectral PXR distribution at small angles $\theta_B < \pi/8$. However, the experimental observation of this split is possible only in the case of small multiple scattering, because of

$$\Delta u = 2\sqrt{2}\,(1+\cos^2 2\theta_B)^{-1/2}\left[\cos 2\theta_B - \frac{1}{2} - \frac{3}{4}\frac{\overline{\theta_s^2}}{\theta_{ef}^2}(1+\cos^2 2\theta_B)\right]^{1/2} \qquad (2.28)$$

and tends to zero at $\theta_s \approx \theta_{ef}$. The total number of photons with the polarization $\vec{e}_s$, emitted in the diffraction direction $\omega_B^{(\tau)}\vec{u} + \vec{\tau}$ within the diffraction peak by a particle, is given by the following formula (Laue case):

$$N_s^{(\tau)} = \frac{Q^2}{8\sin^2\theta_B}\frac{\left|g_\tau^{(s)}(\omega_B)\right|^2}{\mathrm{Im} g_0(\omega_B)}\left|\ln\left[\left(\gamma^{-2} + \delta_s + g_0'\right)^2 + \left|g_\tau^s\right|^2 - \sigma_s^2\right]\right| \qquad (2.29)$$

where $g_0 = g_0' + ig_0''$, $\sigma_s = \dfrac{\mathrm{Re}\sqrt{g_\tau^s g_{-\tau}^s}\cdot \mathrm{Im}\sqrt{g_\tau^s g_{-\tau}^s}}{g_0''}$. By taking into account (2.19) and (2.23) the divergence of PXR quanta into a diffraction peak can be estimated of the order of magnitude as

$$\Delta\theta \cong \sqrt{\gamma^{-2} + \left|g_0'\right|}\,, \qquad (2.30)$$

and the frequency divergence as

$$\frac{\Delta\omega}{\omega_B} \cong \sqrt{\gamma^{-2} + \left|g_0'\right|}\,. \qquad (2.31)$$

In the experimental situation the measurement of the intensity is made by the detector with the angular size of θ_D. In this case, the integral number of photons emitted in a given reflex and experimentally recorded can be represented by the following expression:

$$N_{PXR} = \sum_{n=1}^{\infty}\frac{Q^2}{8}\frac{\omega_B^{(n)}}{\sin^2\theta_B}\left|g_\tau\left(\omega_B^{(n)}\right)\right|^2 L_a\left(\omega_B^{(n)}\right)\left(1 - e^{-\frac{L}{L_a}}\right),$$

$$\left(1+\cos^2 2\theta_B\right)\left[\ln\left(\frac{\theta_D^2 + \theta_{ef}^2}{\theta_{ef}^2}\right) - \frac{\theta_D^2}{\theta_D^2 + \theta_{ef}^2}\right], \qquad (2.32)$$

where the summation is derived over all harmonics of PXR, radiated in a given direction

$$\omega_B^{(n)} = \frac{\tau}{2\sin\theta_B} = \frac{\pi n}{d\sin\theta_B}, \quad n = 1,2,...$$

d is the interplanar spacing. As for the correct interpretation of the experimental results, it is necessary to take into account the diffraction bremsstralung (DB), especially for electrons, let us give the integral intensity of the radiation of DB in the reflex:

$$N_{DB} = \sum_{n=1}^{\infty} \frac{Q^2}{8} \frac{\omega_B^{(n)}}{\sin^2\theta_B} |g_\tau(\omega_B^{(n)})|^2 L_a(\omega_B^{(n)}) \left(1 - e^{-\frac{L}{L_a}}\right), \tag{2.33}$$

$$\left(1 + \cos^2 2\theta_B\right) \frac{\overline{\theta_s^2}\,\theta_D^2}{\left(\theta_D^2 + \theta_{ef}^2\right)\theta_{ef}^2} .$$

As we pointed out above, the main contribution to the radiation intensity is made by the first harmonic of radiation

$$N_0 = \frac{Q^2}{8} \frac{\omega_B}{\sin^2\theta_B} |g_\tau|^2 L_a \left(1 - e^{-\frac{L}{L_a}}\right)\left(1 + \cos^2 2\theta_B\right) . \tag{2.34}$$

So, the integral number of photons, recorded into a reflex, can be written as

$$N = N_0 \left[\zeta_1(E, \theta_D) + \zeta_2(E, \theta_D)\right], \tag{2.35}$$

where the functions ξ_1 and ξ_2 are defined by the expressions (2.26) and (2.26').

The obtained expressions describe the PXR radiation for the arbitrary reciprocal lattice vector. It means that the total angular PXR distribution is a set of peaks (reflexes) forming the diffraction pattern of this crystal, which is analogous to that appearing under the scattering of external X-ray beam with the angular divergence of $\Delta\theta \sim 1/\gamma$ by the same crystal. In Fig.8 the diffraction pattern, containing the most intensive PXR reflexes, are shown for the different

directions of the particle incidence on a crystal. The magnitudes of the angles θ_B and the frequencies ω_B, corresponding to these reflexes, are given in Table I. The integral number of photons emitted in a given reflex (see Ex.(2.35)) depends on the particle incidence direction, on the lattice parameters and on the functions ξ_1 and ξ_2. At the same time, the fine structure both the angular and spectral distributions of emitted photons also depends on the parameters of the particle beam and crystal. It is interesting to investigate the functions ξ_1 and ξ_2 in the Ex.(2.35) as they determine the radiation intensity as a function of the particle energy.

It is well-known [10], that Vavilov-Cerenkov radiation is distinguished from the other mechanisms of radiation by its dependence on the radiating particle energy. If the refractive index of the medium n does not depend on the wave vector $\vec{k}$ and the frequency of the emitted photon ω, then Vavilov-Cerenkov radiation is possible only if the speed of the charged particle satisfies the condition

$$1 - u\, n \cos\theta = 0 \qquad (2.36)$$

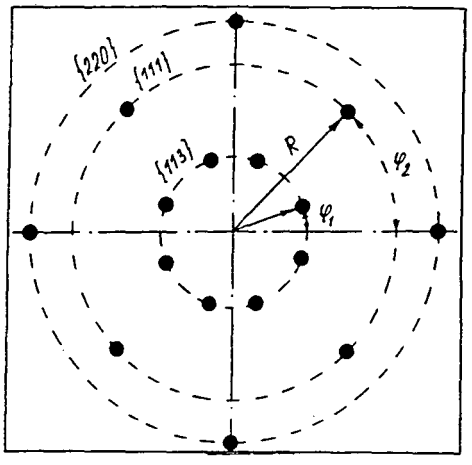

Fig. 8

Table I.

crystal	{hkℓ}	θ_B	ω_B (KeV)
Si			12.60
Ge	{113}	17.55°	12.19
C			19.14
Si			3.44
Ge	{111}	35.02°	3.30
C			5.22
Si			4.58
Ge	{220}	45°	4.39
C			6.96

From (2.36) it follows the inequality determining the threshold energy of the particle E_o, that is

$$E > E_o = \frac{m}{\sqrt{2(n-1)}} \cdot$$

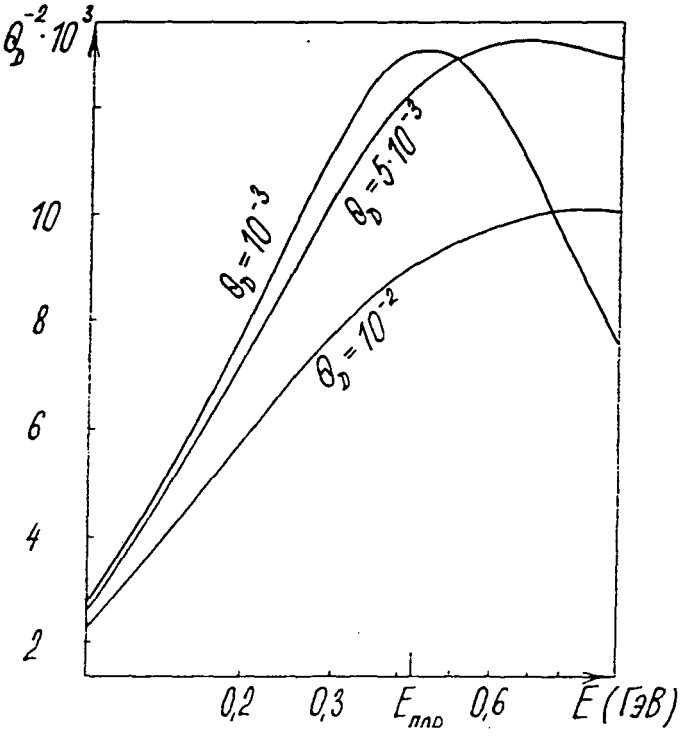

Fig. 9

In the crystal, where there is a strong dimensional dispersion of the refractive index n ($\vec{k}$,ω), the dependence of the PXR intensity on the particle energy essentially changes [37] (see Fig.9). The condition (2.36) is replaced in the crystal by the requirement of the zero value of the real part of the longitudinal momentum transmitted to the medium (see Ex.(2.15)). It can be written in the form

$$\gamma^{-2} + \theta^2 - 2\delta_{\mu s} = 0 \ . \tag{2.37}$$

This equation has a formal solution

$$\theta^2 = -\gamma^{-2} + 2\,\delta_{\mu s} \tag{2.38}$$

for any particle energies. That is why the PXR intensity has not the sharp threshold dependence. However, the deviation from the exact Bragg condition, determined by (2.38), increases with decreasing the particle energy and at the energies

$$E < E_{th} = \sqrt{\frac{m^2 + E_s^2 \frac{L}{Lr}}{\left|g_0'\right| - \Delta_s}} \quad \Delta_s = \frac{Im\sqrt{g_\tau^s g_{-\tau}^s}}{2g_0''}, \tag{2.39}$$

becomes more than $\left|g_0'\right|$. It means that the diffraction wave amplitude, determining the spectral intensity of PXR, falls down according to the law

$$E_\tau \sim \frac{1}{\alpha}\left(\frac{E_{th}}{E}\right)^2 \tag{2.40}$$

The analysis of the function ξ_1 (E) (2.26), determining the energy dependence of the total PXR intensity, shows that the number of photons recorded by the detector at $E << E_{th}$ is estimated as

$$N_D \cong \frac{\pi}{4} N_0 \left(\frac{\theta_D}{\theta_{ef}}\right)^4 = \left(\frac{E}{E_{th}}\right)^4 N_{max} , \qquad (2.41)$$

where N_{max} is the number of photons with the frequency ω_B generated by the particle with the energy $E = E_{th}$. The threshold character of the PXR intensity as a function of the particle energy can be manifest itself stronger if the detector has the high angular resolution $\theta_D << \theta_{ef}$. In this case, the emitted photons will be almost monochromatic$\Delta\omega/\omega_B \sim \theta_D$, i.e. such a detector will record only photons with a definite wave vector $\vec{k}_D$ and the frequency ω_D. As a result, the magnitude of the refractive index will be exactly determined and the condition (2.37) is fulfilled only for the energy

$$E > E_{th}^D = \frac{m}{\sqrt{2n\left(\bar{k}_D, \omega_D\right) - 1}} . \qquad (2.42)$$

In the experimental situation the total intensity of PXR and DB is measured, but the energy dependence of the later one is determined by the function ξ_2 (E) (see Ex.(2.26')). The function ξ_2 contains the term proportional to $\overline{\theta_s^2}$, that is why the function ξ_2 also decreases with decreasing the particle energy as a function of E^{-2}. As a result, the intensity of DB, for the energy E less than a definite energy value E^D, determining on the angular size of the detector and the type of a crystal, can become even more than the intensity of PXR. In this case the total intensity of radiation in a definite reflex has a complicated dependence on the particle energy (see Fig.9). The experimental investigation of this curve is interesting for the correct understanding the process of PXR formation. The interesting feature of PXR is that its integral intensity is not saturated even when the angular size of the detector θ_D is much more than the radiation angle.

According to the formulae, obtained above, both the total PXR intensity and the angular and spectral distributions depend on the particle energy only through the Lorentz factor γ. Consequently, at a definite energy, E,the PXR characteristics are strongly differentiated for various kinds of charged particles. In Table II you can see the magnitudes on the total numbers of photons

Table II

elements	(h,ℓ,k)	keV	grad	electrons		protons		$m^{\pm}$ - mezons		$p^{\pm}$ - mezons	
				$N_D \times 10^3$	$N_D \times 10^3$	$N_D \times 10^6$	$N_D \times 10^6$	$N_D \times 10^4$	$N_D \times 10^4$	$N_D \times 10^4$	$N_D \times 10^4$
		ω_B	θ_B	E = 40 geV	E = 70 geV	E = 40 geV	E = 70 geV	E = 40 geV	E = 70 geV	E = 40 geV	E = 70 geV
	III	200	0.57	I.99	2.20	3.99	25.67	2.58	4.04	1.84	3.3
Si	II3	200	I.08	0.30	0.34	0.61	3.91	0.21	0.33	0.16	0.27
	III	300	0.37	1.39	1.52	2.65	17.10	1.71	2.7	1.27	2.2

emitted in a diffraction peak at $\theta_D \sim 1/\gamma$ by the following particles $e^{\pm}$, p, $\mu^{\pm}$, $\pi^{\pm}$ in Si crystal with the length 1 cm.

It should be noted that parametric X-ray (quasi-Cerenkov) radiation is the main mechanism of radiation in the X-ray range for heavy charged particles due to the smallness of their bremsstralung. The estimations show that the ratio for electron is $N_{DB}/N_{PXR} \sim 10^{-1} - 1$. At the same time, the intensity of the diffraction bremsstralung of protons and $\pi^{\pm}$ at the energy of E = 70 geV are $\sim 10^{-9}$ - 10^{-11} γ/p and $\sim 10^{-6}$ - 10^{-7} $\gamma/\pi^{\pm}$, correspondingly, that is much less than the PXR intensity. The difference increases with increasing the radiating particle energy.

In Figs.10 and 11 the angular and spectral distributions of the total intensity of PXR and DB are shown for different kinds of particles (e, p, π). According to Figs.10 and 11 the dependence of the angular distribution on the factor γ is stronger than the same dependence of spectral distribution. It means that the investigation of the PXR angular intensity curve can provide the information of the composition of the beam, containing the different particles with close energies. Possessing the high spectral and angular density and strongly depending on the factor γ, the parametric X-ray radiation, generated by heavy particles, can be applied for the measurement of the particle energy in the region of the superhigh energies and also for the analysis of the particle beam composition.

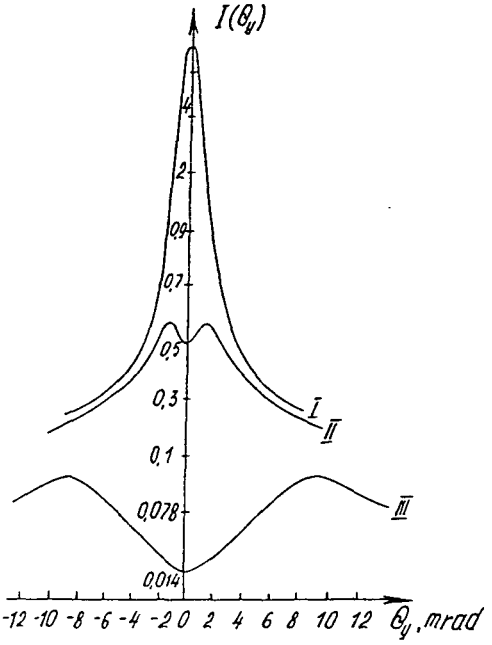

Fig. 10. Here: E = 70 GeV, ω_B = 200 keV; (111) plane in Si; I - e^-; II - p; III - $\pi^{\pm}$

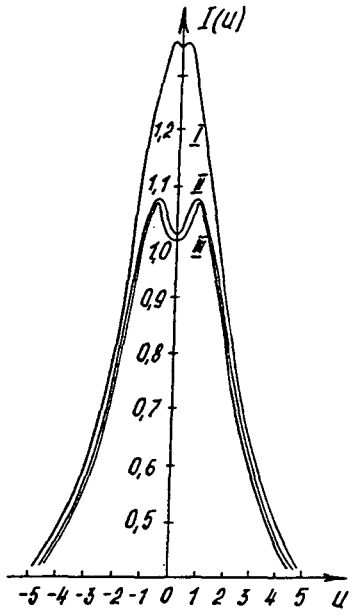

Fig. 11. Here: E = 70 GeV, ω_B = 200 keV; plane (111) in Si; I - e^-; II - p; III - $\pi^{\pm}$

In the conclusion of the theoretical consideration of the main PXR characteristics, we should like to stress that, in our opinion, the main application of PXR connects with the production of X-ray collimated monochromatic beam with continuously turned frequency. The investigation of PXR gives the possibility to analyze the crystal structure, because of the PXR spectrum consists of a set of diffraction reflexes, which contain the information about the structural amplitudes of a crystal [52]. The spectral PXR intensity in a reflex exceeds the analogous magnitude for the synchrotron radiation and allows to obtain the diffraction pattern of high resolution by using the electron beams with moderate energy [52,53]. In [54] it was considered the application of PXR in the X_ray structural analysis for finding the phases of the crystal structural amplitudes just from the measurement of the PXR intensity in reflexes. In was shown that this method can be more effective than the well-known methods, because of the possibility to reduce the time of experimental measurements. It also do not require the strong restriction of the crystal quality.

§3. Experimental Investigation of Parametric (Quasi-Cerenkov) Radiation by Electrons (Positrons).

In spite of comprehensive theoretical description of PXR mechanism formation and its main features, this radiation was experimentally confirmed only several years ago [23-26]. The first experiment in observation of "dynamical maxima" in X-ray spectrum radiated by a relativistic electron beam in a periodic medium was conducted in [61]. But no modifications of radiation intensity under the variation of crystal orientation relative to the electron velocity has been experimentally observed. The analysis of [61] shows that the procedure of this experiment was incorrect and PXR could not be observed during this experiment. The thing is that the intensity of X-ray radiation in [61] was measured within the frequency interval $\Delta\omega \sim \omega$ in the direction of particle velocity. In this case the PXR integral intensity is approximately by the order of magnitude less than the intensity of the ordinary transition radiation, not connected with crystal structure. Just this circumstance has led to negative results of the experiment [61]. Parametric X-ray radiation was first observed in experiments conducted by the collaboration of Institute of Nuclear Problems (Minsk) and Institute of Nuclear Physics (Tomsk) in Tomsk synchrotron "Sirius" [23-26]. It was used the possibility of formation of PXR reflexes (maxima) at a large angle relative particle velocity [16] and, that was important, that the positions of these reflexes did not depend on the energy of radiating particles and was determined only by relative orientation of a particle velocity and crystallographic planes.

$$\omega_\tau^{(n)} = \frac{\tau}{2\sin\theta_0} = \frac{\pi n}{d\sin\theta_0}, \quad n = 1,2\ldots \tag{2.43}$$

where d is the interplanar spacing, θ_0 is the angle of particle incidence relative to the crystallographic planes, corresponding to $\vec{\tau}$, $\vec{\tau}$ is the reciprocal lattice vector of a crystal. The diamond single crystal with the size of 10 x 6 x 35 mm (the axis < 110 > was almost perpendicular

to a large face of diamond) and was fixed in a two-axis goniometer. The electron beam angular spread was 0.1mrad, chromaticity was about 0.5%, the electron energy was E ~ 900meV. The beam pulse duration was τ = 15ms. The measurement of the spectral and angular characteristics of the X-ray radiation was made by a NaI(Tl) scintillator spectrometer with a crystal thickness of about 1mm and a beryllium entrance window. The energy resolution was $\frac{\Delta\omega}{\omega}$ = 35% at ω = 14 keV and $\frac{\Delta\omega}{\omega}$ = 25% at ω = 34 keV. The spectrometer was placed at the angle of $\theta = \pi/2$ relative to the incidence electron momentum on the plane being perpendicular to the vertical goniometer axis at the distance of 1m from the crystal. The size of entrance window of a collimator corresponded to the angular divergence of $\Delta\theta = \pm 3 \cdot 10^{-3}$ rad. The geometry of this experiment [23] is shown in Fig.12. In the case of particle motion along the axis < 110 >, the crystallographic planes (100) are at the angle $\theta_B = 45°$ relative to the particle velocity, and the diffracted radiation (PXR reflex) was observed in the direction perpendicular to the incident particle momentum. The crystallographic axis of the target was aligned with the electron beam direction by using the channeling radiation by the electron beam. In Fig. 13, 14 the PXR spectrum, measured in experiments [24,25], can be seen. In accordance with the theoretical predictions the radiation spectrum has a line structure. You can see in Fig.13 [25] two maxima in a spectral distribution

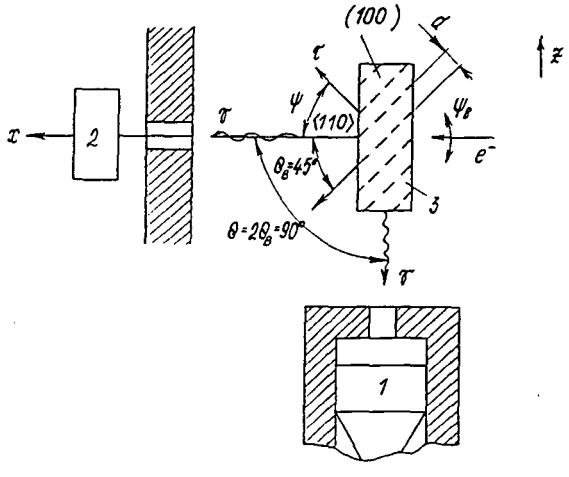

Fig. 12. Here: 1 - x-ray spectrometer; 2-quantometer: 3-diamond crystal.

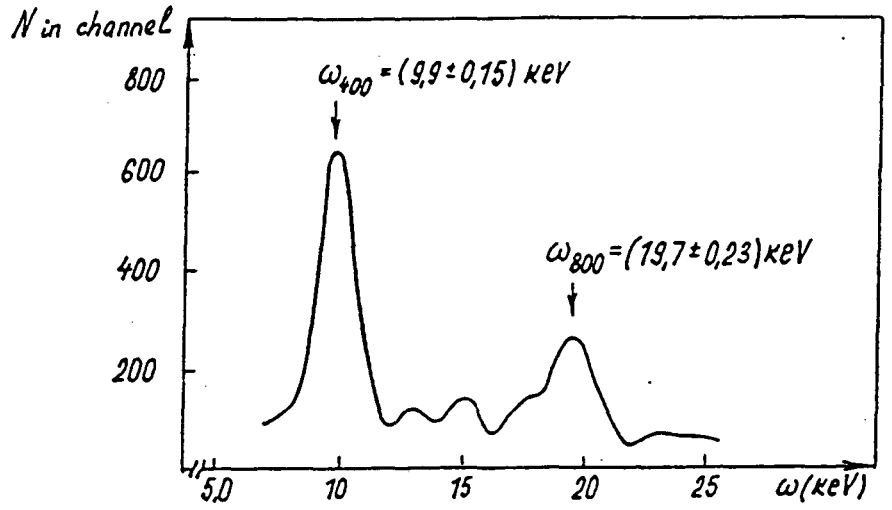

Fig. 13

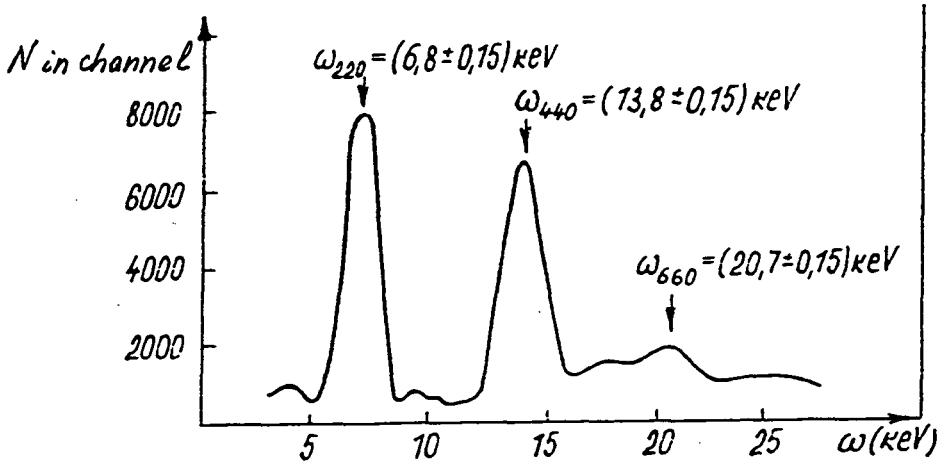

Fig. 14

with energies ω^{ex}_{400} = 9.9 ± 0.15keV and ω^{ex}_{800} = 19.7 ± 0.15 keV, which correspond to the reflections by a set of planes (110) and coincide very well with theoretical magnitudes ω^{th}_{400} = 9.85 keV and ω^{th}_{800} = 19.7keV, correspondingly. In Fig.14 the experimental results, obtained in [24], are shown. In this case the reflection planes were (100). You can see three maxima in a spectral distribution, whose positions coincide with theoretical prediction with a good accuracy:

$\omega_{220}^{th} = 6.99$ keV, $\omega_{440}^{th} = 19.9$ keV and $\omega_{660}^{th} = 20.9$ keV. During these experiments the total yield of the γ-radiation per electron in a diffraction peak was measured: for the peak (440) – $N_\gamma = (6 \pm 3)\cdot 10^{-7}$ γ/e^-, in the peak (660) - $N_\gamma = (0.7 \pm 0.4)\cdot 10^{-7}$ γ/e^-. It should be said that all these first experiments were carried out in the geometry, which corresponds, in dynamical diffraction theory, to the anomalous case of transition between the Laue and Bragg diffraction geometries and calls as asymmetric diffraction case [63]. In this case the general formulae, obtained in § 2, cannot be applied. For the correct interpretation of experimental results, the theory of PXR in the case of the asymmetric diffraction was derived in [43,44]. The specific feature of asymmetric diffraction is that, in this case, it is necessary to take into account the terms of dispersion equation quadratic in α and, making the matching of solutions of Maxwell's equation on the crystal boundaries, we can not neglect the waves reflected by the crystal surface and propagating along the crystal surface in vacuum. In [43,44] the spectral and angular distributions of PXR were obtained. The total number of photons radiated in a diffraction peak can be represented in the following form:

$$N_d^{(n)} = \frac{Q^2}{4} \left|g_\tau\left(\omega_B^{(n)}\right)\right|^2 \frac{L}{a\, g_0''} \left(1 - e^{-\omega_B^{(n)} g_0'' a}\right) x$$

$$x \left\{ \ln\left(\frac{\theta_D^2 + \theta_{ef}^2}{\theta_{ef}^2}\right) - \frac{\theta_D^2}{\theta_D^2 + \theta_{ef}^2} + \frac{\overline{\theta_s^2}\,\theta_D^2}{\left(\theta_D^2 + \theta_{ef}^2\right)\theta_{ef}^2} \right\}, \qquad (2.44)$$

$$\theta_{ef}^2 = \gamma^2 + \left|g_0'\left(\omega_B^{(n)}\right)\right| + \overline{\theta_s^2},$$

where $\overline{\theta_s^2}$ is the mean square angle of multiple scattering, θ_D is the angular spread of the photon beam, a is the transverse size of this beam along the Z-axis. Here, the contribution of photons of diffraction bremsstralung (DB) is taken into account. For the comparison of the theory with experiment it was taken into account that the radiation was absorbed in exit window of acceleration of the length of L_1 and in the air interspace of the length of L_2 between the crystal and a detector

and also the different effectiveness of X-ray detector for different harmonics of PXR. In Fig.15 it can be seen this histogram of intensities corresponding to the different harmonics and crystallographic planes [24,25]. In the histogram it is given the theoretical magnitudes of the X - ray intensity, generated inside the crystal and corrected with the account of experimental conditions and the experimental results of intensities measured by a spectrometer. The analysis of this histogram Fig.15 shows that the coincidence between the theoretical predictions and experimental values can be considered as good if we take into account that some model approximations about the detector's form, a particle distribution in a beam were used in calculations and, on the other hand, the measurements were made with the accuracy not above 20%.

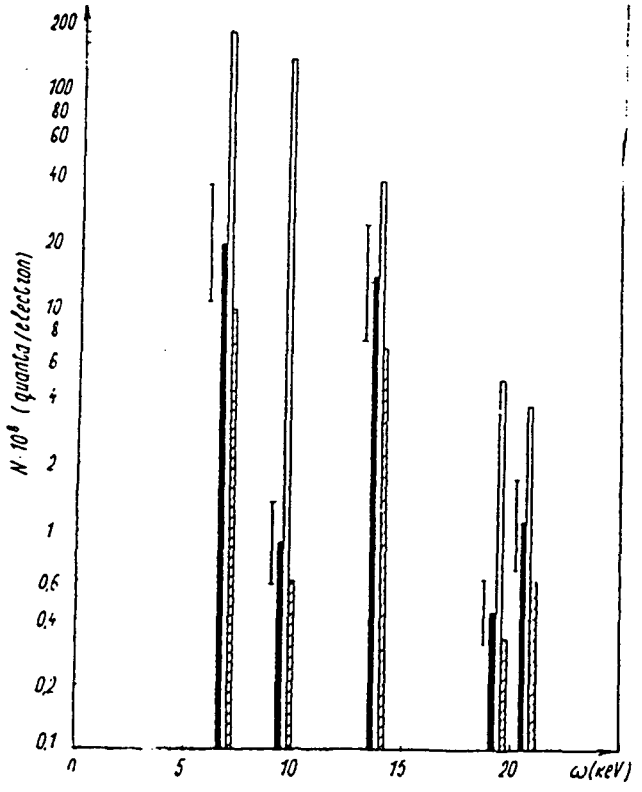

Fig. 15. Solid areas: the number of quanta counted by the detector, N_{ex}; unshaded areas: the number of PX quanta generated in the crystal; shaded areas: the theoretical values N_{pxr} calculated with taking into account the corrections on the photon absorption between the crystal and the dtector and on the detector efficiency.

In Table III the magnitudes of all parameters which are necessary for the calculation of photon numbers recorded by a detector $N_D^{(n)}$ are given.

Table III

diffraction plane	$\omega_B^{(n)}$ keV	$\omega_{ex}^{(n)}$ keV	$g_0 \cdot 10^6$	$\lvert g_\tau \rvert^2 \cdot 10^{13}$	$\theta_{ef}^2 \cdot 10^6$ grad	$L_a^{(c)}$(cm) diamond	$L_a^{(c)}$(cm) window	$L_a^{(a)}$(cm) air	η_n (%)
(400)	9.82	9.7 ± 0.15	15.31	120.0	15.31	0.12	0.148	136	78
(800	19.65	19.7 ± 0.23	3.83	1.0	6.77	0.63	1.003	1058	15
(220)	6.95	6.8 ± 0.15	30.62	883.0	30.62	0.04	0.045	52	94
(440)	13.84	13.8 ± 0.15	7.66	14.8	10.60	0.29	0.342	388	27
(660)	20.84	20.7 ± 0.20	3.40	0.6	6.35	0.75	1.026	1262	15

L cm	L_1 cm	L_2 cm	L_D cm	a cm	d cm	E MeV	L_R cm	$\theta_D \cdot 10^2$
0.10	a) 0.6	155	187	2.5	0.08	900	14.81.30	1.30
	b) 0.005	72	104	0.65				0.63

* the reflections by the planes (100) and (110) is equal to zero

In 1986 several new experiments in the measurement of the PXR integral intensity in various crystals and at various angles of radiation (reflexes) were conducted. In particular, the experiment in observation of PXR generated by electrons with the energy of 4.5 GeV in diamond single crystal was made in Erevan [64]. This experiment was performed with the help of an external Erevan synchrotron beam, that allowed to measure the process cross-section with high accuracy. The geometry of the experiment is shown in Fig.16. The electron beam with angular spread of 10^{-4} rad was incident on a crystal target at the angle of 35° relative to the plane (110). The registration angle of radiation made the angles of 70° and 60° with the initial particle momentum.

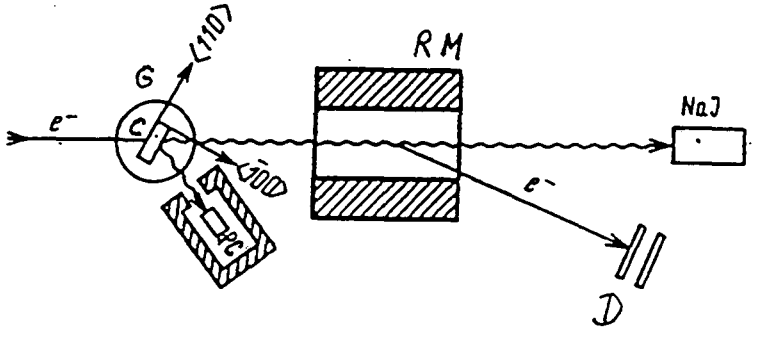

Fig. 16. G-goniometer, C-crystal, PC-proportional counter, RM-rotating magnet, D-detector of electrons.

The crystal target (the lengths were 0.2mm and 1mm) was installed into a goniometer allowing the rotation of the crystal in two mutually perpendicular directions with the accuracy of $4 \cdot 10^{-5}$ rad. The well-known orientational dependence of channeling radiation by electrons in a crystal ware used for the alignment of the crystal relative to the electron beam momentum. The measurements were performed by a proportional counter. The solid angle of quantum registration was $2 \cdot 10^{-4}$ rad. In Fig.17 the spectrum of X-ray radiation at the angle of $2\theta_B = 60°$ is shown after deducting the background (the radiation in a nonoriented crystal). You can see a peak at $\omega_B^{ex} = 11.3 \pm 1.3$ keV with a good accordance with the theoretical value of $\omega_B^{th} = 9.8$ keV.

In [64] the experimental estimation of possible contribution of the ordinary bremsstralung, which was also diffracted by the same crystallographic planes and, consequently, was observed at the same angles and frequencies, was made (see §2). For this purpose, the Al target with the length of 3 mm was placed before the diamond target of the length of 0.3 mm. Up to the accuracy

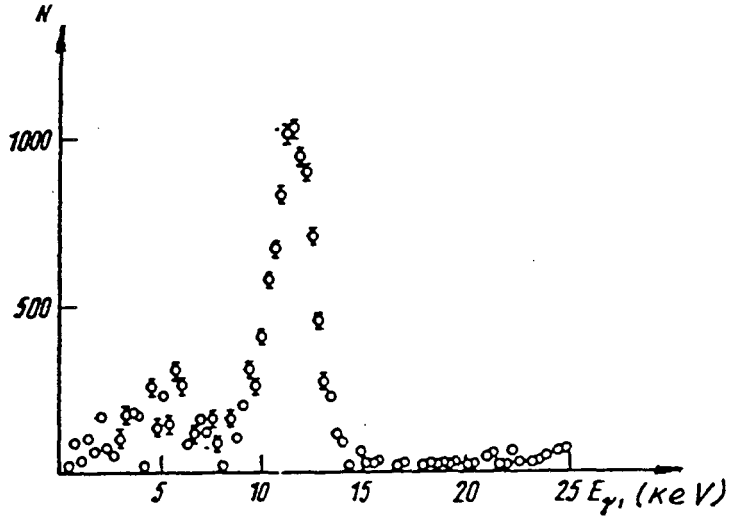

Fig. 17

of experimental errors the increase of the radiation output, introduced by the diffraction of the real photons of bremsstralung produced in Al target, has not been observed. This fact totally coincides with the theoretical estimations of contributions from various mechanisms of radiation to the total yield of X-ray radiation in the diffraction peak (see [43]). According to [43], the ratio of photons produced due to diffraction of bremsstralung (DB) to the photons of PXR in the same reflex is determined by the universal function

$$\zeta = \frac{N_{DB}}{N_{PXR}} \leq \frac{4}{3}\frac{\omega_B}{m} ZQ^2 \left(1 + \frac{\ln\gamma}{\ln\frac{E}{\omega_B}}\right), \qquad (2.45)$$

where Z is the charge of atom nucleus of the medium, E is the particle energy, m is the mass of radiating particle.

According to (2.45) the magnitude of ξ for X-ray region of frequencies is $\xi \approx 3 \cdot 10^{-3}$, that is the main contribution to the radiation intensity in the diffraction peak is made by PXR, indeed.

While comparing the experimental and theoretical results the authors of [64] pointed out that the theoretical magnitude of the number of γ-quanta in a diffraction peak was by an order of magnitude more than the experimental one ($N_{th} = 1.38 \cdot 10^{-5}$ and $N_{ex} = 1.1 \pm 0.1 \cdot 10^{-6}$). Unfortunately, the author did not give the expression which was used for the calculation. The calculation with the help of the formula, obtained in [42,44], gives the result that agrees with the experimental number of quanta with a good accuracy. In Table IV such comparison between the theoretical and experimental numbers of quanta radiated in a diffraction peak are represented for various experiments.

It should also consider one of the first experiments in observation of PXR, which was conducted in Kharkov electron accelerator of Kharkon Phys.-Techn. Institute. The electron beam with the energy of 900 MeV interacted with the Si crystal of the length of 30 μm being oriented in such a way that the Bragg condition was satisfied for crystallographic plane (220) [65,66]. The geometry of this experiment was similar as that represented in Fig.16. The experiment, conducted in Kharkov, is interesting due to the possibility of obtaining very hard quanta ($\omega > 100$ keV) with the help of PXR. The X-ray radiation, generated by relativistic electrons in a crystal, was collimated by a set of collimators being placed on horizontal plane at the angle of θ_B relative to the particle momentum in such a way that the Bragg condition was fulfilled for the small angles $1/\gamma << \theta_B << 1$ (θ_B is the Bragg angle).

The photon collimators provided with the collimation $\Delta\Omega = \pi(\Delta\theta_B)^2$ at the linear angle of collimation of $\Delta\theta_B << \theta_B$. The photon spectrums were measured by a semiconductor X-ray spectrometer with the resolution of ~ 10 keV. The maximum with the frequency of $\omega_{220} = 350$ keV and the width of $\Delta\omega = 25$ keV at the angle of $\theta_B \cong 17.9$ mrad was experimentally observed. The measured spectrum density was 0.3 γ/e·MeV·srad. The rotation of the crystal by the angle of 10^{-3} rad led to the disappearance of this maximum [65-68]. The theoretical value of the PXR intensity, calculated with the help of the formula off §2, gives the value less than experimental one. The theoretical analysis of the result of [66], made in [69], showed that the peak was formed, in this case, by three mechanisms of radiation - PXR, the ordinary diffraction bremsstralung and the

Table IV

Experiments	crystal	L m m	{hkℓ}	θ	ω_δ^{ex} (n = 1) (keV)	ω_δ^{th} (n = 1) (keV)	ΔΩ (srad)	$N_D^{ex} \cdot 10^6$ (γ/e⁻)	$N_D^{th} \cdot 10^6$ (γ/e⁻)
[82]	Si	0.38	(220)	9.5°	19 ± 0.5	19.6	$5.2 \cdot 10^{-5}$	6 ± 1	5.8
			(111)		12 ± 0.5	12.0		1.5 ± 0.17	0.7
[64]	C	0.2	(220)	30°	11.3 ± 1.3	9.8	$2 \cdot 10^{-4}$	1.0 ±0.17	0.7
		0.2		35°	9.2 ± 1.1	8.6		0.66 ± 0.08	0.6
		I		35°	8.9 ± 1.0	8.6		1.1 ± 0.1	1.9
[66]	Si	0.03	(220)	0.52°	350 ± 15	360.0	$2.8 \cdot 10^{-7}$	$(2 \pm 0.2) \cdot 10^{-3}$	$1.66 \cdot 10^{-3}$

diffraction bremsstralung with a photon phase velocity less than the velocity of radiating electrons. This bremsstralung corresponds to the dispersion branch with $n > 1$. The estimation shows that the contribution of all three mechanisms to a diffraction peak, in experimental conditions, are comparable in magnitude. The calculation, taking into account all mechanisms, gives the theoretical value

$$N^{th} = N^{th}_{PXR} + N^{th}_{BD} + N^{th}_{SBD} \cong 0.28 \div 0.32 \ \gamma/e \cdot MeV \cdot srad ,$$

in dependence of the crystal orientation. It means that agreement is rather well. It should be noted that Kharkov experiment considerably differs from the experiments, conducted in Tomsk and Erevan relative to the experimental conditions and, as a consequence, the contributions from the different mechanisms to the total intensity of radiation in a diffraction peak are different. In both later cases the contributions from the other mechanisms in comparison with PXR were very small. In [67], for the explanation of [65,66], the author suggested a new mechanism of coherent bremsstralung connected not with longitudinal crystal periodicity but with a periodicity of the electron density of a crystal on a transverse plane relative to the particle movement direction. However, the author did not make a comparison of a theoretical magnitude of the radiation yield with the experimental results. That is why, this interpretation can not be considered as successful.

The comparison between theoretical and experimental magnitudes of the yield was also made in [70], where the dependence of PXR yield on the crystal length was investigated.

Recently, a series of experiments in the investigation of PXR characteristics have been conducted. They can be divided in several groups: 1) the measurement of PXR spectral density at a given Bragg angle and the integral number of quanta in a given reflex; 2) the investigation of the fine structure of angular and spectral distributions inside a given reflex; 3) the investigation of dependence of PXR characteristics on the radiating particle energy; 4) the measurement of PXR polarization characteristics. Obviously, all first experiments, considered above, can be related to the first group. Recently the observation of PXR under the multi-wave diffraction conditions were performed.

Let us consider each of these groups in detail. After first experiments in which the PXR spectrum was observed and the total radiation yield was experimentally measured, the series of experiments were conducted in order to investigate in detail the spectral [71-78] and angular [26,79-85] distributions inside a definite reflex and also the PXR characteristics in various media [73-78]. The experimental geometry of [71] was the same as in the first experiments, but the measurements were made for the diamond crystal. It was observed three reflexes, which correspond to the reflections (220), (440), (660) and the intensities of radiation in these reflexes were measured. It was shown that the agreement between theoretical and experimental results rather well. It was also shown that, due to the different absorption of photons from different reflexes, the relative magnitudes of intensities of these reflexes were changing with the change of the target length. So, for the target with a small length, the maximum intensity had a reflex with smallest indices. With increasing the target length the contribution of reflexes, corresponding to high reflections, i.e. hard quanta, raises due to weak absorption of hard γ-quanta in the medium. The PXR in GaAs crystal was first observed in [76] and the spectral distribution was measured. It was made the comparison of PXR yield and its spectral width with the X-ray characteristic radiation corresponding to lines GaK and AsK . The total yields of PXR in reflexes for the crystals of Si, quartz and diamond were measured in [77]. The relative comparison of PXR characteristics for various targets were also made. These experiments are interesting for the future application of PXR as a source of X-ray radiation for the different tasks. The paper [73] is devoted to the comprehensive investigation of PXR characteristics in a Si target. It was measured the radiation intensity in different reflexes, the angular and spectral distributions and the threshold dependence of PXR intensity on the energy of radiating particles. In [73-75] the fine structure of PXR spectral distribution in a given reflex was experimentally investigated. By increasing the energy resolution of a detector the authors could observe the fine structure of PXR angular distribution. It was theoretically predicted in [42], but not observed during the first experiments caused by the low resolution of a detector. This fine structure takes place for reflexes corresponding to $2\theta_B < 45$ [42]. It was measured the intensities of two reflexes in Si $\omega_{220} =$

19 keV and ω_{111} = 12 keV. The experimental value of the split of the spectral line was $\Delta\omega^{ex}$ = $0.2\cdot\omega_B$, that was much more than the theoretical magnitude, which was $\Delta\omega^{th} = 2\cdot10^{-2}\ \omega_B$. In [73] it was also analyzed the influence of a detector size on the total yield of PXR in a reflex. It was shown that the relative magnitude of radiation intensities in different reflexes changed with decreasing the angular size of the detector. In this case, the relative contributions of photons generated in the higher reflexes increased. This is explained by the fact that the width of the angular distribution decreases with increasing reflex indices.

The paper [78] is devoted to the experimental investigation of PXR characteristics near the K-line of absorption in Ge crystal. It was shown that the considerable modification of spectral and angular distributions took place in this case. The direct measurement of PXR angular distribution was firstly performed in [25] in the case of asymmetric diffraction, that was at $\theta_B = 45$ in diamond monocrystal. The measurement was made with the help of a coordinate detector of X-ray, consisting of a number of square cells with the size of 1.3cm. Each of these cells is an ionization chamber. The detector contained 16x16 cells and was placed at the distance of L_D = 100 cm from the crystal target. The fine structure was not observed during this experiment because the angular size of the detector was more than the effective radiation angle. However, it was observed the asymmetry of radiation angular distribution along the Y-axis, which was the most prominent in this geometry. Afterwards, a slit collimator was applied in [79-82] in order to investigate in detail the angular distribution of radiation in a given reflex for the crystals of diamond [79-81] and Si [81-82]. This slit collimator allowed to increase the angular resolution of a detector. This was a narrow rectangular slit with the size (2.5x16) mm which corresponded to the angular aperture $\Delta\theta_x = \pm2.5$ mrad and $\Delta\theta_y = \pm16$ mrad. The geometry of these experiments is shown in Fig.18. During these experiments the theoretical prediction of the existence of two maxima in the one-dimensional PXR angular distribution in the Y-direction was confirmed (see §2 (2.20), (2.21)). The angular distribution of radiation in Si for reflexes (400), (200) and (440) were investigated in [80,82]. According to [80], the angular distribution along the Y-axis has two maxima and the distance between these maxima decreases with increasing the radiation frequency . Along the X-axis the

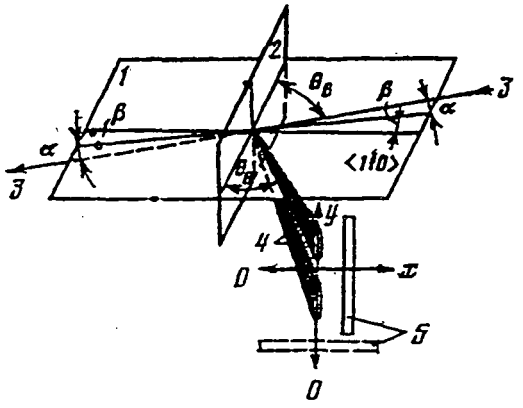

Fig. 18. Here: 1 - (001) plane; 2 - (110) plane; 3 - electron beam; 4 - reflex 400; 5 - slit collimator

angular distribution exhibited only a single maximum at $\theta = \theta_B$, the width of which also decreases with increasing the reflex frequency: ω_{220} = 7.1 keV, $\Delta\theta_x$ = 12 mrad; ω_{400} = 10 keV, $\Delta\theta_x$ = 9 mrad; ω_{440} = 14.2 keV and $\Delta\theta_x$ = 7 mrad. As we have pointed out above, this

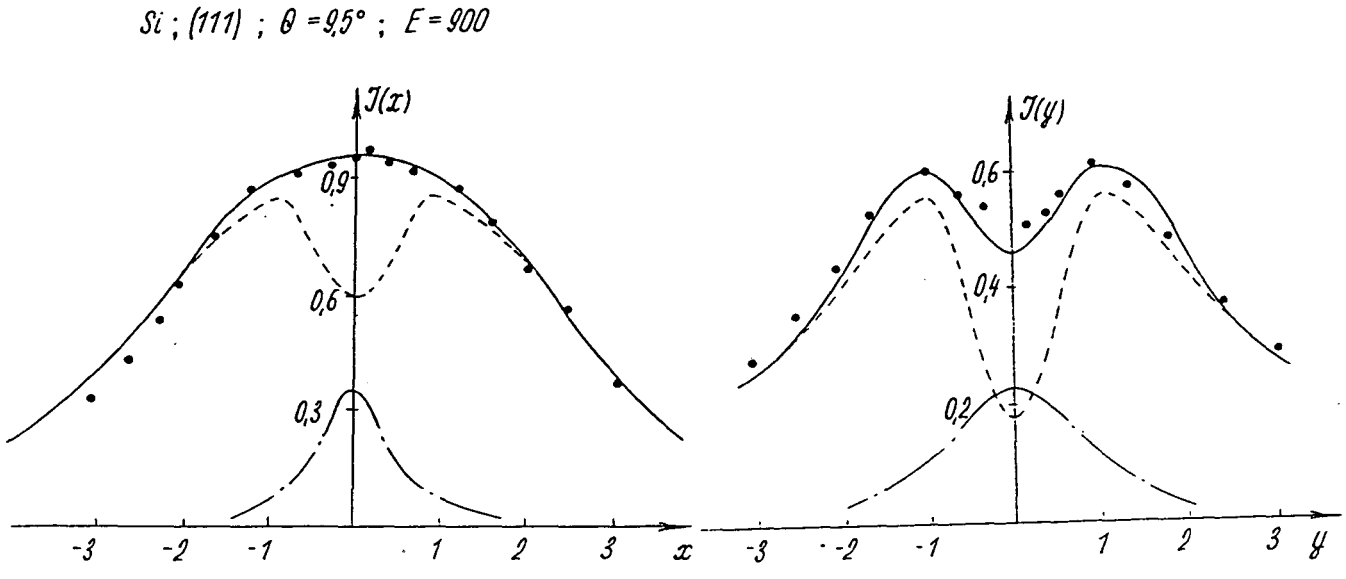

Fig. 19

narrowing of PXR angular distributions with the increase of the reflection indices manifests itself in experiments also in the increase of the relative contribution of these reflexes to the total intensity of radiation, detected at a given angle while decreasing the angular size of a detector [73]. In Fig.19 you can see the comparison of experimental results [82] with the theoretical curves being calculated in [42]. For this comparison, the spectral-angular distribution has been integrated over the size of the slit detector. As a result, the PXR angular distribution, in the case of measurement with the help of a slit collimator, has the following form:

$$N_D(x,y) = \sum_{n=1}^{3} \frac{Q^2}{\pi^2} \frac{\left|g_t\left(\omega_B^{(n)}\right)\right|^2}{\sin^2\theta_B} \omega_B^{(n)} L_a\left(\omega_B^{(n)}\right)\left(1 - e^{\frac{L}{L_a}}\right) x$$

$$x \int_{x-a}^{x+a} d\eta \sum_{\lambda=0,1} (-1)^{\lambda} \left\{ \frac{\left(\eta^2 + \frac{1}{2}\overline{\theta_s^2}\right)\left(1+\cos^2 2\theta_B\right)+\theta_{ef}^2}{\left(\eta^2 + \theta_{ef}^2\right)^{3/2}} \operatorname{arctg} \frac{y + (-1)^{\lambda} b}{\sqrt{\eta^2 + \theta_{ef}^2}} + \right.$$

$$+ \frac{\left[\eta^2\left(\cos^2 2\theta_B - 1\right) + \frac{1}{2}\overline{\theta_s^2}\left(\cos^2 2\theta_B + 3\right) - \theta_{ef}^2\right]}{\eta^2 + \theta_{ef}^2} x \qquad (2.46)$$

$$\left. x \frac{y + (-1)^{\lambda} b}{\eta^2 + \theta_{ef}^2 + \left[y + (-1)^{\lambda} b\right]^2} \right\},$$

where X,Y are the coordinates of a slit center, a and b are the sizes of the slit, L_a is the absorption length, $\overline{\theta_s}$ is the angle of multiple scattering

The analysis showed that for the explanation of experimental results, it is necessary to take into account the contribution of three harmonics of radiation to the total intensity. According to Fig.19 the agreement between theoretical and experimental results is not only qualitative but also quantitative. For example, the split of maximum of angular distribution is $\Delta\theta_y^{ex} = 1.8 \cdot 10^{-2}$ rad ($\Delta\theta_y^{th} = 1.7 \cdot 10^{-2}$ rad, see (2.21)). The papers [84,85] were devoted to the measurement of

angular distributions at various energies of radiating particles and also the investigation of the azimuthal distribution of PXR intensity in a reflex. The methodic and the geometry of these experiments were like as previous one (see Fig.18). It was measured the PXR angular distributions in diamond at the energies of electron beam E = 370 MeV, 500 MeV and 900 MeV.

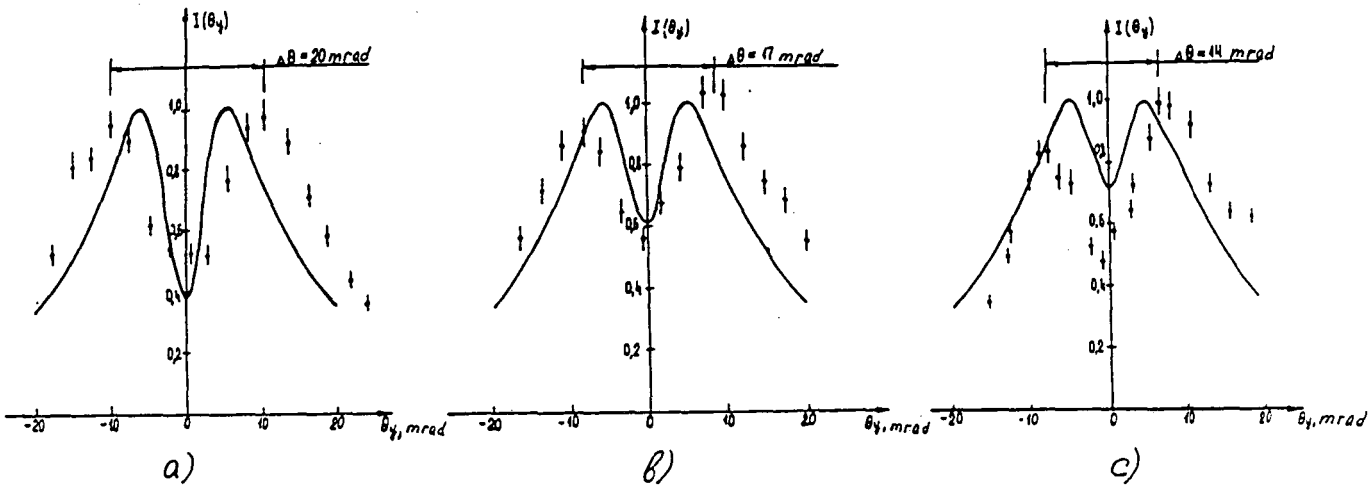

Fig. 20. The vertical PXR angular distribution: a) E = 900 MeV; b) E = 500 MeV; c) E = 370 MeV.

The energy dependence of the distance between two peaks of PXR angular distribution was observed. In Fig.20 was shown the radiation angular distributions along the Y-axis for the reflex (400) at different electron energies. You can see that the distance between the maxima decreases and the width of distribution increases with decreasing the particle energy.

One of the main features of PXR is the threshold energy dependence of radiation intensity (see §2). That is why, the energy dependence of PXR yield in a given reflex was investigated in detail [73,76,79, 82,86]. The comparison of experimental results [82] with the theoretical dependence, calculated according the formulae (2.32) and (2.33) is given in Fig.21(a),(b). You can see a rather good agreement. The calculations were derived taking into account the contribution of diffraction bremsstralung to the total intensity measured by a counter. The measurements of yields were performed within the energy interval of radiating particles from 300MeV till 900MeV.

For diamond crystal and the reflex (400), such energy dependence is presented in Fig.21. The magnitude of the threshold energy is $E_{th}^{ex} \simeq 300$ MeV. The theoretical calculation gives the value E_{th}^{th} = 320MeV [87].

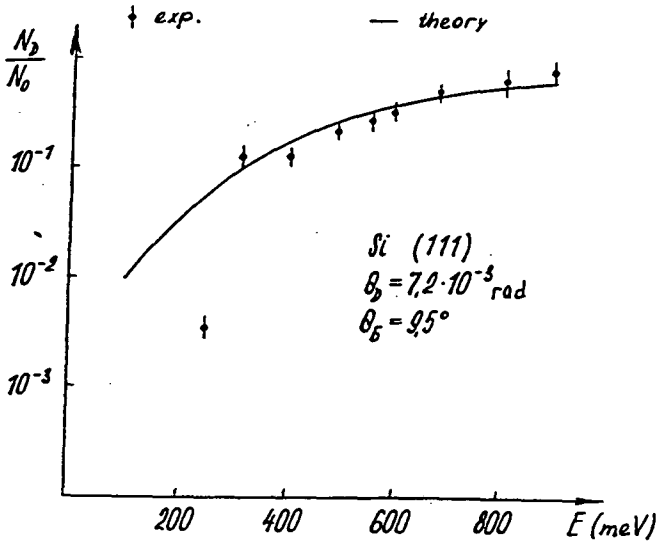

Fig. 21(a)

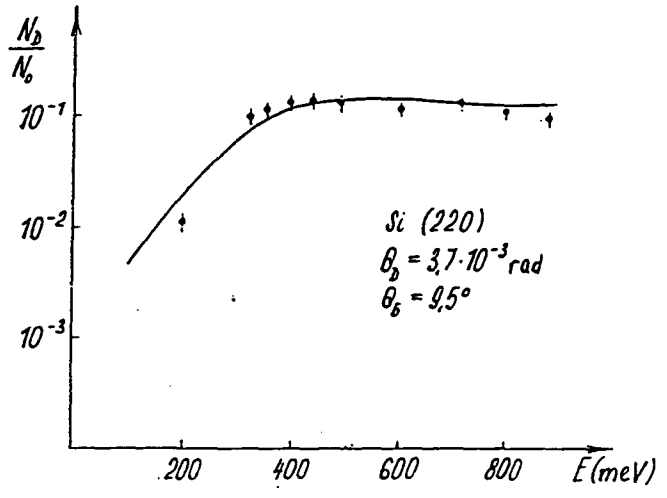

Fig. 21(b) Here: – are the theoretical results; · – are experimental data: a) from Ref. [42]; b) from Ref. [87].

According to theory [2,34-36], PXR is polarized. The papers [88-93] are devoted to the investigation of the polarization characteristics of PXR. Let us consider, for example, the results of [89], where the PXR polarization was measured in Si for the asymmetric diffraction geometry and the reflection plane (220), i.e. $2\theta_B = 90°$, $\omega_B = 19.5 \div 21.5$ keV (it depends on the detection angle relative to the Bragg direction). For the investigation of polarization the compton polarimeter, consisting of a detector and a scatter, was applied. The angular distribution in a reflex was also measured in the independent experiments. In Fig.22, the figures I,II,III point the regions of a PXR reflex, in which the linear polarization of radiation was investigated. In the general case, the PXR

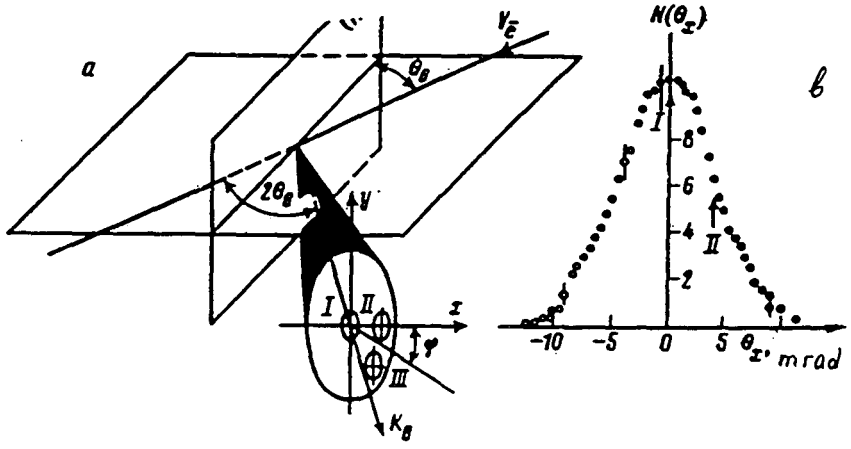

Fig. 22. Here: b) the angular PXR distribution in the horizontal direction.

polarization characteristics depend on the product of the squares of wave amplitude magnitudes of π- and σ- - polarizations and the coherent lengths corresponding to them. In the case of the equaled coherent lengths, the polarization is given as

$$P = \frac{1 - \cos^2 2\theta_B}{1 + \cos^2 2\theta_B} .$$

Besides, the radiation polarization essentially depends on the radiation azimuthal angle in the following way:

$$P(\varphi) = \frac{\sin^2 \varphi - \cos^2 \varphi \cos^2 2\theta_B}{\sin^2 \varphi + \cos^2 \varphi \cos^2 2\theta_B}, \qquad (2.47)$$

ϕ is the azimuthal angle measured from the scattering plane (π-polarized radiation is on the scattering plane, σ-polarized radiation is perpendicular to this plane). The measurement of the azimuthal dependence of PXR distribution permits to obtain the information about the power of polarization P and the inclination angle of the plane of maximum linear polarization ϕ_0. This dependence can be written in the following way:

$$\frac{N(\varphi) - N_0}{N_0} = P\, R \cos 2(\varphi - \varphi_0) \ . \qquad (2.48)$$

The definition of N_0 is given by the formula (2.34). In Fig.23 the results of measurements of the azimuthal dependence of scattered photons are represented for the region II. You can see the good agreement of the curve with the theoretical prediction. The powers of linear polarization P and the inclination angles of the polarization plane ϕ_0, obtained in the experiments [89], are given in Table V.

Table V

region of reflex	angular coordinates of collimator mrad	mrad	P	mrad
I	0 ± 0.5	0 ± 0.5	0 ± 0.06	90.5 ± 3.7
II	4.0 ± 0.5	0 ± 0.5	0.80 ± 0.08	3 ± 2.7
III	3.0 ± 0.6	-3 ± 0.5	0.82 ± 0.12	-51.5 ± 5.6

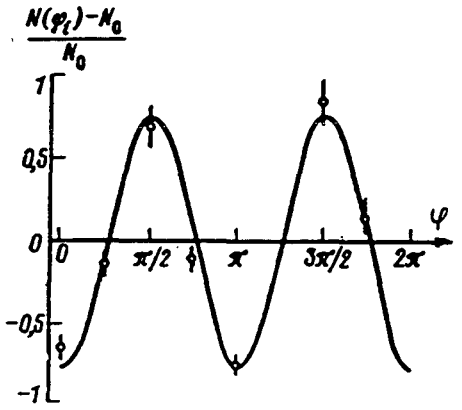

Fig. 23

According to the experimental results the polarization is minimum in the Bragg direction (see the region I) and the inclination angle of the polarization plane, in this case, corresponds to the position of the polarization plane for the ordinary X-ray diffraction. Out of Bragg direction the high power of linear polarization ($P \cong 0.8$) was observed, that agreed with theoretical results. For the regions II and III the polarization plane coincides with the plane of photon wave vector and the vector along the Bragg direction. It means that there is the total analogy between the polarization characteristics of PXR and the ordinary Cerenkov radiation. The high power of polarization of PXR was also demonstrated in [90] by using the original methodic.

In [93] the measurements were performed in GaAs crystal for the reflex (400). This experiment was confirmed that the power of radiation polarization in asymmetric diffraction geometry was close to the unity ($P \cong 1$). It means that the radiation is totally σ- polarized. The angular distribution of PXR, in this case, is described by the expression $I(\theta, \varphi) = \sin^2 \varphi \, I(\theta)$, that agrees very well with the experimental results (see Fig.24).

So, the experimental investigations have confirmed the high power of PXR polarization and proved the possibility to obtain the source of X-ray with high polarization power and with a definite inclination angle of polarization plane by using the collimation of PXR beam out of axis.

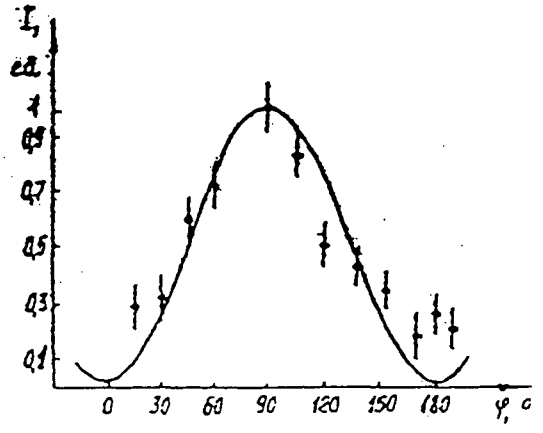

Fig. 24. Here: – is $\sin^2\varphi$; • are experimental data.

§4. Multi-wave Effects in Parametric X-Ray (Quasi-Cerenkov) Radiation.

Up to now the theoretical and experimental investigations of PXR were restricted by the case of two-wave dynamical diffraction. However, due to crystal symmetry the conditions of diffraction can be fulfilled for many waves, consequently, the multi-wave diffraction case of PXR is realized. The analysis shows that multi-wave diffraction can lead to new effects in PXR in comparison with two-wave diffraction case. For example, the spectral-angular PXR distribution depends on the effective refractive index in the crystal and on the photon absorption length. Under multi-wave diffraction conditions the inequality $n(\omega, \alpha) > 1$ can be fulfilled for several refractive indices and for some of them the magnitude of α can be close to zero. This leads to the possibility of Borman effect in PXR, i.e. to the increase of the diffracted wave amplitude due to the decrease of the absorption coefficient, in the comparison with the two-wave diffraction. Besides, under

multi-wave diffraction it is possible to excite the diffraction reflex in the indirect way, i.e. the PXR intensity in the diffraction peak is not equal to zero, even when the reflex under consideration is forbidden because of lattice symmetry [94]. As a result, the regime of multi-wave diffraction leads to the increase of the angular PXR density of radiation within the narrow interval of $\sqrt{g_\tau}$.

Recently PXR has been experimentally investigated in the case of multi-wave diffraction [76, 95-97]. The experiments were conducted for the crystal GaAs. In the papers [95,96] the angular distributions and threshold dependence of PXR in the reflex, corresponding to the 4-wave uncoplanar (000, 220, $1\bar{5}\bar{3}$, 153) diffraction of radiation with the frequency ω_B = 18.4 keV were measured. The energy of electrons was changed within the interval 250 - 900 MeV. The reduction of the width of multi-wave diffraction reflex in comparison with the main two-wave reflex (220) was experimentally observed. Fig.25 shows the angular distribution of PXR radiation in the reflex (220). In this situation the PXR, angular distribution along the X-axis looks like a bell [2]. The multi-wave diffraction changes this angular distribution. Now it has two maxima. On the background of the main two-wave reflex of PXR, the lines corresponding to the conditions of three-wave generation of PXR appear. If we go away from the center of angular distribution the

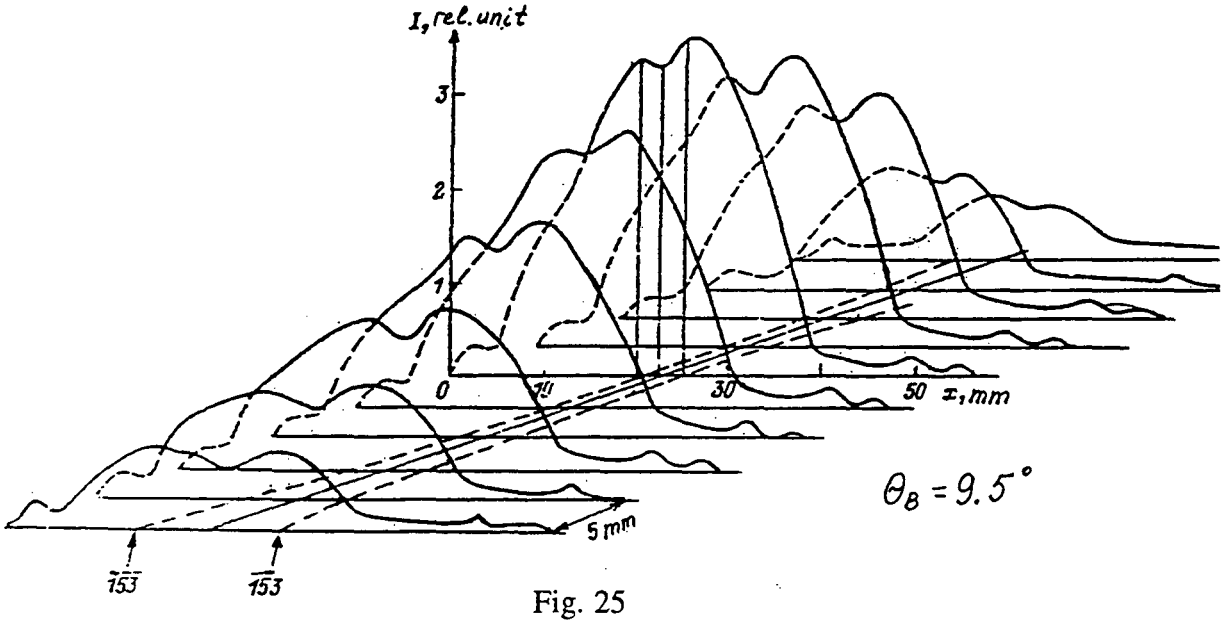

Fig. 25

distance between these maxima will increase. The calculated angle of intersection of reflexes ($1\bar{5}\bar{3}$) and (153) coincides with the measured angle with the accuracy of 10%. The width of the

diffraction multi-wave lines is about two times smaller than the width of the main two-wave reflex (220). The observed picture of PXR angular distribution, in general, is analogous to the distribution of multi-wave diffraction in the case of the external X-rays [94].

In [97] the spectral and angular characteristics of PXR were measured in GaAs for the electrons with the energy of 900MeV. It was shown that near the <110> direction there was a narrow peak caused by multi-wave diffraction on the background of the ordinary two-wave diffraction. The geometry of this experiment corresponds to excitation of 8-wave generation of PXR (000),(022),(0$\bar{2}\bar{2}$,)040),(202),($\bar{2}$0$\bar{2}$),(400) for the photons with the frequency of 6.2keV. It means that two 4-wave diffraction cases are excited simultaneously ((000),)022),(0$\bar{2}\bar{2}$),(040) and (000),(202),($\bar{2}$0$\bar{2}$),(400)). The detection was made at the angle of $2\theta_B = 90°$ in the direction of the two-wave reflex (400). In Fig.26 the angular distribution of PXR along the Y-axis is represented. You can see that there is good agreement between the theoretical and the experimental results

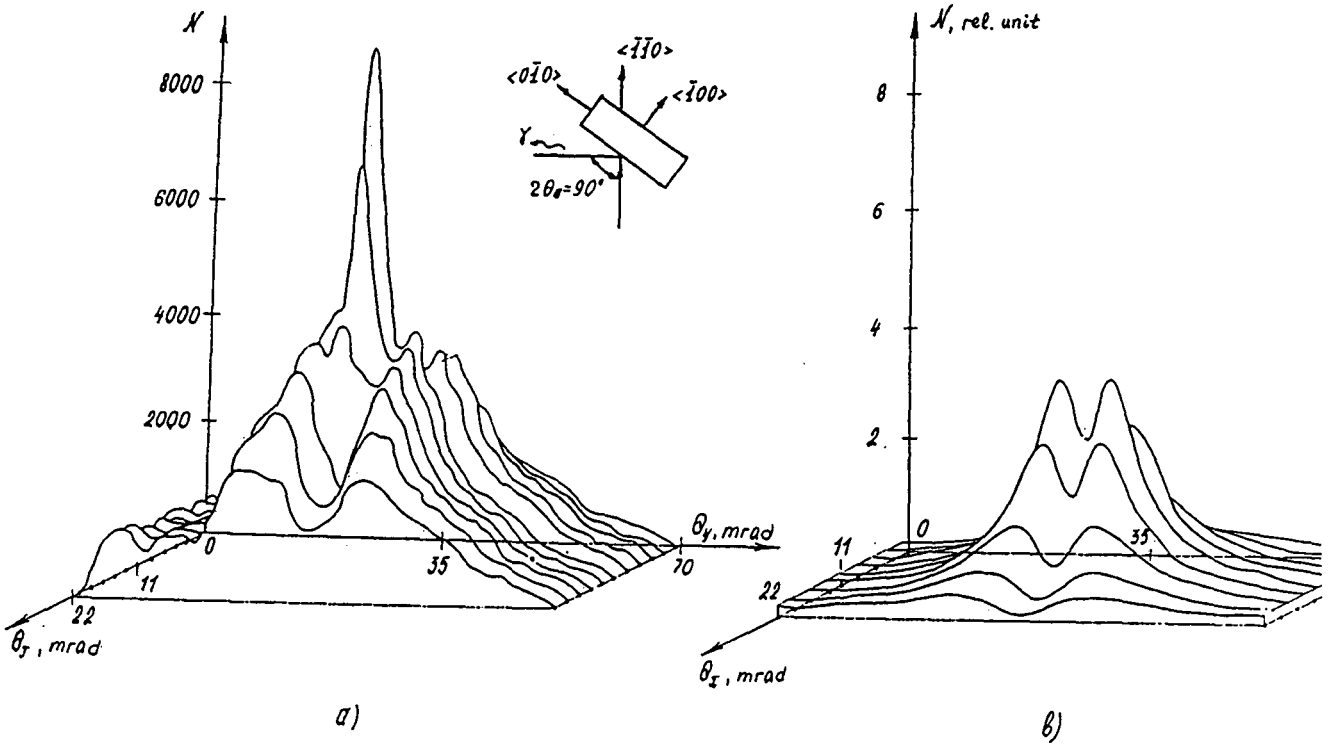

Fig. 26. Here: a) the experimental distribution under multi-wave diffraction; b) the theoretical distribution for (400) reflex under two-wave diffraction.

everywhere excluding the vicinity of the reflex center where the experimental picture shows the narrow peak caused by the multi-wave diffraction of PXR. The intensity of the radiation in this peak is 2.5 times larger and the angular width of the peak is 4 times smaller than the corresponding magnitudes of the main reflex of PXR (400) in the case of two-wave diffraction.

For the explanation of these anomalies the theory of multi-wave generation of PXR was derived in [98-100]. In [101,102] some specific cases were considered.

According to (2.9), to obtain the spectral-angular PXR distribution, we can solve the boundary problem of dynamical diffraction of X-ray by a plate in the arbitrary case of multi-wave diffraction. In [98] the photon wave function $\vec{E}^{(0)s}(\vec{r}, \vec{\omega})$ was obtained by the help of the matrix method. $\vec{E}^{(0)s}(\vec{r}, \vec{\omega})$ is the solution of a set of homogeneous Maxwell's equations and contains incoming spherical waves at $z \to \infty$. In the general case $\vec{E}^{(0)s}(\vec{k}\,\omega)$ are represented as:

$$\vec{E}_{\vec{k}_H}(\vec{r}) = \vec{\varepsilon}\, e^{i\vec{k}\vec{r}}\, G^{-}(\zeta)$$

$$G^{(-)}(\zeta) = \left\{ e^{i\omega Q^{(0)}\zeta}\,\theta(-\zeta) + e^{i\omega Q^{(-)}\zeta}\,\theta(\zeta)\,\theta(L-\zeta) + \right. \qquad (2.49)$$

$$\left. + e^{i\omega Q^{(\infty)}(z-L)}\, e^{i\omega Q^{(-)}L}\,\theta(\zeta - L) \right\} G^{(-)}(0) \ .$$

where $\vec{\varepsilon}$ is the line-matrix of 2N-order consisting of the polarization vectors of all reflections.

$$\vec{\varepsilon} = (..., \vec{e}_{\sigma\vec{G}}, ..., \vec{e}_{\sigma\vec{H}}, ..., \vec{e}_{\pi\vec{G}}\vec{e}_{\pi\vec{H}}, ...) \ .$$

$\vec{K}$ is a diagonal vector matrix consisting of the wave vectors of all reflections outside the crystal $\vec{K}_{u\vec{G}v\vec{M}}$, $= \vec{\varkappa}_{\vec{G}}\,\delta_{u\vec{G}v\vec{M}}$, $\vec{G}$, $\vec{M}$, $\vec{H}$ – are the reciprocal lattice vectors, u and v are the polarization indices. The elements of the $Q^{(\pm)}$ matrix of 2N x 2N order are defined by the following expression:

$$Q^{\pm}_{u\vec{G},\,v\vec{M}} = \frac{1}{2\gamma_G}\left\{\varepsilon^{(\pm)}_{u\vec{G},\,v\vec{M}} - \alpha_{\vec{G}}\,\delta_{u\vec{G},v\vec{M}}\right\}, \qquad (2.50)$$

$\alpha_{\vec{G}} = \left(\text{æ}^2_G - \omega^2\right)/\omega^2$ is the deviation from the exact Bragg condition for the G-reflection, $\delta_{uG,vM}$ is the Kroneker symbol,

$$\delta_{uG,vM} = \begin{cases} 1 \text{ if } G = M \text{ and } u = v \\ 0 \text{ if } G \neq M \text{ and } u \neq v \end{cases},$$

$\gamma_G = \vec{\text{æ}}_G \vec{N}/\omega$ is the cosine of the angle between the wave vector $\vec{\text{æ}}_G$ and the normal to the crystal surface $\vec{N}$, $\vec{N}$ is directed inside the crystal. The matrix $Q^{(0)}$ is obtained from the matrix $Q^{\pm}$ at $\varepsilon^{(\pm)}_{uG,vM} = 0$, $\theta(x)$ is the unit Hevisai function, $\vec{K}_H = \vec{\text{æ}}_H + \omega\lambda\vec{N}$ is the wave vector of photon for the H-reflection inside the crystal, ω is the photon frequency, $\lambda = \lambda\left(\vec{k}\right)$ is the dielectric susceptibility of the crystal which is defined by the help of the matrix Q and can have a lot of magnitudes [98],$\zeta = \left(\vec{r}\vec{N}\right)$, $G^{(\pm)}$ is the 2N-column vector consisting of the amplitudes of waves excited under diffraction inside the crystal, $G^{(\pm)}{}_{(0)}$ and $G^{(\pm)}(L)$ are its magnitude at the crystal boundaries,

$$G(L) = e^{i\omega Q^{(\cdot)}\zeta}\, G(0)$$

The other designations can be found in [98].

By substituting the expression (2.49) into (2.9) the spectral-angular distribution of PXR in the case of multi-wave diffraction can be represented in the following form [98]:

$$W_{s\vec{n}_H\omega} = \frac{e^2\omega^2\beta_1^2}{4\pi^2\cos^2 a}\left|\sum_u e_{u0z}\left[(L_0 - L_D)\left(I - e^{-iQ_0^{(\cdot)}L}\right)G^{(\cdot)^*}(L)\right]_{u0}\right|^2, \qquad (2.51)$$

where $L_0 = \frac{I}{Q_0}$, $Q_0 = \omega - \beta\text{æ}x_{0z} + \frac{\omega\alpha_0}{2\gamma_0}$ is the longitudinal momentum transmitted to the medium, I is the unit matrix, a is the angle of incidence of a particle beam on the plate, $Q_0^{(-)} = q_0 I - \omega Q^{(-)*}$,

the label "0" always corresponds to the wave propagating at the small angle relative to the particle velocity. The Z-axis is chosen along the particle motion direction, $\beta = u/c$. As you can see from (2.51), the PXR spectral-angular distribution is expressed in terms of a function of a matrix $Q^{(-)*}$. As a result, for calculating the PXR spectral-angular distribution under multi-wave diffraction we should know the roots of a minimal polynomial of the matrix $Q^{(-)}$. With the help of a special Lagrange interpolation polynomial [103] we can represent (2.51) in the following form:

$$W_{\vec{sn}_H\omega} = \frac{e^2\omega^2\beta_1^2}{4\pi^2\cos^2 a}\left|\sum_u \sum_{\mu=1}^{m} e_{u0z}\left(e_0 - e_0^{\mu}\right)\left(I \neq e^{-\frac{iL}{L_0^M}}\right)\gamma_{\mu u}\right|^2, \tag{2.52}$$

where $\gamma_{\mu u} \equiv \gamma_{\mu uG}$ and is defined by the expressions:

$$\gamma_{\mu uG} = \left\{\left[\prod_{i\neq\mu} \frac{\left(Q^{(-)^*} - \lambda_i I\right)}{\left(\lambda_\mu - \lambda_i\right)}\right] E^{(-)^*}(L)\right\}_{uG}, \; i, \mu = 1, \ldots, m \tag{2.53}$$

or, depending on the diffraction geometry, by

$$\gamma_{\mu uG} = e^{-i\omega\lambda_\mu L}\left\{\left[\prod_{i\neq\mu} \frac{\left(Q^{(-)^*} - \lambda_i I\right)}{\left(\lambda_\mu - \lambda_i\right)}\right] E^{(-)^*(0)}\right\}_{uG}. \tag{2.54}$$

In the case of rather thick crystals we can use the approximation

$$\left|\frac{\left(1 - e^{-iq_0^\mu L}\right)}{q_0^\mu}\right|^2 \equiv \pi L_{ef}\sigma\left(\mathrm{Re}q_0^\mu\right), \; L_{ef} = \frac{\left(1 - e^{-2\mathrm{Im}q_0^\mu}\right)}{\mathrm{Im}q_0^\mu}, \tag{2.55}$$

and write the PXR distribution as

$$N_{\vec{sn}_H} = \frac{e^2\beta_1^2}{4\pi e^3\cos^2 a}\sum_i \sum_\mu \omega_\mu^i L_{\mu 0}^{ef}\left(\omega_\mu^i\right)\left|\sum_u e_{u0z}\,\gamma_{\mu u}\left(\omega_\mu^i\right)\right|^2 \left|\frac{\partial \mathrm{Re}q_0^\mu}{\partial\omega}\right|^{-1}_{\omega=\omega_\mu^i},$$

$$q_0^M = \frac{\omega - v x_{0z}}{v \cos a} - \omega\lambda_\mu \tag{2.56}$$

the summation over (i) in taken over the roots λ_μ^i which comply with the dispersion equation

$$R_e\, q_0^\mu(\omega_\mu^i) = 0 \tag{2.57}$$

The term $\partial \mathrm{Re}\, q_0^\mu / \partial\omega$ describes the influence of the dispersion of the medium on the process of PXR formation.

In [100] the detail analysis of some special cases of multi-wave diffraction of PXR were considered. This are three-dimensional symmetrical and three-wave coplanar diffraction. In particular, under the three-wave PXR generation when three strong waves are excited inside the crystal $\vec{K}_0$, $\vec{K}_H = \vec{K}_0 + \vec{H}$ and $\vec{K}_F$, $= \vec{K}_0 + \vec{F}$ ($\vec{H}$ and $\vec{F}$ are the reciprocal lattice vectors), the angular distribution of photons emitted in a diffraction peak is determined by the expression [100]

$$N_{s\vec{n}_H} = \frac{e^2\beta^2\left[f_1^s(\tau_{is}) + f_1^s(\tau_{2s})\right]}{4\pi \sin^2\theta_{0H}\left|1 - \delta_F b_{F0}\right|\left|\tau_{2s} - \tau_{1s}\right|\left(\theta^2 + \theta_q^2\right)} \tag{2.58}$$

for the case without degeneracy of dispersion equation roots ($\left|\tau_{2s} - \tau_{1s}\right| >> \Delta\tau_{21}^s$) and

$$N_{s\vec{n}_H} = \frac{e^2\beta^2 f_2(\tau_{1s})}{4\sqrt{2}\,\pi \sin^2\theta_{0H}\left|1 - \delta_F b_{F0}\right|^2\left(\theta^2 + \theta_q^2\right)^{1/2}} \tag{2.59}$$

when there is the degeneracy ($\left|\tau_{2s} - \tau_{1s}\right| \le \Delta\tau_{21}^s$), where τ are the real part of roots of dispersion equation $\tau \equiv \mathrm{Re}\lambda_{sHsH} = \theta_{ef}^2 - \alpha_0 - g_0'\delta_H$, $\theta_{ef}^2 = \gamma^{-2} + \theta^2 + \overline{\theta_s^2}L/\gamma_0$, $\theta_q^2 = \gamma^{-2} + \overline{\theta_s^2}L/\gamma_0 - g_0'$, $\delta_H = \gamma_0/\gamma_H$ γ_0, γ_H and γ_F are the cosines of the angles between the corresponding wave vectors $\vec{K}_0$, $\vec{K}_H$ and $\vec{K}_F$ and the normal to the crystal surface, θ is the radiation angle, $\lambda_{sH,sF}$ are the

elements of the matrix Λ, L is the crystal length, s = σ, π.

The analysis shows that at the radiation angles θ_x, for which the relation $|c_{F0}| \geq |g_0'|$ is fulfilled (see [100]), the contribution to the PXR intensity is made only one dispersion branch and the angular distribution of three-wave PXR generation does not practically differ from the ordinary two-wave case. The multi-wave effect manifests itself only in the vicinity of the small values of radiation angles θ_x, when $|c_{F0}| \leq |g_0'|$. In this region,which corresponds to the degeneration of roots τ_{1s} and τ_{2s}, there is the amplification of the radiation intensity in comparison with the ordinary two-wave generation. This amplification, in general case, is asymmetric relative to the angle of θ_x and its magnitude depends on the radiation angle θ_y. The gain R can be written as

$$R = \frac{N^{d}_{\vec{sn_H}}(three)}{N_{s\bar{n}_H}(two)} = \frac{1}{\sqrt{2}\,|1 - \delta_F b_{F0}|^{1/2}} \left|\frac{Re g_0}{Im\, g_0}\right|^{1/2} . \qquad (2.60)$$

From (2.60) we see that the gain depends on the geometric factor $(1-\delta_F b_{F0})$ and the crystal parameters g_0' / g_0''. This amplification is observed in the narrow interval near the degeneration region. At the same time, inside the degeneration region the radiation intensity has a deep gap caused by the complexity of the roots τ_{1s} and τ_{2s} in this region.

The result of numerical calculation of the angular PXR distribution for a coplanar three-wave diffraction (000),(131),(111) is represented in Fig.27. This diffraction case includes a strong join reflection (040). A beam of 1.2GeV electrons is incident on a 50 μm silicon plate, cut in the plane of (101), at the angle of $a \cong 29.5°$ in a diffraction plane (101). The PXR yield is recorded at the angle $2\theta_B = 109.47$ with respect to the particle beam direction. The effective PXR angle is $\theta_{ef} \cong 68 \cdot 10^{-3}$ rad, $N = N_\sigma + N_\pi$. As one can see, the PXR multi-wave effect is observed only in a narrow band (near degeneracy region) close to the line x = 0 (i.e. the reflection plane). This region of degeneracy is shown scaled up in the X-direction (25:1) in Fig.28. The degeneracy region has a

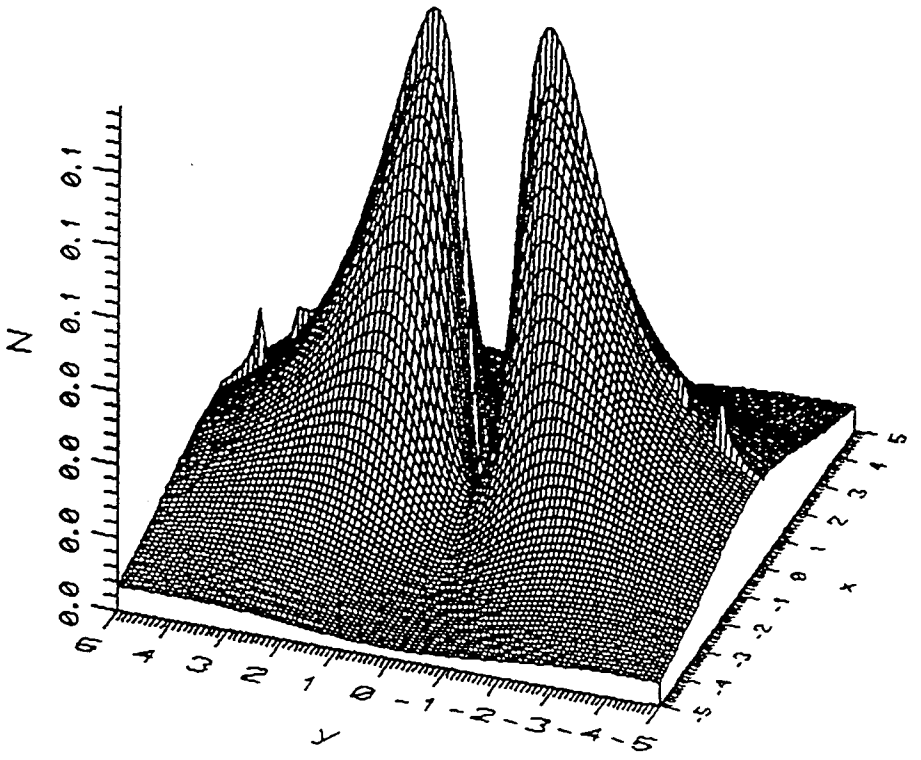

Fig. 27

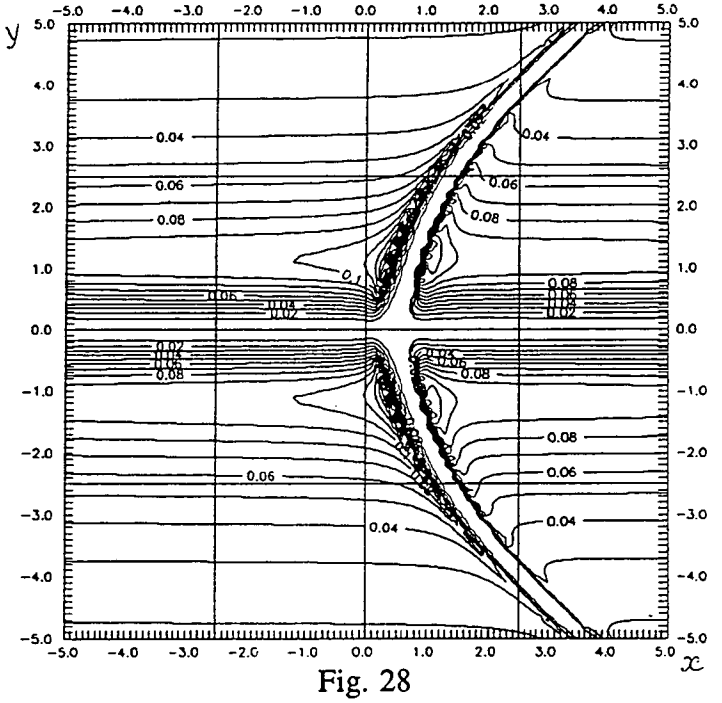

Fig. 28

deep gap and two narrow lines of amplified intensity. The distance between them is approximately 0.02 θ_{ef} ($x = \theta_x/\theta_{ef}$, $y = \theta_y/\theta_{ef}$, θ_x and θ_y are the components of photon radiation angle, counted off in diffraction and reflection planes, respectively).In Fig.29 the one-dimensional PXR angular distribution at a sectional point y = 1 is shown scaled-up in the X-direction. According to Fig.29

two asymmetric peaks are visible at the boundaries of the degeneracy region. The width of these peaks is approximately equal to 0.01 θ_{ef} and the height depends on the value of the coordinate X. The fine structure of the PXR angular distribution may be experimentally observed while studying the angular distribution near the degeneracy region with the help of a detector having an angular size $\Delta\theta_D \leq 10^{-4}$ rad and using the electron beam with the angular divergence not greater than $\Delta\psi = \sqrt{2\Delta\theta_D\theta_{ef}} < 10^{-3}$ rad. Although the obtained results cannot be applied for the explanation of the experimental data [95-97], observed in the 4- and 8-wave diffraction cases, the general rules of multi-wave generation of PXR, observed in the experiments, manifest themselves in the three-wave diffraction case, considered in [98-100]. The characteristics of PXR in the case of three-wave asymmetric coplanar diffraction were analyzed in [101-102].

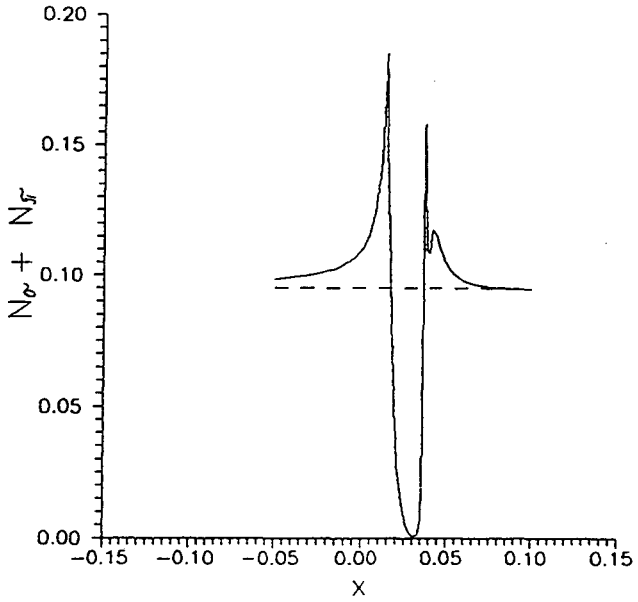

Fig. 29. Here: - - - is the result of two-beam approximation. – is the result of calculation in the case of three-wave coplanar diffraction.

§5 Surface Parametric X-Ray (Quasi-Cerenkov) Radiation (SPXR).

When a particle travels in a vacuum near the surface of a spatially periodic medium, a new kind of parametric (quasi-Cerenkov) radiation arises [104,105] - surface parametric (quasicerenkov) X-ray radiation (SPXR). The phenomenon takes place under the condition of uncoplanar surface diffraction, considered firstly in [32], when the effective refractive index of electromagnetic wave in X-ray region can become more than unity. The effect under consideration should differ from the well-known effect of Smith-Parcell radiation, in which photons are formed from diffraction reflection back from the surface of a body with spatially periodic dielectric constant along the motion of a particle (the direction of the velocity coincides with the direction of the reciprocal lattice vector). A surface wave is not formed in this case, and the wave field consists of two waves propagating in opposite directions, in contrast to uncoplanar surface diffraction, in which at least three waves participate, whose directions of propagation form angles different from π (see Fig.30). The solution of Maxwell's equation $\vec{E}_{\vec{k}}^{(+)}(\vec{r})$ in the case of uncoplanar surface diffraction was derived in [32]. It was shown that the surface diffraction is characterized, in the two-wave case, two angles of total reflection (several in the case of multi-wave diffraction [107]). The solution, obtained in [107], contains the component, which describes a state that damps with

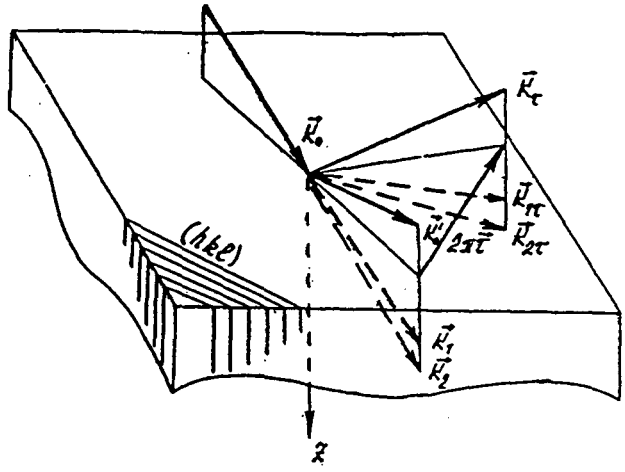

Fig. 30

greater distance from the surface of the medium, both within the material and in the vacuum, and which describes a surface wave, i.e., a wave in which the energy flux is directed along the boundary of the surface of a spatially periodic target (see revue [108]). According to [106], this solution, describing the scattering of the plane wave by the target under the surface diffraction geometry, can be written in the following form:

$$\vec{E}_{\vec{k}}^{(+)s} = e_s\, e^{i\vec{k}\vec{r}} + A_s\left(\vec{k}, \omega\right) e^{i\vec{k}_1\vec{r}} + B_s\left(\vec{k},\omega\right) e^{i\vec{k}_2\vec{r}}\,, \tag{2.63}$$

where the wave vector in the vacuum $\vec{k} = (\vec{k}_t, \vec{k}_\perp)$, $\vec{k}_1 = (\vec{k}_t, -\vec{k}_\perp)$ $|\vec{k}_{2\perp}| = \sqrt{k^2 - k_{2t}^2}$, $\vec{k}_2 = (\vec{k}_{2t}, -\vec{k}_{2\perp})$, $\vec{k}_{2t} = \vec{k}_t + 2\pi\vec{\tau}$, $\vec{k}_t$ is the wave vector component parallel to the target surface, $\vec{\tau}$ is the reciprocal lattice vector, ω is the photon frequency. The amplitudes A_S and B_S are given in [105, 32]. By substituting the solution $\vec{E}_{\vec{k}}^{(-)s} = \left(\vec{E}_{-\vec{k}}^{(+)s}\right)^*$ into (2.3) and taking into account, that the radiation condition can be realized only for the third term of (2.63), the differential number of emitted photons can be represented as (see, also [106])

$$\frac{d^2N_s}{d\omega d\Omega} = \frac{e^2\omega T}{2\pi\hbar c^3}\left|\vec{u}\vec{B}_s(\vec{k},\omega)\right|^2 \delta\left(\vec{k}_t\vec{u} + 2\pi\vec{\tau}\vec{u} - \omega\right) e^{-2Imk_{2\perp}|z_d}\,. \tag{2.64}$$

Here we assume that a particle is moving parallel to the target surface at the distance Z_0 with the constant velocity $\vec{u}$, T is the flight time. The argument of δ-function, from (2.64), is equal to zero for the frequencies $\omega_u = \dfrac{|2\pi\vec{\tau}\vec{u}|}{1 - \vec{n}_t\vec{u}/c}$, where $\vec{n}_t$ is the component of the unit vector in the direction of the vector $\vec{k}$, which is parallel to the surface.

After integrating (2.64) over frequencies, the angular distribution of radiation has the following form:

$$\frac{dN_s}{d\Omega} = \frac{e^2\omega_u T}{2\pi\hbar c^3}\left|\vec{u}\vec{B}_s(\vec{k},\omega_u)\right|^2 e^{-2Imk_{2\perp}(\omega_u)z_d} \qquad (2.65)$$

The spectral-angular distribution of SPXR generated by a particle incident on the crystal at a small angle relative to the crystal surface was obtained in [109]. It was assumed that the reciprocal lattice vector $\vec{\tau}$ makes the angle of $\psi < (g_0)^{1/2}$ relative to the surface and an arbitrary angle φ relative to the tangential component of the particle velocity (see Fig.31). The authors solved the

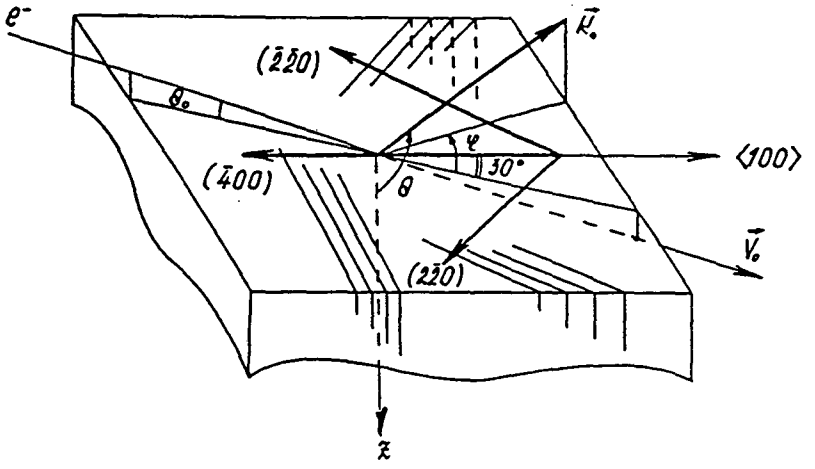

Fig. 31

boundary problem for the wave function of a photon with the wave vector $\vec{k}$ in the vacuum and the frequency ω and obtained the spectral-angular distribution of SPXR ($\hbar = c = 1$);

$$\frac{d^2dN_\pi}{d\omega d\Omega} = \frac{e^2\omega}{4\pi^2\beta^2}\left(\vec{\beta}\vec{e}_{\tau\pi}\right)^2\left|B\,\ell_{0\tau} - \sum_{\mu=1,2} E_\mu C_\mu \ell_{\mu\tau}\right|^2, \qquad (2.66)$$

where the coherent lengths

$$\ell_{0\tau}^{-1} = q_{0\tau} = \beta^{-1}\left(\omega - \vec{k}_{\tau_t}\vec{\beta}_t\right) - k_{\tau_t}\theta_0 ,$$

$$\ell_{\mu\tau}^{-1} = q_{\mu\tau} = \frac{1}{\beta}\left(\omega - \vec{k}_{\tau_t}\vec{\beta}\right) - k_{\mu z}\theta_0 .$$

The formula (2.66) is written for the π-polarization,i.e.

$$\vec{e}_\pi \| \left[\vec{k}\left[k, \vec{k}_\tau\right]\right], \vec{e}_{\pi\tau}\left[\vec{k}_\tau\left[\vec{k}\vec{k}_\tau\right]\right] ,$$

$$k_{z1,2} = k\left[\frac{k_z^2}{k^2} + g_0 - \frac{\alpha}{2} \pm \frac{1}{2}\sqrt{\alpha^2 + 4g_{\tau_\pi}\, g_{-\tau_\pi}}\right] , \qquad (2.67)$$

$$g_{\pm\tau_\pi} = g_{\pm\tau}\left(\vec{e}_\pi\vec{e}_{\pi\tau}\right) , \vec{k}_\tau = \vec{k} + \vec{\tau}$$

The amplitudes B, C_μ, E_μ are obtained from the boundary conditions

$$B = \frac{2C_1C_2\left(k_{1z} - k_{2z}\right)}{C_1\left(k_z + k_{2z}\right)\left(k_{\tau_z} + k_{1z}\right) - C_2\left(k_z + k_{1z}\right)\left(k_{\tau_z} + k_{2z}\right)};$$

$$E_{1(2)} = \frac{2C_1C_2\left(k_{\tau_z} + k_{2(1)z}\right)}{C_1\left(k_z + k_{2z}\right)\left(k_{\tau_z} + k_{1z}\right) - C_2\left(k_z + k_{1z}\right)\left(k_{\tau_z} + k_{2z}\right)};$$

$$C_{1,2} = \frac{2g_{-\tau\pi}}{\alpha \pm \left(\alpha^2 + 4g_{\tau_\pi}\, g_{-\tau\pi}\right)^{1/2}} .$$

In (2.67) it was taken into account that, when $\left(\frac{\pi}{2} - \theta_0\right) \sim \sqrt{g_0'}$ and $\psi \sim \sqrt{g_0'}$, the difference between the diffraction plane and the crystal surface can be ignored. It gave the possibility to consider the diffraction and the radiation of π- and σ- components of the electromagnetic field independently. The analysis of (2.67) shows that at $\alpha \geq k_z^2 / k^2$, a damping solution appears on

both sides of the crystal surface (surface wave). The phase velocity of such wave is smaller than the particle speed. It means that Cerenkov mechanism of radiation can be realized. Damping of waves along the Z-axis is, thus, not associated with a crystal self-absorption but is determined by the effect of a total external reflection under diffraction condition.

In (2.66) the firs term corresponds to the particle radiation along the path in the vacuum as far as the crystal surface intersection and the term with E_μ^γ to the particle motion inside the medium. The estimation of the coherent lengths shows that the vacuum coherent length $|\ell_{0\tau}|_{max} = L_{0\tau} = |\mathrm{Im} K_{\tau_z}\theta_d|^{-1}$ is determimed by the damping of the surface wave and the particle incidence angle θ_0. Under the exact Bragg condition $(\alpha \to 0)\, L_{0\tau} = \gamma/\omega\theta_0$, where γ is the Lorentz factor of the radiating particle. Thus, the particle starts to radiate effectively at a distance from the surface of the order of magnitude $c\gamma/\omega$, i.e., a factor of γ larger than the radiation wave length. At the same time, the coherent length value $L_{\mu\tau} = |\ell_{\mu\tau}|_{max}$, corresponding to the radiation of the elector inside the crystal, is substantially affected by the self-absorption of quanta in a crystal and the process of multiple-scattering of particles by atoms. We can represent it as

$$L_{\mu\tau} \cong \left(\mathrm{Im} k_{\mu z}\theta_0 + k_\mu \frac{\overline{\theta_s^2}}{2} L_{\mu\tau}\right)^{-1},$$

where $\overline{\theta_s^2}$ is a mean square angle of multiple-scattering per unit of length. As a result, the magnitude of $L_{\mu\tau}$ is limited first of all to the value of the coherent bremsstralung length

$$L_{br} = 2E/E_s\,(L_r c/\omega)^{1/2} \quad .$$

With $\theta_0 \to 0$, $L_{0\tau} >> L_{br}$ and, in (2.67) the main contribution to the SPXR intensity is made by the part of a particle trajectory before the crystal target. By taking into account this fact and integrating (2.66) over frequencies the angular distribution of SPXR can be written in the following form:

$$\frac{dN_\pi}{d\Omega} = \frac{e^2\left(\vec{\beta}\vec{e}_{\tau\pi}\right)^2}{4\pi\beta} \frac{|B(\omega_{0\tau})|^2 L_{0\tau}(\omega_{0\tau})\,\omega_{0\tau}}{1-\vec{n}_t\vec{\beta}}, \tag{2.68}$$

where $\omega_{0\tau} = \dfrac{|2\pi\vec{\tau}\vec{\beta}|}{1-\vec{n}_t\vec{\beta}}$.

It is worth noting that, as an electron moves in the medium, the bremsstralung arising can also diffract by a set of planes under consideration. This diffracted bremsstralung (DB) manifests itself as an additive to SPXR. Under certain conditions, the DB contribution may be substantial and it should be taken into account.

The angular distribution and lines of constant radiation intensity for one of the Ge crystal reflections are shown in Figs.32 and 33, when the electron energy is 500 MeV and the angle of the incidence upon the surface is $\theta_0 = 10^{-5}$ rad (see Figs.30,31). The angle φ is taken from the

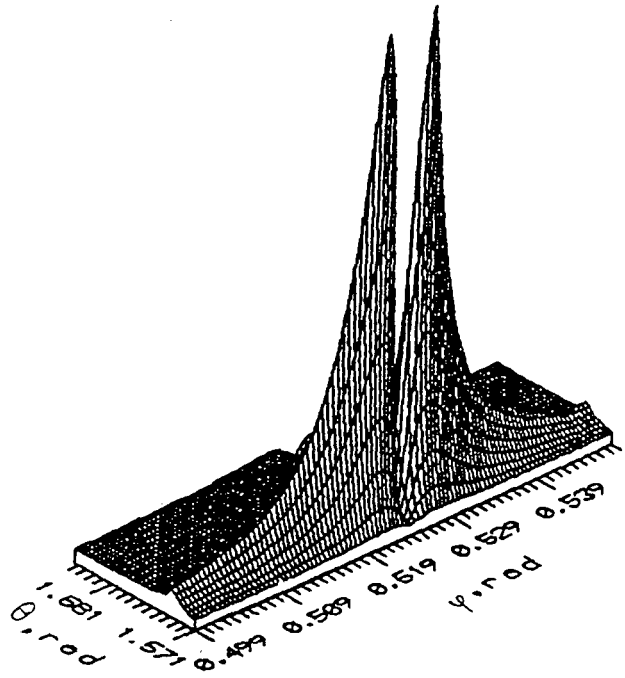

Fig. 32

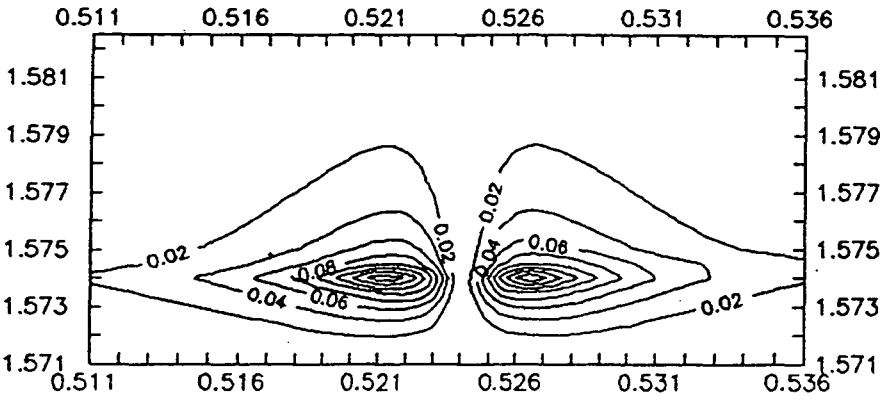

Fig. 33

direction of the tangent component of the electron velocity vector and the angle θ is the angle between the wave vector $\vec{k}$ and the Z-axis. The tangent component of the particle velocity makes an angle of 30° with the crystal direction <100>. Diffraction occurs on (220) planes. The distribution has a typical double-peaked form for the parametric radiation mechanism with a gap in the direction of the double Bragg angle of $\varphi = 2\varphi_B = 30°$. Under such conditions the coherent lengths are $L_{\mu\tau} = 2 \cdot 10^{-2}$ cm, $L_{0\tau} \cong 5 \cdot 10^{-1}$ cm, i.e., $L_{0\tau} >> L_{\mu\tau}$. That is why the main contribution to the distribution is made by a vacuum term. In Fig.34 the dependence of the coherent lengths, $L_{\mu\tau}$ and $L_{0\tau}$ on the incidence angle θ_0 of the electron on the surface is given. In Fig.35 the number N_{γ/e^-} of SPXR quanta at the fixed angle θ, $\Delta\Omega = 10^{-5}$ srad is given as a function of the electron energy. Such quasithreshold dependence of radiation intensity on the particle energy is attributed to the fact that the radiation conditions are satisfied at any energies and at any $\alpha > 0$. However, the radiation intensity is substantial only in the case when a radiated photon is close to the exact Bragg condition of $\alpha \leq |g_0|$. In the case, shown in Fig.35, the threshold particle energy can be estimated as $E_{th} \sim 100$ MeV.

Table VI gives the main parameters of a spectral-angular distribution of SPXR for some reflections of Ge, Si and C crystals. We can see that Ge has the largest quanta yield at the expense of a higher $|g_\tau|$ value. The angular width of peaks in φ is determined from the relation

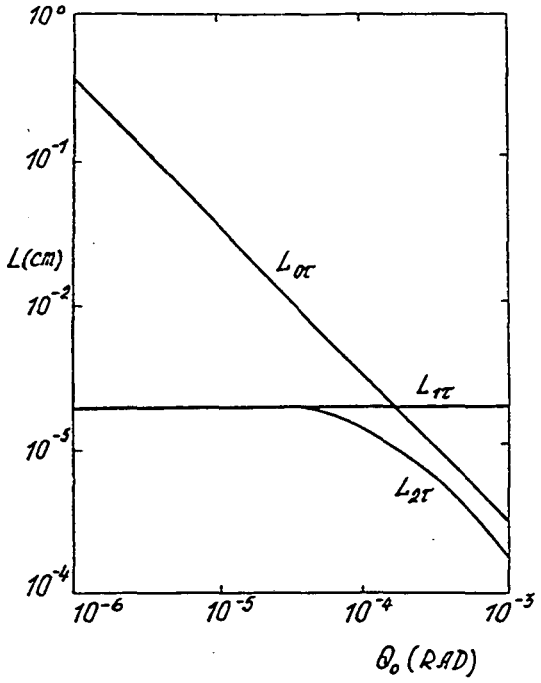

Fig. 34. Here: $L_{0\tau}$ is the vacuum coherent length, $L_{1\tau}$ and $L_{2\tau}$ are the coherent lengths inside the medium, θ_0 is the beam particle incidence angle.

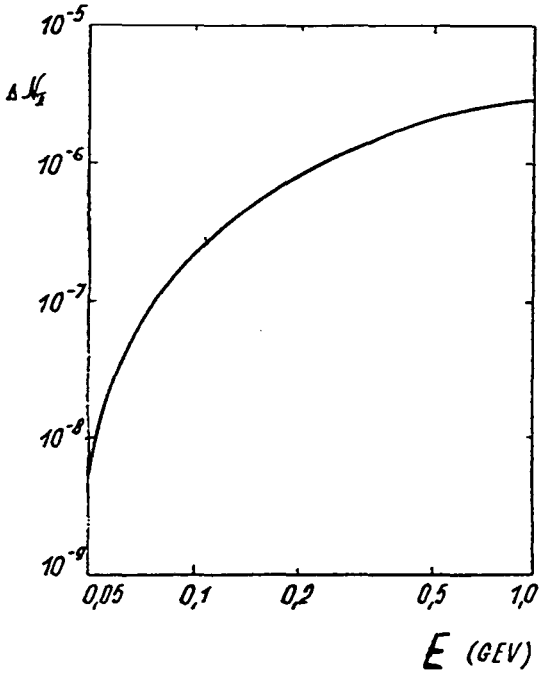

Fig. 35

$\Delta\varphi \cong (\gamma^{-2} + |g_0|)^{1/2}$. The position of SPXR maximum with respect to θ corresponds to the critical angle of total reflection under diffraction condition [104].

Thus, the characteristics of the spectral and angular distribution and energy dependence of the quantum yield of SPXR are analogous to that for PXR generation inside the crystal. At the same time, at the sufficiently small incidence angle of an electron on the crystal surface the main

Table VI

(h,k,ℓ)	ω_5, кэВ	$2\phi_5$, grad	$\lvert g_0 \rvert$ x 10^6	$\lvert g_\tau \rvert$ x 10^6	θ_c, mrad	$\Delta\theta$, mrad	$\Delta\phi$, mrad	ΔN_π x 10^6
(400)	5.06	120	84.6	24.5	8.4	5.0	12.0	1.1
(220)	11.85	30	14.8	8.3	3.1	1.2	4.5	1.9
(220)	3.20	210	208.9	116.5	12.0	11.1	25.1	19.3
(220)	12.4	30	7.3	3.5	2.2	1.0	3.4	0.6
C								
(220)	19.01	30	4.7	1.2	1.9	0.9	3.3	0.13

contribution to the surface radiation intensity may be made by the vacuum trajectory. In this case, multiple scattering does not affect to the radiation process and the vacuum coherent length is limited to the real length of the plate. The estimation of the possibility of observing SPXR experimentally gives [109]: let an electron beam with the energy 500 MeV, the transverse width of 10^{-1} cm, an angular spread of 10^{-4} rad and an energy current of 1μA is incident on Ge crystal with the surface length of the order of 1 cm. In this case, approximately 0.01% of all particles experience effective radiation. As a result, for the (220) reflection of Ge, the photon yield will be of the order of 10^2 quanta/s.

In conclusion it should be noted that, according to the analysis made by Kaminsky, Andriyanchik and us, it is possible the formation of circular polarized quanta under the surface diffraction and, as a consequence, such circular-polarized quanta can be produced at SPXR process.

§6. Parametric X-Ray Radiation in Crystals being Subjected to the Action of High Frequency Ultrasonic Waves.

According to [2,32], in the presence of an external variable field (for example, ultrasonic field) a crystal is characterized by an effective refractive index depending on external field parameters. Changing these parameters we can change the properties of parametric radiation.

As the characteristics and yield of PXR depend on the solution $\vec{E}^{(-)}(\vec{r},\omega)$ of homogeneous Maxwell's equation describing diffraction process in crystals, then the investigation of the external ultrasonic (US) field influence on diffraction of X -ray points to the strong influence of an US external field on the PXR process. It was shown in [112] that the action of US wave can be resonant in the case of intersection of dispersion surface branches and, as a consequence, the degeneration of refractive indices. In [114] it was pointed to the essential modification of scattering process and X-ray radiation process under diffraction condition in crystals. Due to dynamical character of PXR formation, according to [115], the influence of US wave on this process will be maximum under the coincidence of the wave length of US with the period of extinction beatings.

The theory of PXR under the action of an external US wave to a crystal target was derived in papers [116-120]. The boundary problem of diffraction of X-rays by a crystal target being subjected to an US external wave was solved in the case of two-wave diffraction in [121-123]. We do not give here the expressions for photon wave functions $\vec{E}^{(-)}(\vec{k},\vec{r})$ because they are very clumsy. The spectral-angular PXR distribution in the presence of US wave was obtained in [117-

118]. It was pointed to two new effects which manifest themselves at definite conditions in the PXR generation process.

The first effect, acoustic-parametric resonance, manifests itself as an increase of PXR absorption length under the action of US wave and leads to the increase of angular density of radiation in thick crystals within a narrow angular region. Indeed, it is well-known (see also §1) that the refractive index of centresymmetric crystal under diffraction conditions in X-ray spectrum range is represented in the form:

$$n_{1,2} = 1 + \frac{1}{4}\left(-\alpha\beta_1 + g_0(1+\beta_1) \pm \sqrt{(\alpha\beta_1 + g_0(1-\beta_1))^2 + 4\beta_1 g_\tau^s g_{-\tau}^s}\right), \quad (2.69)$$

where all definitions are given in §1.

The Cerenkov condition

$$1 - \beta n \cos\theta = 0$$

is fulfilled, as pointed out in §1, only for n_1, for a rather big deviation from the exact Bragg condition. In this case the absorption coefficient is practically the same as in amorphous medium $\mu_0 = \frac{1}{2} k g_0''$ and the effect of anomalous X-ray transition under diffraction [124] is not realized. The action of the US wave leads to the change of dielectric properties of a crystal. The modified refractive index in the case of

$$æ < \frac{k(\theta^2 + \theta_{ef}^2) + \beta_1 r_s'}{2\zeta(\theta^2 + \theta_{ef}^2)}, \quad (2.70)$$

can be written in the following form:

$$n_{1,2}^{p} = n_{1,2} + p\frac{æ\zeta}{k}, p = 0, \pm 1$$

where $\vec{æ}$ is the US wave vector, θ is the photon radiation angle, $\vec{k}$ is the photon wave vector, $\theta_{ef}^2 = \gamma^2 + g_0' + \overline{\theta_s^2}$, $\zeta = \cos\left(\vec{k} \wedge \vec{æ}\right)$, $r_s' = R_e\left(g_\tau^s g_{-\tau}^s\right)$, $\beta = u/c$. The analysis shows that, if

$$æ = \frac{k}{2\zeta}\left(\theta^2 + \theta_{ef}^2 + g_\tau^2 \frac{g_\tau^{s''}}{g_0''}\right), \tag{2.71}$$

then the Cerenkov condition for one of the branches n_1^{+1} is satisfied under the simultaneous fulfillment of condition of anomalous X-ray penetration. In this case the absorption length of PXR increases, consequently, the coherent length of PXR formation also increases (at the condition of Req = 0, the coherent length is restricted by the photon absorption length in crystals). The growth of coherent length, obviously, leads to the increase of the spectral and angular densities of radiation. The spectral-angular distribution of PXR within the narrow region close to the exact Bragg direction $\vec{k\beta} + \vec{\tau}$ for the case of Laue diffraction in a crystal being subjected to the action of the transverse US wave can be represented in the form:

$$\frac{d^2N^s}{d\omega d\Omega} = \frac{e^2\left(\vec{e}_s\vec{\beta}\right)^2}{4\pi^2}\left|\sum_{a,b,p,p'} A_{ab}^{spp'}\left[e^{iL/L_{ab}^{spp'}} - 1\right]\left[\ell_0 - \ell_{ab}^{spp'}\right]\right|^2, \tag{2.72}$$

where ℓ_0 and $\ell_{ab}^{spp'}$ are the coherent lengths in the vacuum and in a crystal, correspondingly,

$$\ell_0 = (kq_0)^{-1},\ q_0 = \frac{1}{2}\left(\theta^2 + \gamma^2\right);\ \ell_{ab}^{spp'} = \left(kq_{ab}^{spp'}\right)^{-1}$$

$$q_{ab}^{spp'} = \frac{1}{2}\left(\theta^2 + \gamma^2 + \overline{\theta_s^2} - 2p\frac{æ}{k}\zeta - \lambda_{ab}^{sp'}\gamma_0\right),$$

$\lambda_{ab}^{sp'}$ is the solution of the diffraction dispersion equation in the presence of the transverse US wave, the amplitudes $A_{ab}^{spp'}$ are given in [116].

The analysis shows that the cross-section of photon radiation in a crystal being subjected to the action of a transverse US wave, in general case, is determined by 36 coherent lengths. For each from waves with the wave vectors $\vec{k} + p\vec{æ}$ ($p = 0, \pm 1$) there are six coherent lengths corresponding to different stationary superpositions of electromagnetic waves which are formed by the interaction of incident and diffracted waves with a definite polarization in a crystal. The same number of coherent lengths characterizes the formation process of radiation with the another polarization. Let us recall, that the radiation process in an amorphous medium is determined by one coherent length and in unperturbed crystal there are four coherent lengths determining the radiation formation. However, it should be said, that the requirement of Cerenkov condition fulfillment strongly restricts a number of coherent lengths which are determined the PXR intensity.

In [117] it was given the detailed analysis of radiation in a weakabsorbing and strong-absorbing (thick) crystals. The most interesting situation the later; when $L >> L_{abs}$. In this case the influence of the US oscillations on PXR can be essential. If the coherent length in an unperturbed crystal is restricted by

$$L_1^0 \cong 2\left(k\beta_1 g_0''\right)^{-1},$$

then, under the fulfillment of the condition (2.71), we have

$$L_1^{-1} \cong L_1^0,\ L_1^{+1} \cong L_1^0\frac{\beta_1 r_s' + \delta_s^2}{r_s^1 - \delta_s^2} >> L_1^0 .$$

Here $\delta_s = r_s''/2g_0''$, $r_s'' \equiv \mathrm{Im}(g_\tau g_{-\tau})$. Because the angular radiation density is proportional to the square of coherent length (see (2.72)) then, obviously, the increase of PXR intensity is possible. The analysis of (2.72) and the angular distribution, obtained in [116,117], shows, that this increase takes place within the narrow angular interval in which the influence of US oscillations is the greatest

$$\Delta\theta_{vs} = \left(r_s' - \delta_s^2\right)^{1/4} .$$

As in the unperturbed crystal $\Delta\theta_{ef} = \left(\gamma^{-2} + \overline{\theta_s^2} - g_0'\right)^{1/2}$, then you can see that $\Delta\theta_{vs} << \Delta\theta_{ef}$. It is important to note that the angular width of the region of PXR intensity growth is determined only by crystal parameters and does not depend on generating particle characteristics and the US amplitude.

The angular density of PXR is quadratically depends on the US amplitude when this amplitude is much less than the interplanar distance of a crystal. In [116,117] it was obtained the angular and spectral PXR characteristics in crystal under the action of longitudinal and transverse US waves, which amplitudes are less than a crystal interplanar distance ($\vec{\tau}\vec{a} << 1$) for the geometries of Laue and Bragg. In Fig.36, the result of numerical calculation of the angular distribution of PXR generated by electrons with the energy of 500 MeV in the reflex (220) of Si crystal being subjected to the action of transverse US wave (ω_B = 8 keV) is shown. It is important to note that the considered effect becomes stronger with decreasing the crystal temperature [117-119]. The temperature dependence of the additional intensity to the PXR angular distribution on the crystal temperature is shown in Fig.37. The authors of [117,119] suggested to apply the effect of acoustic-parametric resonance for the investigation of the temperature dependence of the imaginary part of the crystal susceptibility.

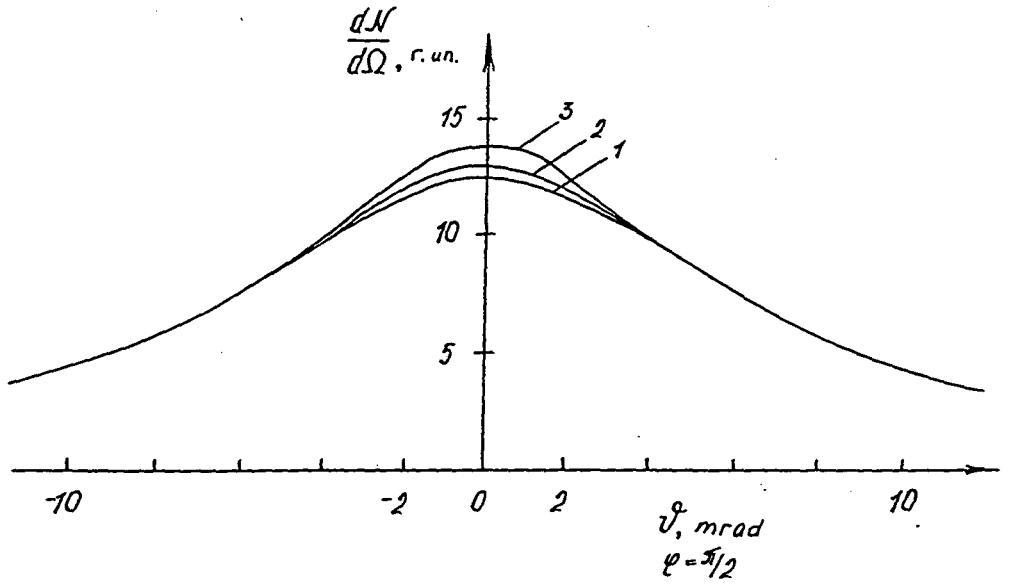

Fig. 36. Here: L = 2 mm, æ = æ$_{th}$, the US frequency $\nu \cong 7.54 \cdot 10^8$ Gz, g = 1/2 $\vec{\tau}\,\vec{a}$ are 1) 0; 2) 0.06; 3) 0.1.

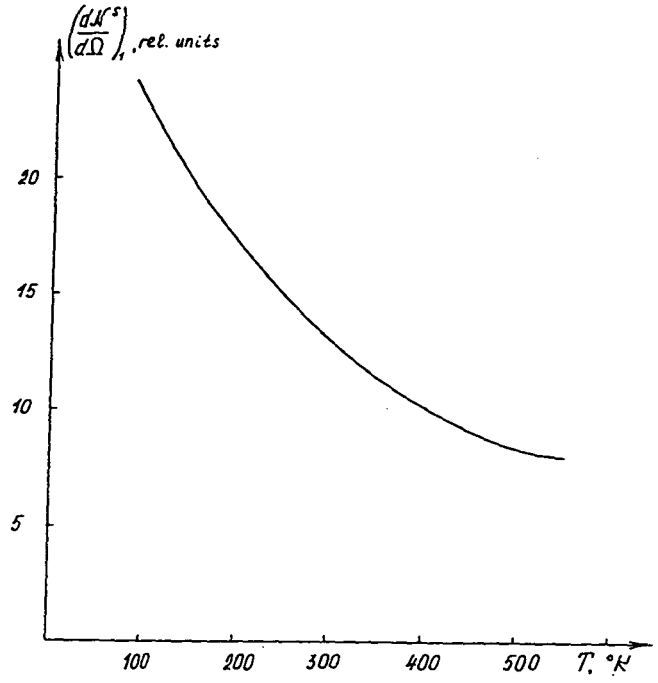

Fig. 37

The second effect, resulting from the action of US wave to the crystal, is the X-ray-acoustic resonance. It manifests itself under simultaneous fulfillment of both Cerenkov and X-ray acoustic resonance conditions. Under the X-ray-acoustic resonance it is possible the oscillations in the OXR spectral-angular distribution with the period depending on the amplitude of US wave. The corresponding theory is given in [117-120].

It is known that the action of US wave can result in the intersection of diffraction dispersion branches, that is the degeneration of refractive indices take place at the zero amplitude of oscillation. The degeneration of refractive indices is possibly only from some threshold magnitude of the US wave vector. The US wave with the amplitude $a \neq 0$ destructs the degeneration within the region of $\Delta\alpha \sim \zeta g_\tau^s$ where $\zeta = \frac{1}{2}\vec{\tau}\vec{a}$. It is interesting that the US wave with the wave vector close to the threshold magnitude does not influence the PXR, because the degeneration of refractive indices of a crystal takes place far from the Cerenkov condition. The influence on the OXR characteristics will be resonant under simultaneous fulfillment of both Cerenkov condition and the condition of X-ray-acoustic resonance. The calculation shows that the US wave vector, in this case, should satisfy the condition

$$æ = \frac{k\left(\theta_{ef}^2 + \theta_r^2\right) + \beta_1 r_s'}{2\zeta\left(\theta_r^2 + \theta_{ef}^2\right)},$$

where θ_r is the angle which corresponds to the resonance condition. In the case of the resonant field there are the waves the refractive indices of which differ from each other only by the small magnitude $|\zeta g_\tau^s|$ being proportional to the US amplitude.

The interference of the waves with the different refractive indices results in the oscillation dependence of the PXR spectral-angular density on the US amplitude in a weakabsorbing crystal. Besides, the PXR angular density, under the condition of X-ray-acoustic resonance, can essentially change. In most cases the angular density in the direction of diffraction reflex decreases.

At the same time , the angular density in the forward direction, i.e., in the particle motion direction, increases. The angular interval of the effect observation is $\Delta\theta \sim |\zeta g_{\tau}^{s}|$. The magnitude of the angular density, in this case, does not depend on the oscillation amplitude and is determined only by characteristics of a crystal and of a charged particle. In Fig.38 the modification of PXR angular density as a function of the US wave vector is shown. The third situation corresponds to the X-ray-acoustic resonance condition.

The ultrasonic oscillations influence not only the radiation angular distribution but also its polarization and the energy dependence of radiation intensity [119,120]. The thing is that the resonant action of US oscillations changes the angular density of parametric radiation and, consequently, changes a photon number recorded by a detector with a definite angular size. The

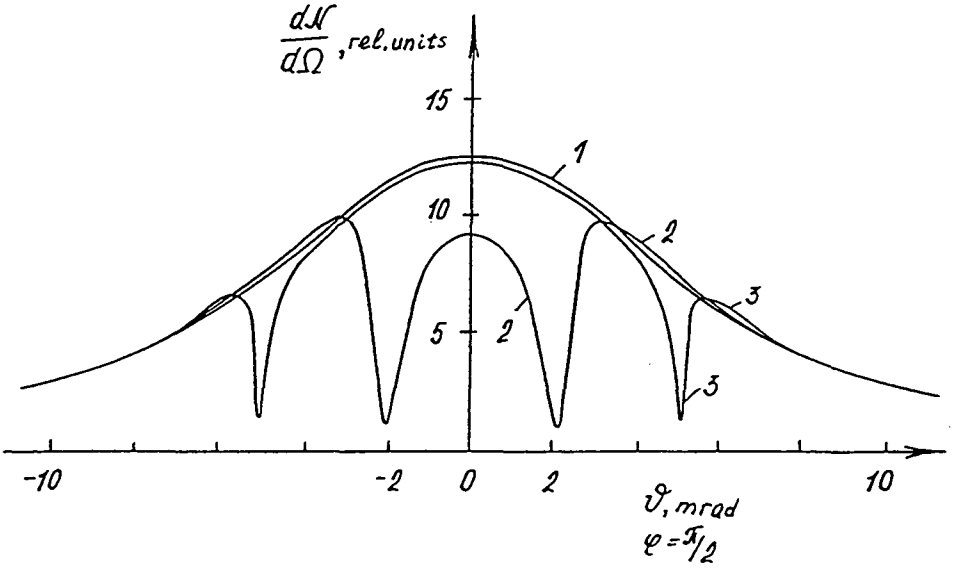

Fig. 38Here: The PXR angular distribution in Si (220), E = 900 MeV, the asymmetry factor β = 1, ω_B = 8 keV, æ = z æ$_{th}$: 1)g = 0, z = 0; 2) g = 0.1, z = 1.9, $\nu_s = 5.87 \cdot 10^8$ Gz; 3) ζ = 0.1, z = 3, $\nu_s = 9.28 \cdot 10^8$ Gz.

resonant conditions depend on the energy of radiating particles and, as a consequence, a number of photons, incident on a detector, can increase or decrease with changing the particle energy. As a result, the energy dependence of PXR intensity, recorded by a detector with the angular size of

$\Delta\theta_D$, becomes more complicated. The modification of the threshold dependence of PXR intensity as a function of the US wave amplitude is shown in Fig. 39 ($\hbar\omega_B$ = 8 keV,.$\theta_D = 10^{-3}$ rad, the plane (220) in Si):

The US oscillations influence the polarization characteristics of PXR as well. Because the conditions of the resonant influence of US waves on the π- and σ-polarizations are different, the polarization of produced radiation will depend on the parameters of an external US wave. This can allow to change the PXR polarization by the resonant action of a US wave. The change of the PXR polarization with changing the US wave vector relative to the threshold magnitude is shown in Fig.40. You can see that the action of US wave can essentially modify the polarization degree of the detected radiation indeed.

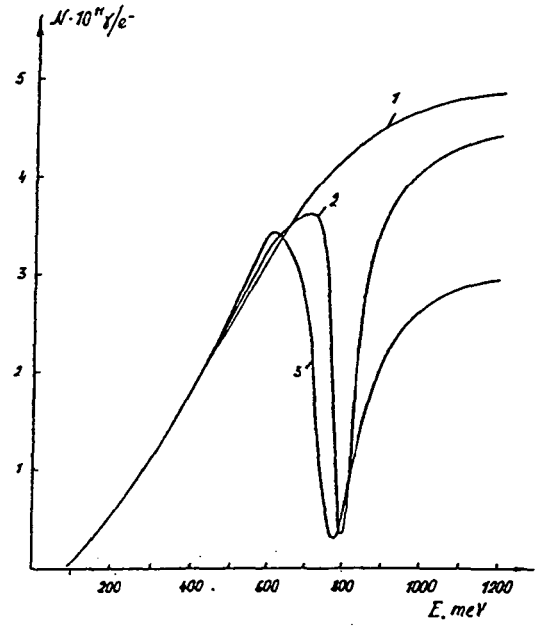

Fig. 39

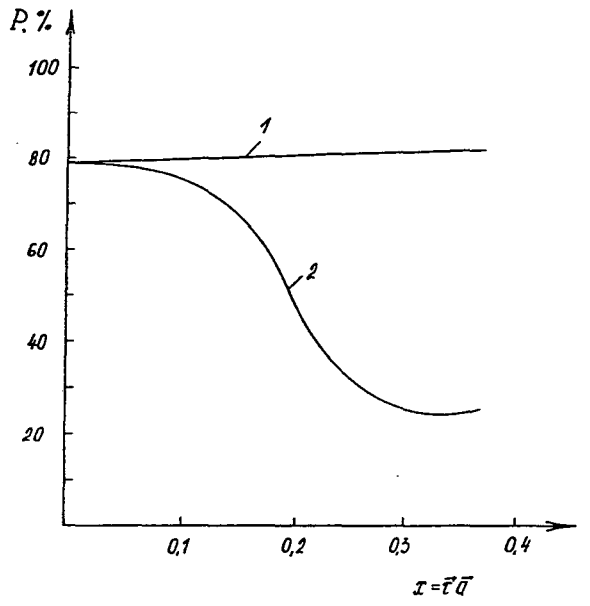

Fig. 40. Here: P is the PXR polarization power in Si (220), $\theta_D = 10^{-3}$ rad, æ = zæth: 1) z = 1, $\nu_S = 4.17 \cdot 10^8$ Gz; 2) z = 1.5, $\nu_S = 6.26 \cdot 10^8$Gz.

Part III. DIFFRACTION X-RAY RADIATION BY RELATIVISTIC OSCILLATOR (DRO).

As we discussed above, the X-ray radiation of a relativistic oscillator in a crystal essentially modifies under diffraction conditions of emitted photons. A new diffraction radiation of iscillator (DRO) appears as a result of coherent summation of two processes — photon radiation and photon diffraction, but it can not be reduced to the sequence of these two processes. The relativistic oscillator itself can be or a relativistic atom or a relativistic charged particle channeled in the potential well of averaged crystallographic potential of axes (planes), or an oscillator formed by an external electromagnetic field (ultrasonic, laser). It was shown in [2,13,19,27,28] that the DRO spectrum is rather complex and is determined by complex and anomalous Doppler effect (see §1).

It is known that the transverse energy of channeled electrons (positrons) is discrete and state to state transitions result in the radiation , i.e., in this case a channeled particle is like an one-dimensional or two-dimensional oscillator with the eigenfrequency in the laboratory frame $\Omega_{nf} = \varepsilon_n - \varepsilon_f$, where ε_n and ε_f are the eigenvalues of corresponding one- or two-dimensional Schrodinger's equation, in which the particle rest mass is replaced by its total energy $m\gamma$.

For the analysis of DRO characteristics it is necessary to obtain the spectral-angular distribution. The description of channeled particle motion by the help of one- or two-dimensional Bloch functions was given in [125]. The expressions for spectral-angular DRO distribution for different cases of photon dynamical diffraction were obtained in [17-19]. For example, in the case of two-wave Laue diffraction the spectral-angular distribution of DRO can be written in the following way[17-19]":

$$\frac{d^2N_s^\tau}{d\omega d\Omega} = \frac{e^2\beta_1^2\omega}{\pi^2\hbar c^3}\sum_{nf} Q_{nn}\left|\vec{e}_{0s}^{\,\tau}\,\vec{g}_{nf}\right|^2\left|\sum_{\mu=1,2}\zeta_{\mu s}^{\tau}\frac{1-e^{-iq_{znf}^{\mu s}L}}{q_{znf}^{\mu s}}\right|^2, \qquad (3.1)$$

where

$$q_{znf}^{\mu s} = \omega\left(1 - \beta_{\parallel}\cos\theta\right) - \Omega_{nf} - \frac{\omega}{\gamma_0}\delta_{\mu s} \qquad (3.2)$$

$\varepsilon_{\mu s}$ was determined in §2, θ is the angle between the photon wave vector $\vec{k_\tau}$, directed at a small angle relative to the particle velocity, and the Z-axis. In the dipole approximation, that is true for the X-ray radiation, we have

$$\vec{g}_{nf} = -i\left[\beta_{\parallel}\vec{n}_z\left(\vec{k}_{\perp}\vec{\rho}_{nf}\right) + \Omega_{nf}\vec{\rho}_{nf}\right]$$

in an arbitrary nondipole case $\vec{g_{nf}}$ is defined in [17,18],

$$\vec{\rho}_{nf} = \int_{\Delta} \varphi_{n\vec{k}}(\vec{\rho})\,\vec{\rho}\,\varphi^{*}_{f\vec{k}}(\vec{\rho})\,d^2\rho\ ,$$

$\varphi_{n\vec{k}}$ and $\varphi_{f\vec{k}}$ are the two-dimensional Bloch-functions satisfying the equation like Schrodinger's one (see [17-19], L is the crystal target length, Q_{nn} is the population probability of a particle transverse energy state n.

According to (3.1) the maximum intensity should be observed at the angles and frequencies which satisfy the equation

$$\omega\left(1 - \beta_{\parallel}\cos\theta\right) - \Omega_{nf} - \frac{\omega}{\gamma_0}\delta_{\mu s} = 0 \qquad (3.3)$$

The solutions of this equation were obtained in §1.

In the case of rather thick crystals the angular distribution of DRO was obtained in [2,18,19].For example, the angular distribution of radiation generated by plane-channeled particles can be written as [2]:

$$\frac{dN_\tau^s}{d\Omega} = \frac{e^2 L_{ef} \beta_1^2}{2\pi} \sum_{nf} Q_{nn} |x_{nf}|^2 \sum_{\mu} \frac{(\omega_{nf}^{\mu s})^2}{\Omega_{nf}} \left|\zeta_\tau^{\mu s}(\omega_{nf}^{\mu s})\right|^2 \left[1 - \frac{(\omega_{nf}^{\mu s})^2}{\gamma_1 \Omega_{nf}} \mathrm{Re}\left(\frac{\partial \delta_{\mu s}}{\partial \omega}\right)\right]^{-1}_{\omega = \omega_{nf}^{\mu s}} \cdot F_s(\theta, \varphi) \qquad (3.4)$$

for r -polarization:

$$F_r(\theta, \varphi) = \left\{\beta_1 \omega_{nf}^{\mu\sigma} \sin^2\theta \cos\varphi \frac{\tau_y \cos\varphi - \tau_x \sin\varphi}{|\vec{\tau}_\perp|} + \Omega_{nf} \frac{\tau_z \sin\theta \sin\varphi - \tau_y \cos\theta}{|\vec{\tau}_\perp|}\right\}^2$$

and for π-polarization

$$F_\pi(\theta, \varphi) = \left[\frac{\beta_1 \omega_{nf}^{\mu\sigma} \sin\theta \cos\varphi [\cos\theta (\vec{n}, \vec{\tau}) - \tau_z]}{|\vec{\tau}_\perp|} + \Omega_{nf} \frac{[\sin^2\theta \cos\varphi (\vec{n}_1 \vec{\tau}) - \tau_x]}{|\vec{\tau}_\perp|}\right]^2$$

where $\omega_{nf}^{\mu s} = \Omega_{nf}\left(1 - \beta \cos\theta - \gamma_1^1 \mathrm{Re}\, \delta_{\mu s}(\omega_{nf}^{\mu s})\right)^{-1}$,

x_{nf} is the matrix element, determined through the one-dimensional Bloch-functions, L_{ef} is the effective length (at $L < L_{abs}$, $L_{ef} = L$, $L >> L_{abs}$, $L_{ef} = L_{abs}$, where L_{abs} is the absorption length). The term in square brackets takes into account the influence of medium dispersion on the angular distribution. Because the frequency, satisfying the dispersion equation (3.3), belongs first to one dispersion branch and then the another one with changing the radiation angle θ,(see the analysis in §1) the summation over the solutions μ means that we select the corresponding root of the dispersion equation for each definite radiation angle θ, $\vec{n_1}$ is the unit vector directed along the wave vector of the photon propagating at a small angle relative to the mean velocity of a channeled particle.

The numerical calculation of the angular DRO distribution taking into account the dispersion characteristics of the medium under diffraction conditions, was made in [29]. According

to Fig.41 the angular distribution has a fine structure which corresponds to the region of transition from one dispersion branch to the another one. You can see that the DRO distribution looks like two narrow rings — the first one corresponds to the solution $\mu = 2$ and the second one to $\mu = 1$

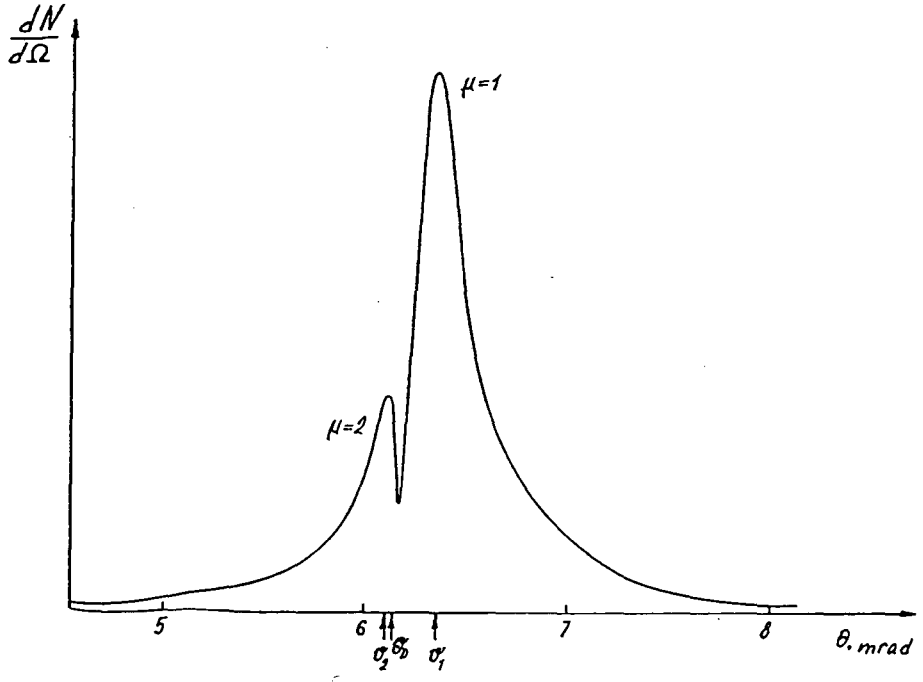

Fig. 41

(in the case of PXR generation only one solution satisfies Cerenkov condition). The angular position of maxima in the DRO distribution can be estimated in the first approximation as:

$$\theta_{1,2} = \sqrt{\theta_D^2 \pm \frac{\sqrt{\beta r_s'}}{\sqrt{1 + 2\sin^2\theta_B}/\frac{\Omega}{\omega_B}}}\ , \qquad (3.5)$$

where θ_D is the angle which satisfies the following equation

$$\theta^2 + \gamma^{-2} + \frac{\omega_L^2}{\omega_B^2} - \frac{2\Omega_{nf}}{\omega_B} = 0$$

θ_B and ω_B are the angle and the frequency satisfying the exact Bragg condition. For example, according to Fig.40, the values of these angles are $\theta_1 = 6.1 \cdot 10^{-3}$ rad and $\theta_2 = 6.2 \cdot 10$ rad. The ratio of the angular width to the value of the angle θ is about of $\Delta\theta/\theta_D \cong 0.1$. The expressions for the radiation angular distribution are essentially simplified if the particle energy is rather small ($1 - \beta \gg 1/\gamma_{0,1}$ Re $\delta_{\mu s}$). In this case we can consider the frequency, corresponding to the maximum intensity, not to depend on the dielectric properties of a crystal and to be determined only by the radiation angle. The DRO characteristics, in this case, were considered in [126].

In [127] the possibility of the DRO experimentally observation by measuring the angular distribution was analyzed. It was shown that this experiment demanded particle beams of high quality because the radiation characteristics were very sensitive to the particle beam parameters. Indeed, the DRO angular distribution, shown in Fig.41, takes place only for the particle beam which characteristics satisfy the following inequality:

$$\frac{\Delta\gamma}{\gamma} + \frac{(\Delta\theta_{ef}\gamma)^2}{2} + \frac{2\pi\gamma^2}{k_B L_0} < \frac{\gamma^2\sqrt{\beta r_s'}}{2} \qquad (3.6)$$

where γ is the Lorentz factor, $\Delta\theta_{ef}$ is the angular spread, $\Delta\gamma/\gamma$ is the energy spread, $\Delta\Omega = \frac{2\pi c}{L}$ is the divergence of the oscillator eigenfrequencies.

In the opposite case the angular width of maxima is equal to

$$\Delta\theta = \frac{1}{\gamma}\left(\frac{2\Delta\gamma}{\gamma} + (\theta_{ef}\gamma)^2 + \frac{4\pi\gamma^2}{k_B L_0}\right)^{1/2} \qquad (3.7)$$

As an example, the dependence of DRO angular distribution characteristics on the energy divergence of the particle beam is shown in Fig.42. You can see that this dependence is rather sharp indeed.

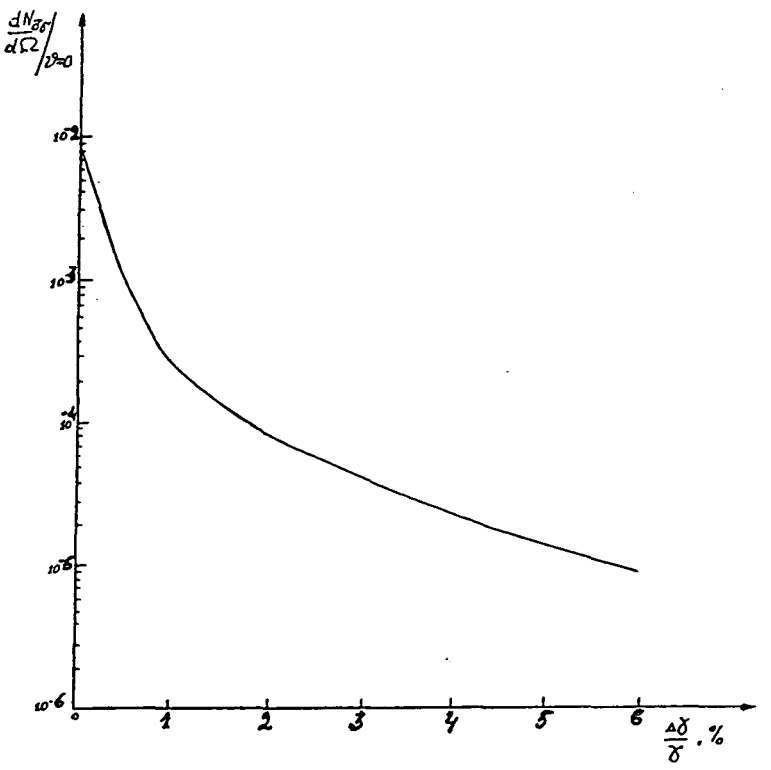

Fig. 42

The dependence of the radiation angular density on the relativistic oscillator energy, which has a "resonance" character at a given angle of the radiation observation, was also considered in [127]. If the observation angle is equal to zero, the maximum of the angular distribution sharply increases with $\gamma \to \gamma^R = (\omega_B/2\Omega)^{1/2}$. When the frequency ω_B equals $\omega_B = \omega_m\theta_x = 2\Omega\gamma^2$ the maximum value of the radiation density is observed at γ being a little more than γ_R. The angular distribution , in this case, looks like a bell and its width decreases sharply with $\gamma \to \gamma_R$ (see Fig.43). In the region of $\gamma > \gamma_R$ ($\omega_B < \omega_{max}$) the single narrow maximum splits into two peaks (φ is fixed), which shift to the region of larger radiation angles θ with increasing the particle energy E. In [127] the relative estimations was given for the contributions from different radiation mechanisms to the total radiation angular distribution which can be observed in a definite reflex. It

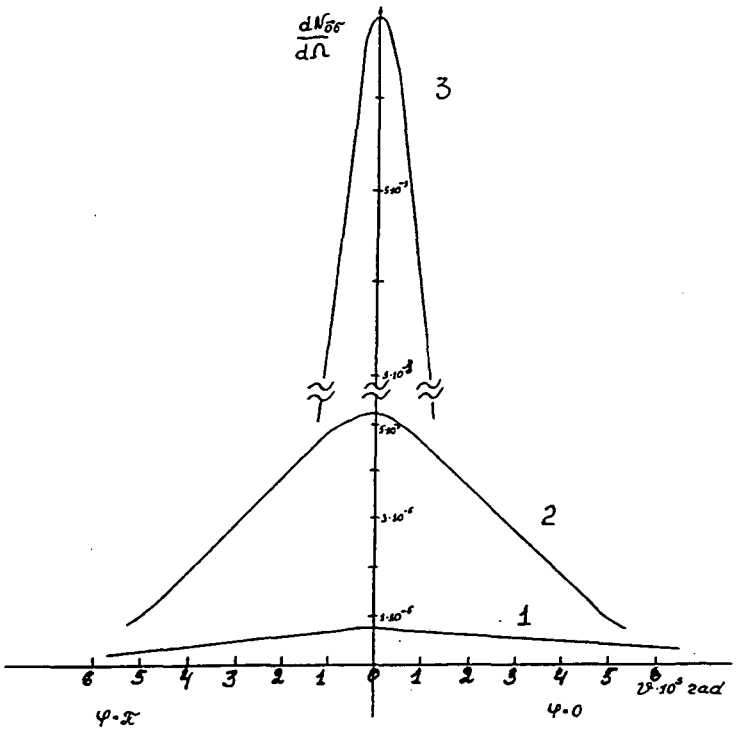

Fig. 43

was shown that at $\Delta\gamma/\gamma \sim 1\%$ the ratio of the DRO angular density to the density of diffraction bremsstralung at $\theta = 0$ was

$$R_1 = \frac{I_{DRO}}{I_{DB}} = \frac{Q_{nn}\theta_L^2\left(\sin^2\psi + \cos^2 2\theta_B \cos^2\psi\right)}{\left(1 + \cos^2 2\theta_B\right) 4\,\overline{\theta_s^2}\, L\left(\Delta\gamma/\gamma\right)^2} \qquad (3.7)$$

where the estimation is given for a channeled electron (positron), θ_L is the Lindhard's angle, ψ is the angle between the particle oscillation plane and the diffraction plane, $\overline{\theta_s^2}$ is the mean square angle of multiple scattering per unit length, $1/4\ \theta_L^2$ is the classical estimation of the magnitude $|x_{nfi}|^2\ \Omega^2\ c^{-2}$. For Si crystal, the channeled electron with the energy of E = 23.6 MeV ($\gamma \approx \gamma_R$) (planes of channeling (100), $\theta = 0$, diffraction plane is (220)) the value of the ration is $R_1 = 25$, that is the DRO intensity is 25 times larger than the intensity of the diffraction bremsstralung at $\Delta\gamma/\gamma \cong 1\%$ and $\Delta\psi^2\gamma^2 < \Delta\gamma/\gamma$. If the diffraction radiation is observed at the angle $\theta \neq 0$, we should compare it with the contribution from the parametric (quasi-Cerenkov) radiation. In this case the analogous ratio is estimated as [127]

$$R_2 = \frac{I_{DRO}}{I_{RxR}} \cong Q_{nn} \left(\frac{\theta_L}{4\frac{\Delta\gamma}{\gamma}\theta_D} \right)^2 \frac{\left(1 + \theta_D^2\gamma^2 + \gamma^2\gamma_n^{-2}\right)^2 \left(\sin^2\psi + \cos^2\psi\cos^2 2\theta_B\right)}{\left(\sin^2\varphi + \cos^2\varphi\cos^2 2\theta_B\right)}, \tag{3.8}$$

where φ is the angle between the wave vector $\vec{k}$ and the diffraction plane, $\gamma_n = \omega_B/\omega_L$ is the Lorentz factor corresponding to the threshold magnitude of the energy $E = mc^2\left(g_0'\right)^{-1/2}$. You can see that this ratio essentially depends on the value of azimuthal angle φ. For example, for Si this ratio is estimated as $R_2 \cong 5$ if the electron with energy of E = 34 MeV is channeled between the planes (100) and the diffraction plane is (220).

Thus, the experimental observation of the diffraction radiation of oscillator is possible by the help of the particle beams with the high quality.

Relativistic oscillator can be formed not only by an unperturbed crystal channel but also by an external ultrasonic or laser field which subjects to the crystal and forms a bent crystal channel. In [128] the radiation of electrons (positrons) in a crystal, being subjected by the action of a laser wave, which forms an oscillator, was considered. The estimations for the intensity of such radiation were given. A relativistic oscillator can be a channeled particle, which moves in a plane channel, bent by a variable external field (ultrasonic or laser wave), i.e., in some electromagnetic undulator [14]. In this case, the oscillator frequency in the laboratory frame is $\Omega' = æ_z u - \Omega$, where $\vec{æ}$ is the wave vector of an external wave in a crystal, Ω is its frequency (the Z-axis is chosen along the direction of an average particle velocity $\vec{u}$). The diffraction radiation of oscillator, being formed by an external ultrasonic wave, was considered in [129].

According to [14], the trajectory of a particle moving in the dynamic ultrasonic undulator is written in the following form (see Fig.44)

$$\vec{r}(t) = \vec{r}_{ch}(t) + \vec{r}^{s}(t) = \vec{r}_{ch}(t) + \vec{a}\cos\left(\Omega' t + \delta\right), \tag{3.10}$$

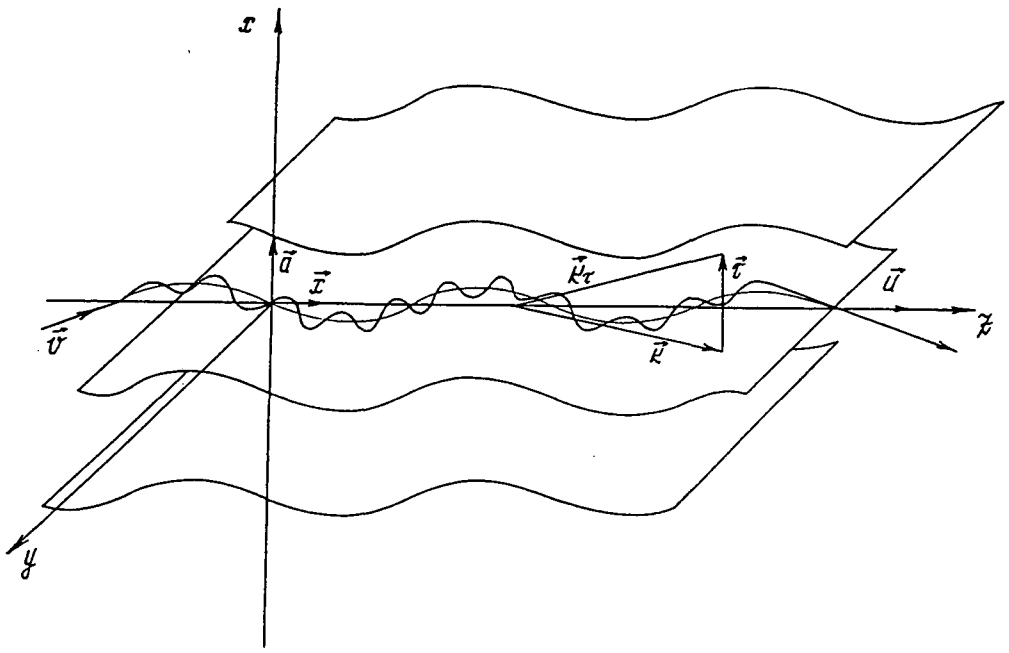

Fig. 44

where $\vec{r}_{ch}(t)$ is the radius vector describing the ordinary high-frequency channeled particle motion and $\vec{r}^{s}(t)$ is the radius vector describing the motion of particle in the dynamic undulator. Assuming that the frequency of ultrasonic wave is much smaller than the frequency of particle oscillations in a crystal channel, we can consider these two kinds of particle motion independently: the ordinary channeled particle motion and the motion of the equilibrium trajectory center of particle gravity inside the bent channel formed under the action of the external variable field. $\vec{a}$ and δ are the amplitude and the initial phase of particle oscillation in the ultrasonic channel. It should be noted that, if the ultrasonic wave amplitude satisfies the condition $a << uU(Ed\text{æ}^2)^{-1}$ (E is the particle energy, d is the crystal channel width and V is the depth of the potential well for a crystal channel), then the radius of the crystal curvature due to the action of the ultrasonic wave is much larger than the radius of the trajectory curvature for the channeled particle incident on the crystal at the Lindhard angle. In this case, the equilibrium trajectory of a positively charged particle gravity center corresponds to the trajectory of a stable channeling regime, and the curvature of the crystal

channel, caused by the action of the ultrasonic wave, leads only to the displacement Δ of the equilibrium trajectory center of gravity during the particle movement through the crystal. That is why, for positively charged particles, for which $a_f + \Delta \leq d/2$, we can take into account the dechanneling effect, because of channel curvature, by considering the mean square angle of multiple scattering in this bent channel in the same way as in an amorphous medium [129] (a_f is the amplitude of particle oscillation for the ordinary channeling regime).

In the case under consideration an essential difference arises compared with the diffraction radiation from the oscillator caused by a channeled particle. This is that the atomic (nuclear) oscillations, resulting in the formation of the ultrasonic undulator, will simultaneously lead to the dielectric constant modulation in a crystal and, consequently, can change the diffraction process itself. As a result, the photon wave function changes. The Maxwell's equations describing this situation is given in [129]. The case when the influence of ultrasonic wave on the X-ray diffraction process can be reduced only to the change of the magnitude of Fourier-components of crystal dielectric susceptibility was considered in detail. It was obtained the spectral-angular distribution and was separated the contributions of parametric (quasi-Cerenkov) radiation and DRO itself. The spectral and angular characteristics were analyzed and the total number of photons in a diffraction peak was estimated.

It was shown that, if the following inequality

$$(a\Omega')^2 > (a_f\Omega_f)^2$$

is fulfilled, the intensity of the diffraction radiation by a particle in the external field will be more intensive than DRO by ordinary channeled particle (a_f and Ω_f are the amplitude and the frequency of particle oscillations in an unperturbed channel). According to [14], this inequality can be realized for a standard ultrasonic field source and, as shown by the estimations, the influence of this wave on dechanneling process can be ignored in this situation.

In conclusion, it should be noted that the diffraction radiation can also be formed under the motion of oscillator over the crystal surface, by analogy to the surface parametric (quasi-Cerenkov) radiation. The main difference of the surface DRO from the SPXR is that, in this case, both radiation dispersion branches give the contribution to the radiation intensity. It is also possible to observe in the vacuum not only normal but also anomalous Doppler effect which is accompanied by the excitation of the radiating oscillator itself.

Part IV. COOPERATIVE EFFECTS in X-RAY RADIATION by CHARGED PARTICLES in CRYSTALS.

The high spectral and angular densities of parametric (quasi-Cerenkov) and diffraction radiation of oscillator and also narrow spectral and angular widths of radiation reflex give the basis of application of considered spontaneous mechanisms of X-ray radiation for construction of X-ray coherent radiation source by using relativistic particle beams in crystals. Such system can be considered as a crystal X-ray free electron laser (FEL). The idea of parametric X-ray generator on the basis of channeled electron (positron) beams in crystals was firstly expressed in [130-132]. In [130-134] it was obtained the dispersion equation for eigenstates of system, consisting of electromagnetic radiation, a beam of relativistic oscillators and a crystal. The increment of the beam instability was also analyzed. The possibility, in principle, of obtaining X-ray coherent radiation with the help of a beam of relativistic oscillators in crystals was shown. In [135] the Cerenkov relativistic beam instability in a crystal was considered and the corresponding increment was obtained. Thus, in [130-135] the new kind of X-ray FEL - solid X-ray free electron laser (SXFEL) was suggested. As we have pointed above, two mechanisms of spontaneous X-ray radiation, generated by a relativistic electron beam in crystals, can constitute the basis of such SXFEL: parametric (quasi-Cerenkov) X-ray radiation and diffraction radiation of oscillators formed in crystals, for example, by channeling [130-134, 140-143] or under the action of an external field [142,144].

The main feature of such X-ray generator is that the crystal target, in this case, not only forms the mechanism of spontaneous radiation but also is a three-dimensional resonator for X-ray radiation which produces a distributed feedback (DFB). Recently, the construction of X-ray generator by using channeled electron beams in crystals was also considered in [145-149] and on the basis of resonance transition radiation in [150,151]. The possibility of using crystal as a resonator which produces one-dimensional distributed feedback for X-ray coherent generator was

firstly expressed in [152]. This idea was used for the formation of one-dimensional DFB in solid X-ray FEL on the basis of channeled particles in [148,149]. However, in all these papers the DFB was traditionally considered in one-dimensional geometry when the radiated and diffracted waves propagated along one line in opposite directions. The authors [148,149] obtained a low generation threshold for such system with one-dimensional DFB only due to the ignoration of radiation self-absorption inside the crystal. The correct consideration of absorption, as it has been shown in [143], leads to the threshold beam density of the order of $j^{th} \sim 10^{12}$ A/cm^2 for this DFB geometry.

In the solid X-ray free electron laser, suggested in [130-144], the crystal resonator produces the three-dimensional DFB, that allows to optimize the system and essentially decrease the generation threshold. The distributed feedback in X-ray region in crystals is possible due to diffraction of X-ray radiation by crystal planes, which act like mirrors in a Fabry-Perot resonator. The case, under consideration, is distinguished from the ordinary one-dimensional DFB by the direction of propagation of diffracted wave. This is a large angle, but not π, relative to the particle motion direction and, consequently, relative to the radiated wave. The analysis shows that the process of amplification and generation in such solid resonator essentially modifies and, under definite conditions, is developing more intensive. It was shown that the interaction between the particle beam and electromagnetic field is the strongest near the region of degeneration of roots of diffraction dispersion equation, particularly, in the case of multi-wave diffraction.

Let us consider in detail two kinds of X-ray solid generators, suggested in [130-144]. Each of them has own advantages and disadvantages.

8. Parametric (Quasi-Cerenkov) X-ray Generator.

The quasi-Cerenkov instability of a relativistic electron (positron) beam in three-dimensional periodic medium in X-ray region was firstly considered in [135]. The authors have formulated the problem of X-ray parametric radiation amplification in infinite medium caused by quasi-Cerenkov instability of a relativistic particle beam. It was obtained the dispersion equation in

the case of two-beam diffraction and the increment of instability. It was shown that the strongest interaction between the particle beam and radiation was close to the region of degeneration of dispersion equation roots, which was possible only in the geometry of three-dimensional distributed feedback. The boundary problem of amplification radiation in a finite parallel-plane crystal target was solved and the generation threshold for the particle density was obtained. It was assumed that a relativistic particle beam with a mean velocity of $\vec{u}$ was incident at a definite angle ψ_0 on the parallel-plane crystal target with the length of L. The orientation of a particle beam relative to crystallographic planes was made in such a way that spontaneous photons radiated by a particle beam, were under diffraction conditions for planes with low indices. The fulfillment of diffraction condition not only results in the possibility of quasi-Cerenkov radiation in the X-ray region itself but also produces three-dimensional distributed feedback.

The closed set of equations describing the interaction of radiating beam with a crystal, in the general case, consists of Maxwell's equations for electromagnetic field and an equation for particle motion in the field (for "cold" particle beam, $\theta\psi < (kL)^{-1}$, where θ is the radiation angle, ψ is the angular spread of particles in a beam, $\vec{k}$ is the photon vector) or the equation for a distribution function (in the case of "hot" particle beam). For example, in the case of a "cold" beam we have:

$$\vec{\nabla} \times \vec{\nabla} \times \vec{E}(\vec{r},\omega) = \frac{4\pi i\omega}{c^2}\vec{j}(\vec{r};\omega) + \frac{\omega^2}{c^2}\vec{D}(\vec{r},\omega),$$

$$\frac{d\vec{v}_\alpha(t)}{dt} = \frac{e}{m\gamma}\left\{\vec{E}(\vec{r}_\alpha(t),t) + \left[\frac{\vec{v}_\alpha(t)}{c}\vec{H}(\vec{r}_\alpha(t),t)\right] - \right. \tag{4.1}$$

$$\left. - \frac{\vec{v}_\alpha(t)}{c}\left(\frac{\vec{v}_\alpha(t)}{c}\vec{E}(\vec{r}_\alpha(t),t)\right)\right\},$$

where $\vec{j}(\vec{r},t) = e\sum_{\alpha} \vec{v}_{\alpha}(t)\,\delta(\vec{r} - \vec{r}_{\alpha}(t))$ is the microscopic current density of particles in a beam, $n(\vec{r}, t) = e\sum_{\alpha} \delta(\vec{r} - \vec{r}_{\alpha}(t))$ is the corresponding charge density, $\vec{r}_{\alpha}(t)$ and $\vec{v}_{\alpha}(t)$ are the trajectory and the velocity of α-th particle in a beam, $\vec{E}(\vec{r},t)$ and $\vec{H}(\vec{r},t)$ are the electric and magnetic strengths of field, $\vec{D}(\vec{r},\omega) = \varepsilon(\vec{r},\omega)\vec{E}(\vec{r},\omega)$, $\varepsilon(\vec{\pi},\omega) = \sum_{\tau} \varepsilon_{\tau}(\omega)e^{-i\vec{\tau}\vec{r}}$ is the crystal dielectric constant, $\varepsilon_0 = 1 + g_0 \cong 1 - \omega_L^2/\omega^2$, $\omega_L^2 = 4\pi e^2 n_0/m_e$, n_0 is the electron density in a crystal, $g_{\tau} \equiv \varepsilon_{\tau}$ is the Fourier-component of dielectric constant, $\vec{\tau}$ is the reciprocal lattice vector.

Considering two-wave generation and representing the trajectory and velocity of a particle as $\vec{r}_{\alpha}(t) = \vec{r}_{0\alpha} + \vec{u}t + \delta\vec{r}_{\alpha}(t)$ and $\vec{v}_{\alpha}(t) = \vec{u} + \delta\vec{v}_{\alpha}(t)$, where $\vec{\tau}_{0\alpha}$ is the position of α-th particle in a beam at the moment of intersection of the crystal boundary, the system (4.1) can be rewritten as a system of Maxwell's equations for electromagnetic fields $\vec{E}(\vec{k},\omega)$ and $\vec{E}_{\tau}(\vec{k},\omega)$ in the following way[136-139]

$$\begin{aligned}
&\left(k^2c^2 - \omega^2\varepsilon_0 + \frac{\tilde{\omega}_L^2}{\gamma} - \omega^2\varepsilon_b(\vec{k})\right)E_{\sigma} - \omega^2 g_{\tau} E_{\sigma}^{\tau} = 0 \\
&-\omega^2 g_{-\tau} E_{\sigma} + \left(k_{\tau}^2c^2 - \omega^2\varepsilon_0 + \frac{\tilde{\omega}_L^2}{\gamma} - \omega^2\varepsilon_b(\vec{k}_{\tau})\right)E_{\sigma}^{\tau} = 0\,,
\end{aligned} \tag{4.2}$$

where $\vec{k}_{\tau} = \vec{k} + \vec{\tau}$, $E_{\sigma} = \vec{E}(\vec{k}, \omega)\vec{e}_{\sigma}$, $E_{\sigma}^{\tau} = \vec{E}(\vec{k}_{\tau}, \omega)\vec{e}_{\sigma}$, $\vec{e}_{\sigma} \| [\vec{k}\vec{\tau}]$. The set of equations (4.2) is written for σ-polarization of radiation, because it is excited with maximum probability at parametric (quasi-Cerenkov) radiation (see Part II), $\tilde{\omega}_L^2 = 4\pi e^2\tilde{n}_0/m_e$, $\tilde{n}_0$, is the mean density of an unperturbed particle beam.

The comparison of (4.2) with the ordinary set of Maxwell's equations describing X-ray dynamical diffraction in a crystal allows to conclude that the boundary problem of X-ray amplification (generation) under penetration of a particle beam through a periodic medium can be

reduced to the problem of X-ray diffraction by an "active" periodic medium, which consists of the crystal+radiating particle beam and is characterized by the following dielectric constant:

$$\tilde{\varepsilon}_0(\vec{k},\omega) = \varepsilon_0 - \frac{\tilde{\omega}_L^2}{\gamma\omega^2} - \frac{\tilde{\omega}_L^2}{\gamma\omega^2}\frac{(\vec{u}\vec{e}_\sigma)^2}{c^2}\frac{k^2c^2-\omega^2}{(\omega-\vec{k}\vec{u})^2},$$

$$\tilde{\varepsilon}_0(\vec{k}_\tau,\omega) = \varepsilon_0 - \frac{\tilde{\omega}_L^2}{\gamma\omega^2} - \frac{\tilde{\omega}_L^2}{\gamma\omega^2}\frac{(\vec{u}\vec{e}_\sigma)^2}{c^2}\frac{k_\tau^2c^2-\omega^2}{(\omega-\vec{k}_\tau\vec{u})^2}. \qquad (4.3)$$

As the electron density in a beam is much smaller than that in a crystal, the second term on the right-hand side of (4.3) can be neglected. The last term has a resonance behavior under the fulfillment the synchronism condition between a particle beam and electromagnetic field $\omega - \vec{k}\vec{u} \cong 0$. In X-ray region the fulfillment of this condition for a diffracted wave is impossible, that is why, it is possible to consider $\tilde{\varepsilon}_0(\vec{k}_\tau,\omega) \cong \varepsilon_0$.

In the case of "hot" beam, dielectric constant of a such "active" medium is represented as:

$$\tilde{\varepsilon}_0(\vec{k},\omega) \cong \varepsilon_0 - \frac{\tilde{\omega}_L^2}{\gamma\omega^2}\frac{xe^{-x^2\theta^2}}{(\psi_1\cos\varphi + \psi_2\sin\varphi + \psi_{||}/\gamma^2\theta)^2},$$

where $x = \omega - \vec{k}\vec{u}$, ψ_1, ψ_2, $\psi_{||}$ are the transverse and longitudinal divergences of the particle velocities in a beam, φ is the azimuthal angle of a photon, θ is the angle between the photon wave vector and the Z-axis, directed inside the crystal as a normal to the crystal surface.

Thus, the reduction of analysis of amplification and generation processes in X-ray FEL to the solution of a boundary problem of X-ray dynamical diffraction by "active" crystal target with the length of L allows to find generations thresholds of such system for different regimes of FEL operation and to do the optimization of parameters [138,139].

The dispersion equation determining the solutions for electromagnetic wave vector inside the "active" medium in the case of two-wave generation is written as follows:

$$\left(\omega - \vec{k}\vec{u}\right)^2 \left\{\left(k^2c^2 - \omega^2\varepsilon_0\right)\left(k_\tau^2c^2 - \omega^2\varepsilon_0\right) - \omega^4 g_\tau g_{-\tau}\right\} =$$

$$= -\frac{\tilde{\omega}_L^2}{\gamma}\frac{\left(\vec{u}\vec{e}_\sigma\right)^2}{c^2}\left(k^2c^2 - \omega^2\right)\left(k_\tau^2c^2 - \omega^2\varepsilon_0\right). \qquad (4.4)$$

and the general solution of a set of equations (4.2) can be represented in the form

$$\vec{E} = \sum_{\mu=1}^{4} \vec{e}_\sigma C_\mu e^{i\vec{k}_0\vec{r}}\left(1 + S_\mu e^{i\vec{\tau}\vec{r}}\right) e^{i\delta_\mu z}, \qquad (4.5)$$

where $S_\mu = \dfrac{\omega^2 g_{-\tau}}{k_{\mu\tau}^2c^2 - \omega^2\varepsilon_0}$, $\vec{k}_\mu = \vec{k}_0 + k_0\delta_\mu\vec{n}_z$ are the roots of dispersion equation of (4.4). The wave amplitudes C_μ are found from the matching conditions for the electromagnetic field (4.5) on the boundaries of the crystal target and are written in [139].

As a result, the generation conditions in the case of two-wave distributed feedback and the different cases of "cold" and "hot" beams and also for different regimes (weak and high gain regimes) were obtained. It was shown that, in all cases, the generation threshold has the simple meaning: on the left-hand side of equality is always the term describing "production" of radiation inside the crystal and on the right-hand side - two terms describing the radiation losses. Particularly, the first of these terms connects with the radiation losses through the crystal boundaries,and the second one corresponds to the self absorption of radiation inside the crystal.

The analysis shows that the conditions of generation threshold are optimal near the region of degeneration of roots of dispersion equation (4.4). This region corresponds to the edge of

nontransparentcy region in dynamical diffraction theory and the interaction of electromagnetic field with a particle beam and with a crystal is here the most effective.

It should be noted that the condition of the degeneration of dispersion equation roots leads to the requirement for the photon radiation angle $\theta^2 = (-\beta_1)^{-1/2}|g_d| - |g_0'| - \gamma^{-2}$, and this, in its turn, gives the restriction, in the X-ray region, for the possible geometry of Bragg diffraction

$$-\frac{r'}{|g_0'| + \gamma^2} < \beta_1 < 0 ,$$

where $r = g_\tau g_{-\tau}$.

The estimations of the threshold magnitude of the beam current density show that the case of two-wave solid distributed feedback is not optimal case for the achievement of generation regime in the X-ray region. If for "cold" particle beam in LiH and $\psi_\perp < 10^{-6}$ rad, $\psi_{||} < 10^{-8}$ rad the threshold current is of the order of 10^9 A/cm^2 at L ~ 0.1 cm, then the multiple scattering of electrons makes the beam "hot" and leads to the increase of the threshold particle beam density to $j_{th} \geq 10^{10}$ A/cm^2.

Caused by the destructive influence of multiple scattering process on the relativistic particle beam quality and, consequently, on the threshold conditions, it is necessary to decrease the crystal target length as much as possible. From the optical laser theory it is well-known that the mirror resonator, like as Fabry-Perot, is used for this purpose. In the X-ray region mirrors can be replaced by crystal plates which are oriented in such a way that the radiation wave vector is under Bragg condition. Due to the radiation generation process takes place in a narrow angle and spectral interval $\Delta\omega/\omega \sim \Delta\theta \leq 10^{-5}$,the high effectiveness of the radiation diffraction reflection by an external crystal resonator can be obtained under the corresponding coordination of resonator and the crystal target("active" medium). This allows to reduce essentially the radiation losses through target boundaries. In [138] the generation threshold for the system with the external Bragg mirrors

was derived and it was shown that the term connected with losses through boundaries could be reduced in (1 - |R|) times, where R is the reflection coefficient of Bragg mirror. As a result, we can decrease the crystal length being necessary for the generation threshold achievement. However, the estimation shows the threshold magnitude holds rather high.

As the analysis in [138] shows the transition to the distributed feedback under the surface uncoplanar diffraction, when the radiating particle beam is incident on a crystal at a small angle $\psi \sim \sqrt{g_0'}$ relative to the crystal surface (see Fig.30 in §5), allows to step down the generation threshold. First of all, the destructive influence of multiple scattering on the particle beam is suppressed. Besides, the behavior of dispersion equation roots changes and this modifies the process of radiation amplification.

The disadvantage of the case of two-wave diffraction distributed feedback is that the coordination between the degeneration condition of dispersion equation roots and the requirement of Cerenkov synchronism hardly fixes the geometry of distributed feedback and leads to the small magnitudes of the diffraction asymmetry factor β_1. It, in its turn, leads to the enhancement of self-absorption of radiation inside the crystal target. In [132] it was pointed that the transition to the multi-wave diffraction allows to modify the functional dependence of the increment of the particle beam instability and, consequently, to step down the threshold density of a beam as well. The dispersion equation for the three-wave coplanar diffraction geometry of distributed feedback was obtained and the rule for writing the dispersion equation for an arbitrary multi-wave diffraction distributed feedback was formulated. In [138] it also was derived the expression for the generation threshold in the case of three-wave coplanar diffraction. It was shown that, in this case, the Cerenkov condition was fulfilled for two dispersion branches that gave the possibility for the coincidence of diffraction roots with Cerenkov synchronism condition near the exact Bragg condition and, consequently, the possibility to optimize the threshold magnitude. In the case of the Laue-Bragg diffraction geometry the threshold density of the beam can be reduced to $j_{th} \sim 10^8$ A/cm^2, at ψ $5 \cdot 10^{-5}$ rad) in the vicinity of the double degeneration of dispersion equation roots. It

should be noted, that even in the case of three-wave generation, it becomes possible to apply the phenomenon of anomalous X-ray penetration under diffraction condition and, as a result, to step down self-absorption of radiation inside the crystal.

Thus, we can conclude that the most suitable geometry for the achievement of the generation regime of quasi-Cerenkov X-ray radiation by the help of relativistic electrons (positron) beams in crystals is the grazing geometry of the particle beam incidence on a target with the distributed feedback formed by multi-wave surface diffraction.

The spectral-angular distribution of the coherent PXR near the generation threshold was obtained in [139].

In [136] it was derived the spectral-angular distribution of coherent radiation far from the generation threshold in the frame on the perturbation theory and the possibility of experimental observation of the coherent PXR in existing accelerators was analyzed. It was shown that the observation of coherent parametric (quasi-Cerenkov)radiation far from the generation threshold was a very complicated problem for the X-ray region, but, it was possible to observe the coherent radiation in an optical region even nowadays.

9. The X-Ray Generator on the Basis of Relativistic Beam of Oscillators.

The second type of crystal generator is based on the application of diffraction radiation by oscillator (DRO) as a spontaneous radiation mechanism [140-144]. As it was said above, the radiating oscillator can be formed in the different ways. This can be electrons, channeled in an averaged crystallographic potential of plane or axes, or electrons moving in a electrostatic viggler [142] or, for example, oscillator formed by an external ultrasonic (optical) wave in a crystal [144]. It is obvious that the general approach to the consideration of generation problem by the help of a relativistic oscillator beam does not depend on the formation mechanism of oscillator itself.

Because the oscillator is a quantum system, the calculation of polarizability tensor of a particle beam is more correct to be performed in the frame of quantum electrodynamics. The reduction of the problem of radiation application (generation) by a particle beam in a finite crystal target to the problem of diffraction of X-ray by an "active" medium , consisting of a crystal and a beam of radiating oscillator, is true in this case as well.

The expression for the polarizability of such an "active" medium in the case of channeled particles in unperturbed averaged crystal potential was obtained in [141]:

$$\tilde{\varepsilon}_0(\vec{k},\omega) = \varepsilon_0 - \frac{\tilde{\omega}_L^2}{\gamma\omega^2} - \frac{4\pi e^2 n_0}{\omega^2}(W_2 - W_1)\frac{\left|\vec{\alpha}(\vec{k})_{21}\vec{e}_\sigma\right|^2}{\omega - \vec{u}\vec{k} - \Omega_{21} + i\Gamma}; \qquad (4.7)$$

where $\vec{\alpha}_{21}(\vec{k})$ is the matrix element of the operator $\hat{\alpha}\exp(i\vec{k}\vec{r})$ and in the dipole approximation it takes the form

$$\vec{\alpha}(\vec{k})_{21} = -ix_{21}(\Omega_{21}\vec{n}_x + k_x\vec{u}_z).$$

the axis $\vec{n}_x$ is chosen to lie along the transverse particle oscillations in a channel, $\vec{u}_\parallel$ is the longitudinal velocity parallel to the channeling planes, ($k_x = \vec{k}\vec{n}_x$, $\vec{u}_\parallel\vec{n}_x = 0$), Ω_{21} is the frequency of the transition (see §1 Part I), $\vec{e}_\sigma \parallel [\vec{k}\vec{\tau}]$, W_1 and W_2 are the populations of the states of 1 and 2, Γ is the phenomenological constant, taking into account inelastic collisions and can be estimated in the order of magnitudes as $(L_d)^{-1}$, where L_d is the dechanneling length. While obtaining (4.7) it was taken into account that the synchronism condition could be fulfilled only for the wave propagating at the small angle relative to the longitudinal velocity of a particle. The fulfillment the synchronism condition for the diffracted wave is impossible in the X-ray region (see also §8). As the analysis showed [141], although there were a lot of zones (states) of transverse energy of a channeled particle, the main contribution to the polarizability tensor was made by a definite

transition with the frequency Ω_{21}. It means that the consideration is reduced to the two-level problem.

Indeed, the contribution to the beam polarizability from the transition between the levels m and n is determined by the deviation from the exact synchronism condition of the radiation field with the oscillator, i.e., $\mathrm{Re}\left(\omega - \vec{u}\vec{k} - \Omega_{mn}\right) = 0$. This contribution should be taken into account only if

$$\left|\mathrm{R_e}\left(\omega - \vec{u}\vec{k} - \Omega_{mn}\right) \le \left|\mathrm{Im}\left(\vec{k}\vec{u} - \omega\right) + \Gamma_{mn}\right|\right| \tag{4.8}$$

If the magnitudes of $\mathrm{Re}\omega$ and the angle between $\vec{u}$ and $\vec{k}$ are fixed, a number of transitions contributing to the polarizability depends on the relationship between $\Delta\Omega$ and $\left|\mathrm{Im}\left(\vec{k}\vec{u} - \omega\right) + \Gamma_{mn}\right|$ where $\Delta\Omega$ determines the typical value of the difference of $\Omega_{n+1,n} - \Omega_{n,n-1}$ which characterizes the unharmonism of the averaged potential (for the harmonic potential $\Delta\Omega = 0$).The analysis of the magnitude of $\Delta\Omega$ for the different kinds of averaged crystallographic plane potentials shows that

$$\Delta\Omega >> \left|\mathrm{Im}\left(\vec{k}\vec{u} - \omega\right) + \Gamma_{mn}\right|,$$

and, consequently,the synchronism condition can be fulfilled only for the definite transition Ω_{21}. The other terms of a polarizability tensor can be neglected as unresonant ones. It was shown that the most effective interaction between the oscillator beam and the radiated wave takes place near the degeneration region of roots of the dispersion equation determining the eigenstates of the field in an "active" medium (see also §8). But, in the contrary to the parametric (quasi-Cerenkov) generator, for which the radiation condition is realized only at large deviation from exact Bragg condition, now there is a possibility to overlap the synchronism condition with the exact diffraction condition. As a result, in the case under consideration, the manifestation of the effect of anomalous X-ray penetration through resonator under dynamical diffraction (Borman effect) is possible. This

circumstance is much important because of strong absorption of X-ray inside a crystal target. In [141] the boundary problem of X-ray diffraction by an "active" medium of a finite size was solved and the generation condition was obtained. It was shown that the beam can be in synchronism with one of modes of "active" medium. They correspond to the waves with the wave vectors being the solution of dispersion equation (δ_1 and δ_2). According to [141] the generation condition can be realized in two cases: for the wave, corresponding to the root δ_2 at the positive magnitude of $\alpha = \alpha_+$, and for the wave, corresponding to the root δ_1 for the negative deviation from the exact Bragg condition $\alpha = \alpha_-$. It was shown that the solutions of generation equation for different modes are identical in a structure. All of them lead to the phase condition like

$$\delta_1^{(0)} - \delta_2^{(0)} = \frac{2\pi n}{\omega L} \tag{4.9}$$

where $\delta_1^{(0)}$ and $\delta_2^{(0)}$ are the solutions of diffraction dispersion equation, and to the amplitudes conditions of generation, which are written for the case of channeled particle in [141] and for the case of electrostatic and magnitostatic viggler in [142].

If the condition (4.9) is fulfilled the longitudinal structure of modes turns to be close to a stand wave structure. That is $|E|^2$ and $|E_\tau|^2$ are proportional to $\sim \cos^2 \frac{2\pi n}{\omega L}(z - L)$. This condition, in such a way, is analogous to the well-known phase condition of the stand wave appearance in a mirror resonator of an ordinary laser [144]. The meaning of amplitude conditions are the same as in the case of quasi-Cerenkov X-ray generator (see §8). The field amplification, due to radiation process, should be equal to the radiation losses caused by absorption inside the crystal and output of radiation through boundaries of crystal target. Because the gain, in the weak-gain regime, is proportional to the current density of a beam, the formula for the threshold gain gives the requirement for the current density. Instead of current density the invariant characteristics of a particle beam are often used, that is the current I, the normalized emittance $\varepsilon_n = \gamma r \langle\psi\rangle$ and the

normalized brightness $B_n = I/\pi^2\varepsilon_n^2$, where r is the beam radius, $\langle\psi\rangle$ is the angular spread. The angular spread corresponds to the divergence of the longitudinal velocity $\sigma_\varepsilon \cong u\langle\psi^2\rangle/2$ and corresponding divergence of the particle energy is

$$\left(\frac{\Delta\gamma}{\gamma}\right)_e = \gamma_{||}^2 \frac{\langle\psi^2\rangle}{2}.$$

For the crystal LiH, the diffraction plane (220) the values of the threshold normalized brightness of the beam, which correspond to the generation threshold for magnetic, optical undulators and channeled particles, are given in Table VII. According to this Table the value of brightness in the case of two-wave distributed feedback is rather high. But, as it was shown for parametric quasi-Cerenkov generator, using the surface multi-wave diffraction for the formation of distributed feedback, one can decrease the threshold characteristics of a particle beam and can provide with the achievement of generation regime.

In [141] the underthreshold spectral-angular distribution of radiation was analyzed and it was shown that the observation of collective radiation by relativistic oscillators was a very complicate problem in the X-ray spectrum region.

Thus the parallel consideration of two kinds of crystal three-dimensional X-ray generators, which are distinguished by the mechanisms of spontaneous radiation, shows that three dimensional distributed feedback allows to decrease the current density of the particle beam, in comparison with the other papers [145-149] by several orders of magnitude. It makes it possible to consider the construction of FEL in the hard X-ray region as a scientific problem of nowadays, which can be analyzed not only theoretically but also experimentally.

In conclusion we briefly consider the question of the time of formation of radiation, generated by a particle passing through a crystal. At the first sight, the duration of radiation impulse is of the order of L/c, where L is the target length. But in [155] it was shown that the

Table VII

Parameters	Magnitostatic Wiggler	Optical Wiggler	Channeled Particle
Accelerator			
Energy	= 5 GeV	= 290 MeV	= 500 MeV
Normalized brightness	$= 3.5 \cdot 10^{9}$	$= 1.7 \cdot 10^{10}$	$= 5 \cdot 10^{9}$
Energy spread	$= 2.4 \cdot 10^{-3}$	$1.2 \cdot 10^{-5}$	
Density of current	$= 5.3 \cdot 10^{7}$	$= 1.3 \cdot 10^{6}$	$= 3.3 \cdot 10^{8}$
Wiggler			
Wave length	= 1 mm	= 5 μm	
Magnetic field strength	= 17.5 kG		
Laser energy		= 0.75 gW	
Crystal			
Wave length of radiation	= 0.05 Å	= 0.15 Å	= 1 A
Asymmetry parameter	= 9	= 1	
Diffraction plane	(220)	(220)	(100)

transmission of the short impulse of X-ray and γ-radiation through crystals was accompanied by an essential delay of radiation inside the target even in the absence of resonance scattering.

Let the electromagnetic impulse pass through the medium with the refractive index $n(\omega)$ The group velocity of wave packet inside the medium is

$$v_{gr} = \left(\frac{\partial \omega n(\omega)}{c \partial \omega}\right)^{-1} = \frac{c}{n(\omega) + \omega \dfrac{\partial n(\omega)}{\partial \omega}}, \tag{4.10}$$

where c is light speed, ω is the quantum frequency.

In the X-ray region (~ 10 keV) the refractive index is a universal function of frequency $n(\omega) = 1 - \omega_L^2/2\omega^2$, $4\pi e^2 n_0/me$ and $n - 1 \cong 10^{-6} << 1$. By introducing $n(\omega)$ into (4.10) we obtain $v_{gp} \cong c\left(1 - \omega_L^2/\omega^2\right)$, that is the group velocity is does not differ practically from a light speed. As a consequence, the time delay of wave packet inside the medium makes up only a small part of a time of light passage of the distance L in the vacuum.

$$\Delta T = \frac{L}{v_{gr}} - \frac{L}{c} \cong \frac{L}{c}\frac{\omega_L^2}{\omega^2}. \tag{4.11}$$

Let the impulse be diffracted by a crystal. Let us consider, for simplicity, the case of two-wave dynamical diffraction. The crystal, under these conditions, is characterized by two effective refractive indices (see Part I):

$$n_{1,2} = 1 + \delta^{(1,2)},$$

$$\delta_{1,2} = \frac{1}{4}\left[g_{00}\left(1 + \beta_1\right) - \beta_1\alpha \pm \sqrt{\left[g_{00}\left(1 - \beta_1\right) + \beta_1\alpha\right]^2 + 4\beta_1 g_{10} g_{01}}\right] \tag{4.12}$$

Because we consider the photons with the frequencies in the vicinity of the Bragg frequency ω_B,then the magnitudes of g_{00} and g_{01} can be taken as constants and only the deviation from exact Bragg condition α is a function of a frequency

$$\alpha = \frac{\vec{\tau}\left(\vec{\tau} + 2\vec{k}\right)}{k^2} \cong -\frac{\tau^2}{k_B^2 c}(\omega - \omega_B)$$

where $k = \omega/c$, $\vec{\tau}$ is the reciprocal lattice vector, ω_B corresponds to the condition $\alpha = 0$. As a result, we have from (4.10)-(1.12).

$$v_{gr}^{(1,2)} \cong c\left[n_{1,2}(\omega) \pm \beta_1 \frac{\tau^2}{4k_B^2} \frac{\left(g_{00}(1-\beta_1) + \beta_1\alpha\right)}{\left[\left(g_{00}(1-\beta_1) + \beta_1\alpha\right)^2 + 4\beta_1\, g_{01}g_{10}\right]}\right]. \qquad (4.13)$$

In the general case of diffraction $\left(g_{00}(1-\beta_1) + \beta_1\alpha\right) \cong 2\sqrt{\beta_1}\, g_\tau$ and, consequently, the additional term is of the order of the unity. Moreover, in the case of asymmetric diffraction, when $|\beta_1| >> 1$, v_{gr} can essentially differ from c. It should be noted that the complex character of the electromagnetic field under diffraction in a crystal leads to the possibility that v_{gr} becomes more than the light speed. If β_1 is negative, the expression under the root in (4.13) can be zero (the threshold of Bragg reflection). In this case, v_{gr} tends to zero. The analysis shows that under multi-wave diffraction the duration of radiation impulse can increase.

REFERENCES

1. Ter-Mikaelian Hihg Energy Electromagnetic Processes in Condensed Media, New York, Wiley-Interscience, 1972.

2. Baryshevsky V.G. Channeling, Radiation and Reactions in Crystals at High Energy, Minsk, Izd. Bel. University, 1982.

3. Kalashnikov N.P. Coherent Interaction of Charged Particles in Crystals, Moscow, Atomizdat, 1981.

4. Garibian G.M. and Yang C. X-Ray Transition Radiation, Erevan, Izd. Akad. Nauk Arm.SSR, 1983.

5. Ginzgurg G.M. and Tsytovich V.N. Transition Radiation and Transition Scattering, Moscow, Nauka, 1984.

6. Kumakhov M.A. and Komarov F.F. Radiation from Charged Particles in State Solids, Minsk, Izd.Belor.University, 1985.

7. Bazylev V.A. and Zhevago N.K. Radiation from High Energy Particles in the Medium in External Fields, Moscow, Nauka, 1987.

8. Belyakov V.A. Diffraction Optics of Periodic Media with Complex Structures, Moscow, Nauka, 1988.

9. Bayer V.A., Katkov V.M. and Strakhovenko V.M. Electromagnetic Processes at High Energy in Oriented Crystals, Novosibirsk, Nauka, 1989.

10. Frank I.M. Vavilov-Cerenkov Radiation. Theoretical Questions, Moscow, Nauka, 1988.

11. Vorobiev S.A. Electron Transition throgh Crystals, Moscow, Atomizdat, 1975.

12. Gemmell D.S. Rev. Mod. Phys., 1974, v.46, p.129.

13. Baryshevsky V.G. and Dubovskaya I.Ya. Doklady Akad. Nauk SSSR, 1976, v.231, p.1336.

14. Baryshevsky V.G., Dubovskaya I. Ya. and Grubich A.O. Phys. Lett., 1980, v.777A, p.61.

15. Baryshevsky V.G. Doklady Akad. Nauk Bel.SSR, 1971, v.15, p.306.

16. Baryshevsky V.G. and Feranchuk I.D. Zh. Exp. Theor. Fiz., 1971, v.61, p.944; Corrections: ibid., 1973, v.64, p.760.

17. Baryshevsky V.G., Grubich A.O., Dubovskaya I.Ya. Phys. Stat. Sol.(b), 1978, v.88, p.351.

18. Baryshevsky V.G., Dubovskaya I.Ya., Grubich A.O. Phys. Stat. Sol.(b), 1980, v.99, p.205.

19. Baryshevsky V.G. and Dubovskaya I.Ya. J. Phys.C: Solidi State Phys., 1983, v.16, p.3663.

20. Garibian G.M. and Yang C. Zh. Exp. Theor. Fiz., 1971, v.61, p.930.

21. Garibian G.M. and Yang C. Zh. Exp. Theor. Fiz., 1972, v.63, p.1198.

22. Jelley I.V. Cerenkov Radiation and its Applications, Pergamon press, London-New-York-Paris, 1958.

23. Vorobiev S.A., Kalinin V.N., Pak S. et al. Pis'ma in Zh. Exp. Theor. Fiz., 1985, v.41, p.3.

24. Adishchev Yu.N., Baryshevsky V.G., Vorobiev S.A. et al. Pis'ma in Zh. Exsp. Teor. Fiz., 1985, v.41, p.295.

25. Didenko A.N., Kalinin V.N. et al. Phys. Lett., 1985, v.110A, p.177.

26. Baryshevsky V.G., Danilov V.A., Ermakovich O.L. et al. Phys. Lett., 1985, v.110A, p.477.

27. Baryshevsky V.G., Gradovsky O,T., Dubovskaya I.Ya. Izv Akad. Nauk Bel.SSR, ser. phys.-math., 1987, v.6,p.77.

28. Gradovsky O.T. Phys. Lett., 1988, v.126A, p.291.

29. Grubich A.O. and Lugovskaya O.M. Izv. Akad. Nauk Bel.SSR, ser. phys.-math., 1991, v.1, p.61.

30. Landau L.D. and Lifshits E.M. Electrodinamics of Condensed Media, Moscow, Nauka, 1982.

31. Mors F.M. and Feshbakh G. Methods of Mathematical Physics,

32. Baryshevsky V.G. Nuclear Optics of Polarized Media, Minsk, Izd. Bel. University, 1976.

33. Fainberg Ya.B. and Hizhniak N.A. Zh.Exp. Teor. Fiz., 1957, v.32, p.883.

34. Baryshevsky V.G. and Feranchuk I.D. Izd. Akad. Nauk Bel.SSR, ser. phys.-math., 1973, v.2, p.102.

35. Baryshevsky V.G. and Feranchuk I.D. Doklady Akad. Nauk Bel.SSR, 1974, v.18, p.499.

36. Baryshevsky V.G. and Feranchuk I.D. Phys. Lett., 1976, v.57A, p.183.

37. Baryshevsky V.G. and Feranchuk I.D. J.Physique, 1983, v.44, p.913.

38. Avakian A.P., Aginian M.A., Garibian G.M. and Yang C. Zh. Exp. Teor. Fiz., 1975, v.68, p.2038.

39. Garibian G.M. and Yang C. Zh. Exp. Theor. Fiz., 1976, v.70, p.1627.

40. Aginian M.A. and Yang C. Preprint EFN-953, (3)-87, Erevan, 1987.

41. Garibian G.M. and Yang C. Nucl. Instr. Meth., 1986, v.248A, p.29.

42. Feranchuk I.D. and Ivashin A.V. J. de Physique, 1985, v.46, p.1981.

43. Baryshevsky V.G., Grubich A.O., Feranchuk I.D. and Ivashin A.V. Nucl. Instr. Meth., 1986, v.249A, p.306.

44. Baryshevsky V.G., Grubich A.O. and Feranchuk I.D. Zh. Exp. Teor. Fiz., 1986, v.90, p.1588.

45. Baryshevsky V.G., Grubich A.O. and Le Tien Hai, Zh. Exp. Teor. Fiz., 1988, v.94, p.51.

46. Grubich A.O. and Le Tien Hai Izv. Akad. Nauk Bel.SSR, ser. phys.-math., 1987, v.6, p.90.

47. Fedorov V.V. and Smirnov A.I. Pis'ma in Zh. Exp. Teor. Fiz., 1976, v.23, p.34.

48. Mendlovits H. and Glass Phys. Lett., 1979, v.73A, p.363.

49. Belyakov V.A. and Orlov V.P. Phys. Lett., 1972, v.42A, p.3.

50. Dialetis D. Phys. Lett., 1978, v.17A, p.1113.

51. Afanasiev A.M. and Aginian M.A. Zh. Exp. Teor. Fiz., 1978, v.74, p.570.

52. Feranchuk I.D. Crystallography - Sov. Phys., 1979, v.24, p.289.

53. Ivashin A.V. and Feranchuk I.D. Abstr. XIIV Conf. on Interaction of Charged Particles with Crystals, Moscow, 1987, p.102.

54. Ivashin A.V. and Feranchuk I.D. Sov. Phys. - Crystallography, 1989, v.34, p.39.

55. Baryshevsky V.G. and Feranchuk I.D. Nicl. Instr. Meth., 1985, v.228A, p.490.

56. Ivashin A.V. Cand. Dissertation, Minsk, 1987.

57. Galitsky V.M. and Gurevich I.I. Nuovo Cimento, 1964, v.32, p.396.

58. Baryshevsky V.G., Batrakov K.G. and Dubovskaya I.Ya. Abstr. XX Conf. on Interact. of Charged Particles with Crystals, Moscow, 1990, p.88.

59. Feranchuk I.D., Ivashin A.V. and Polikarpov I.V. J. Phys. D: Appl. Phys., 1988, v.21, p.831.

60. Ivashin A.V., Krylov E.V. and Feranchuk I.D. Dokl. XIX Conf. of Interact. of Charged Particles with Crystals, Moscow, 1990, p.96.

61. Yuan L.C., Alley P.W., Bamberger A. et el. Nucl. Instr. Meth., 1985, v.234A, p.426.

62. Baryshevsky V.G., Cherepitsa S.V., Danilov V.A. et al. J. Phys.D: Appl. Phys. 1986, v.19, p.171.

63. Kaganer V.M., Indenbom V.L., Vraha M. et al. Phys. Stat. Sol.(a), 1982, v.71, p.371.

64. Avakian R.O., Avetisian A.E., Adishchev Yu.N. et al. Pis'ma in Zh. Exp. Teor. Fiz., 1987, v.45, p.33.

65. Adeshvili D.I., Blazhevich S.V., Boldyshev V.F. et al. Abstr. XVI Conf. on Interact. of Charged Particles with Crystals, Moscow, 1986, p.80.

66. Adeishvili D.I., Blazhevich S.V., Boldyshev V.F. et al. Dokl. Akad. Nauk SSSR, v.298, p.844.

67. Morohovsky V.L. Coherent X-Ray Radiation from Relativistic Electrons in a Crystal, Revue, Moscow, 1989.

68. Morokhovsky V.L., Adeishvili D.I., Blazhevich S.V. et al. Questions of Atomic Science and Teknics, ser. "Physics of Radiation Demages and Radiation", 1988, v.4, p.66.

69. Baryshevsky V.G., Grubich A.O. and Le Tien Hai, Izv. Akad. Nauk Bel.SSR, ser. phys.-math., 1988, v.4, p.100.

70. Aginian M.A. and Yang C. Izv. Akad. Nauk. Arm.SSR, ser. phys.,1986, v.21, p.280.

71. Adishchev Yu.N., Vorobiev S.A., Kalinin B.N. et al. Zh. Exp. Teor. Fiz., 1986, v.90, p.829.

72. Adeishvili D.I., Blazhevich S.V., Bochek G.Ya. et al. Abstr. XVII Conf. on Interact. of Charged Particles with Crystals, Moscow, 1987, p.75.

73. Adishchev Yu.N., Babadzhanov R.D., Vorobiev S.A. et al. Zh. Exp. Teor. Fiz., 1988, v.58, p.754.

74. Adishchev Yu. N., Mun V.V., Uglov S.R. Abstr. XVII Conf. on Interact. of Charged Particles with Crystals, Moscow, 1987, p.74.

75. Adishchev Yu.N., Vorobiev S.A., Mun V.V. et al. Pis'ma in Zh. Tekn. Fiz., 1987, v.13, p.83.

76. Afanasenko V.P., Baryshevsky V.G., Gradovsky O.T. et al. Pis'ma in Zh. Tekn. Fiz., 1988, v.14, p.57.

77. Adishchev Yu. N., Apanasevich A.P., Afanasenko V.P. et al Dokl. XVIII Conf. on Ineract. of Charged Particles with Crystals, Moscow, 1989, p.99.

78. Adishchev Yu. N., Babagzhanov R.D.. Versilov V.A. et al. Pis'ma in Zh. Tekn. Fiz., 1990, v.16, p.15.

79. Didenko A.N., Adishchev Yu.N., Kalinin V.N. et al. Phys. Lett., 1986, v.118A, p.363.

80. Adishchev Yu.N., Babadzhanov R.D., Vorobiev S.A. et al. Zh. Exp. Teor. Fiz., 1987, v.93, p.1943.

81. Didenko A.N., Adishchev Yu.N., Vorobiev S.A. et al. Dokl. Akad. Nauk SSSR, 1987, v.296, p.1360.

82. Adishchev Yu.N., Didenko A.N., Mun V.V., et al. Nucl. Instr. Meth., 1987, v.21B, p.49.

83. Aginian M.A. and Yang C. Dokl. XVIII Conf. on Interact. of Charged Particles with Crystals, Moscow, 1988, p.107.

84. Adishchev Yu.N., Apanasevich A.P., Afanasenko V.P. et al. Abstr. XIX Conf. on Interact. of Charged Particles with Crystals, Moscow, 1988, p.338.

85. Adishchev Yu.N., Apanasevich A.P., Afanasenko V.P. et al. Izv. VUSOV, ser. phys., 1989, v.8, p.112.

86. Adishchev Yu. N., Babadzhanov R.D., Muminov T.M. et al. Pis'ma in Zh. Tekn. Fiz., 1986, v.12, p.1507.

87. Baryshevsky V.G., Grubich A.O., Ivashin A.V. et al. Dokl. XVI Conf. on Interact. of Charged Particles with Crystals, Moscow, 1987, p.111.

88. Adishchev Yu.N., Versilov V.A., Vorobiev S.A. et al. Abstr. XVIII Conf. on Interact. of Charged Particles with Crystals, Moscow, 1988, p.62.

89. Adishchev Yu.N., Versilov V.A., Vorobiev S.A. et al. Pis'ma in Zh. Exp. Teor. Fiz., 1988, v.48, p.311.

90. Afanasenko V.P., Baryshevsky V.G., Gradovsky O.T. et al. Abstr. IV Conf. on Coherent Interact. of Radiation with Medium, Moscow, 1988, p.337.

91. Adishchev Yu.N., Versilov V.A., Potylitsin A.P. et al. Nucl. Inetr. Meth., 1989, v.44B, p.130.

92. Adishchev Yu.N., Versilov V.A., Potylitsin A.P. et al. Dokl. XIX Conf. on Interact. of Charged Particles with Crystals, Moscow, 1990 p.83.

93. Adishchev Yu.N., Versilov V.A., Vorobiev S.A. et al. Abstr. XX Conf. on Interact. of Charged Particles with Crystals, Moscow, 1990, p.61.

94. Chang Shin-Lin, Multiple Diffraction of X-Rays in Crystals, Springer-Verlag, 1984.

95. Afanasenko V.P., Baryshevsky V.G., Gradovsky O.T. et al. Phys. Lett., 1989, v.141A, p.311.

96. Afanasenko V.P., Baryshevsky V.G., Zhuevsky R.F. et al. Pis'ma in Zh. Tekn. Fiz., 1989, v.15, p.33.

97. Afanasenko V.P., Baryshevsky V.G., Gatsykha S.V. et al. Pis'ma in Zh. Exp. Teor. Fiz., 1990, v.51, p.213.

98. Truong Ba Ha, and Dubovskaya I.Ya. Phys. Stat. Sol.(b), 1989, v.155, p.685.

99. Dubovskaya I.Ya. and Truong Ba Ha Abstr. XX Intern. Congress of Crystallography, Moscow, 1990.

100. Dubovskaya I.Ya., Truong Ba Ha and Le Tien Hai Phys. Stat. Sol.(b), 1991, v.165, p.571.

101. Dubovskaya I.Ya. and Savchuk G.K. Phys. Stat. Sol.(b), 1989, v.156, p.687.

102. Ivashin A.V. and Feranchuk I.D. Abstr. XVIII Conf. on Interact. of Charged Particles with Crystals, Mockow, 1988, p.78.

103. Gantmakher F.R. Matrix theory, Moscow, Nauka, 1988.

104. Baryshevsky V.G. Dokl. Akad. Nauk SSSR, 1988, v.299, p.1336.

105. Baryshevsky V.G. in "Some Problems of Modern Nuclear Physics" to 80-th Anniversary of I.M.Frank, Moscow, Nauka, 1989, p.156.

106. Baryshevsky V.G. Pis'ma in Zh. Tekn. Fiz., 1976, v.2, p.112.

107. Baryshevsky V.G. and Dubovskaya I.Ya. Phys. Stat. Sol. (in Russia), 1977, v.19, p.597.

108. Andreev A.V. Uspekhi Fiz. Nauk, v.145, p.113.

109. Andriyanchik A.A., Dubovskaya I.Ya. and Kaminsky A.I. J. Phys. C: Condenced Matter, 1991, v.3, p.5579.

110. Entin I.R. Zh. Exp. Teor. Fiz. 1979, v.77, p.214.

111. Entin I.R. Phys. Stat. Sol. (b), 1985, v.132, p.355.

112. Kolpakov A.V. and Khanacev Yu.P. "Crystallography (in Russia), 1973, v.18, p.474.

113. Baryshevsky V.G. Dokl. Akad. Nauk Bel.SSR, 1980, v.24, p.132.

114. Baryshevsky V.G. Izv. Akad. Nauk Bel.SSR, ser. phys.-math., 1980, v.3, p.117

115. Baryshevsky V.G. Abstr. XVI Conf. on Interact. of Charged Particlea with Crystals, Moscow, 1986, p.53.

116. Baryshevsky V.G. and Polikarpov I.V. Izv Akad. Nauk Bel.SSR, ser. phys.-math., 1988, v.2, p.86.

117. Baryshevsky V.G. and Polikarpov I.V. Zh. Exp. Teor. Fiz., 1988, v.94, p.109.

118. Baryshevsky V.G. and Polikarpov I.V. Izv. Bel. University, ser.1, 1989, v.1, p.8.

119. Baryshevsky V.G. and Polikarpov I.V. Phys. Lett., 1989. v.190A, p.205.

120. Baryshevsky V.G. and Polikarpov I.V. Izv. Akad. Nauk Bel.SSR, ser. phys.-math., 1989, v.2, p.81.

121. Polikarpov I.V. and Skadorov V.V. Phys. Stat. Sol.(b), 1987, v.143, p.11.

122. Polikarpov I.V. and Skadorov V.V. Izv. Akad. Nauk Bel.SSR, ser. phys.-math., 1878, v.6, p.95.

123. Polikarpov I.V. and Skadorov V.V. Izv. Akad. Nauk Bel.SSR, ser. phys.-math., 1988, v.3, p.83.

124. Pinsker Z.G. "X-Ray Crystallography", Moscow, Nauka, 1982.

125. Baryshevsky V.G. and Dubovskaya I.Ya. Phys. Stat. Sol.(b), 1977, v.82, p.403.

126. Dubovskaya I.Ya. and Truong Ba Ha, Izv. Bel. University, 1988, ser.1, v.1, p.11.

127. Grubich A.O. and Lugovskaya O.M. Izv. Akad. Nauk Bel.SSR, ser. phys.-energ., 1991, v.3, p.61.

128. Andriyanchik A.A. and Kaminsky A.N. Izv. Bel. University, 1988, ser.1, v.2, p.54.

129. Baryshevsky V.G. and Dubovskaya I.Ya. J. Phys. C: Condens. Matter, 1991, v.3, p.2421.

130. Baryshevsky V.G. and Feranchuk I.D. Dokl. XI Conf. on Interact. of Charged Particles with Crystals, Moscow, 1982, p.208.

131. Baryshevsky V.G. and Feranchuk I.D. Dokl. Akad. Nauk Bel.SSR, 1983, v.27, p.995.

132. Baryshevsky V.G. and Feranchuk I.D. Dokl. Akad. Nauk Bel.SSR, 1984, v.28,p.336.

133. Baryshevsky V.G. and Feranchuk I.D. Phys. Lett., 1984, v.102A, p.141.

134. Baryshevsky V.G. and Feranchuk I.D. Izv. Akad. Nauk Bel.SSR, ser. phys.-math., 1985, v.2, p.79.

135. Baryshevsky V.G., Dubovskaya I.Ya. and Feranchuk I.D. Izv. Akad. Nauk Bel.SSR, ser. phys.-math., 1988, v.1, p.92.

136. Baryshevsky V.G. , Batrakov K.G. and Dubovskaya I.Ya. Dokl. XIX Conf. of Interact. of Charged Particles with Crystals, Moscow, 1990, p.105.

137. Batrakov K.G. and Dubovskaya I.Ya. Izv. Akad. Nauk Bel.SSR, ser. phys.-math., 1990, v.5, p.82.

138. Baryshevsky V.G., Batrakov K.G. and Dubovskaya I.Ya. Izv. Akad. Nauk Bel.SSR, ser. phys.-energ., 1991, v.1, p.53.

139. Baryshevsky V.G., Batrakov K.G. and Dubovskaya I.Ya. J. Phys. D: Appl. Phys., 1991, v.24, p.1250.

140. Baryshevsky V.G., Dubovskaya I.Ya. and Zege A.V. Dokl. XIX Conf. on Interact. of Charged Particles with Crystals, Moscow, 1990, p.102.

141. Baryshevsky V.G., Dubovskaya I.Ya. and Zege A.V. Nucl. Instr. Meth., 1990, v.135A, p.368.

142. Baryshevsky V.G., Dubovskaya I.Ya. and Zege A.V. Izv. Akad. Nauk Bel.SSR, ser. phys.-energ., 1990, v.3, p.49.

143. Baryshevsky V.G., Dubovskaya I.Ya. and Zege A.V. Phys. Lett., 1990, v.149A, p.30.

144. Baryshevsky V.G. and Dubovskaya I.Ya. Izv. Akad. Nauk Bel.SSR, ser. phys.-energ., 1990, v.1, p.30.

145. Fridman A., Gover A., Kurizki G. et al. Rev. Mod. Phys., 1988, v.60, p.471.

146. Kurizki G. in "Relativistic channeling", Eds. Carrigan R.A. and Ellison S.A., M.Y.Plenum Press., 1987, p.505.

147. Bogaez S.A. and Ketterson J.B. J. Appl. Phys., 1986, v.60, p.177.

148. Strauss M., Amend P., Rostoker N. and Ron A. Appl. Phys. Lett., 1988, v.52, p.866.

149. Strauss M. and Rostoker N. Phys. Rev., 1989, v.39A, p.579.

150. Pistrup M.A. and Finman P.E. IEEE J. of Quantum Electronics, 1983, v.QE-19, p.357.

151. Piestrup M.A. IEEE, J. of Quantum Electronics, 1988, v.QE-24, p.591.

152. Yariv A. Appl. Phys., 1974, v.24, p.105.

153. Kogelnik H. and Shank C. Appl. Phys., 1972, v.43, p.2327.

154. Karlov N.V. "Lectures on Quantum Electronics", Moscow, Nauka, 1988.

155. Baryshevsky V.G. Izv. Akad. Nauk Bel.SSR, ser. phys.- energ., 1989, v.5, p.58.

LAWRENCE BERKELEY LABORATORY
UNIVERSITY OF CALIFORNIA
INFORMATION RESOURCES DEPARTMENT
BERKELEY, CALIFORNIA 94720